

**ADVANCED CONTROL STRATEGIES FOR PHARMACEUTICAL
ANTISOLVENT CRYSTALLIZATION PROCESSES**

VAMSI KRISHNA KAMARAJU

NATIONAL UNIVERSITY OF SINGAPORE

2014

**ADVANCED CONTROL STRATEGIES FOR PHARMACEUTICAL
ANTISOLVENT CRYSTALLIZATION PROCESSES**

VAMSI KRISHNA KAMARAJU

2014

**ADVANCED CONTROL STRATEGIES FOR PHARMACEUTICAL
ANTISOLVENT CRYSTALLIZATION PROCESSES**

VAMSI KRISHNA KAMARAJU
(B.Tech., Osmania University, India)

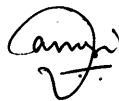
**A THESIS SUBMITTED
FOR THE DEGREE OF DOCTOR OF PHILOSOPHY
DEPARTMENT OF CHEMICAL AND BIOMOLECULAR ENGINEERING
NATIONAL UNIVERSITY OF SINGAPORE**

2014

Declaration

I hereby declare that this thesis is my original work and it has been written by me in its entirety. I have duly acknowledged all the sources of information which have been used in this thesis.

This thesis has also not been submitted for any degree in any university previously.



Vamsi Krishna Kamaraju

20 August 2014

This thesis was prepared with the \LaTeX document preparation system.

\TeX is a trademark of the American Mathematical Society.

This thesis was edited and composed using WinEdt 6.0 text editor on a Dell Opti-plex 780 running the Microsoft Windows 7 operating system.

Copyright © 2014 by Vamsi Krishna Kamaraju.

All rights reserved. No part of this publication may be reproduced, stored in any retrieval system, or transmitted, in any form or by any means, electronic, mechanical, photocopying, recording or otherwise, without the prior written permission of the author.

Printed in Singapore.

To my parents, teachers, philosophers, and well-wishers ...

Acknowledgements

I would like to sincerely thank all the authorities and administrative staff at the National University of Singapore (NUS) for enabling and providing me with an opportunity to pursue the Doctoral program at this prestigious university with all the necessary facilities and research scholarship. I regard myself very fortunate to have joined the Department of Chemical and Biomolecular Engineering, that enabled me to meet some of the wonderful people who have influenced, mentored and taught some great values, philosophies and experiences in life.

Firstly, I would like to sincerely thank and express my deepest gratitude to Dr. Min Sen Chiu for his constant support, encouragement and patience in providing valuable suggestions and constructive criticism regarding my research work throughout the Doctoral program. I am very thankful for his care and concern in nurturing me into a confident young researcher with ambitious ideas and aspirations. I would like to express my sincere gratitude towards Dr. Balasubrahmanyam Srinivasan (École Polytechnique Montréal) for his collaborative work on *Necessary Conditions of Optimality* tracking based control schemes and generous efforts in teaching interesting concepts and sharing his knowledge on batch process control. It has been an overwhelming experience interacting with him, which has definitely helped me in better visualizing some of the intricate concepts of linear systems theory. I am greatly indebted to Dr. Lakshminarayanan Samavedham not only for his courses on mathematical methods, but also for influencing and inspiring me towards effective teaching and learning. I would like to express my gratitude for the

encouragement and support I have received from him and his subordinate staff at the Centre for Development of Teaching and Learning (CDTL, NUS) for making me a part of facilitating the workshops and sessions. My sincere thanks to Dr. Qing-Guo Wang and Dr. Rajagopalan Srinivasan for providing valuable suggestions and comments during my research proposal presentation.

I warmly thank my colleagues Su Qinglin, Li Yan, Huang Wen, and Xu Yuenchen at the Laboratory of System Identification and Control for interesting and thought-provoking technical discussions on variety of topics, and also for the moral support that was necessary in lot of situations during my Doctoral program. My special thanks to the group alumni, Dr. Yang Xin, Dr. Martin Wijaya Hermanto, and Dr. Yasuki Kansha for their occasional visits to our office and unhesitatingly sharing their research experiences. I would also like to thank all the innumerable researchers across the globe, who have inspired and helped me understand various topics through their research contributions, and also all the anonymous reviewers for their time and patience in providing the critiques, valuable suggestions, and remarks regarding my manuscripts.

I would like to thank all my friends and house mates who made my stay in Singapore a memorable experience. Their wise words and thoughtful suggestions have helped me maneuver through tough times. Reaching this stage in my life would have never been possible without the encouragement of my wonderful parents Mr. Rama Rao and Mrs. Janaki, my brother Chaitra, my sister-in-law Shalini, and my nephew Aditya, who have inspired and strongly motivated me into pursuing the PhD with utmost sincerity, dedication and integrity. Their love, care and support has been pivotal in making me achieve this task with undivided attention and diligence. Last but not the least, I would like to extend my gratitude to Swetha for her unconditional love and understanding. I sincerely thank The Almighty for safe guarding and blessing me with good health and peace.

Table of Contents

Acknowledgements	i
Table of Contents	iii
Summary	vii
List of Tables	xi
List of Figures	xiii
Nomenclature	xvii
Abbreviations	xxv
1 Introduction	1
1.1 Motivation	1
1.2 Contributions	4
1.3 Thesis organization	7
2 Literature Review	9
2.1 Fundamentals of crystallization	9
2.1.1 Driving force for crystallization	10
2.1.2 Nucleation	12
2.1.3 Crystal growth	15

2.1.4	Role of solvent composition on the precipitation kinetics . . .	16
2.1.5	Crystal size distribution	17
2.2	Modeling of antisolvent crystallization processes	19
2.3	Recent advances in control of antisolvent crystallization processes	21
3	Improved Operation of Concentration Control	27
3.1	Introduction	27
3.2	Concentration control of semi-batch antisolvent crystallization processes	30
3.2.1	Process model	30
3.2.2	C-control strategy	34
3.3	Proposed integrated modeling framework	36
3.3.1	Overview of LSSVM for multiclass classification	36
3.3.2	Nonlinear dynamic modeling	41
3.3.3	Nonlinear product quality modeling of batch processes . . .	44
3.4	Results and discussions	47
3.5	Conclusions	61
4	Adaptive Concentration Control	63
4.1	Introduction	63
4.2	Methodologies	66
4.2.1	On-line pattern classification	66
4.2.2	Proposed framework	68
4.3	Results and discussions	70
4.4	Conclusions	87
5	Measurement Based Optimal Control	89
5.1	Introduction	89

5.2	Background	92
5.2.1	Model predictive control formulation for batch processes . .	92
5.2.2	Necessary conditions of optimality tracking based control .	93
5.2.3	Neighboring extremal controller for non-singular problems .	94
5.3	NCO-tracking based control of antisolvent crystallization processes	96
5.4	Results and discussions	99
5.5	Conclusions	108
6	Reformulated Neighboring Extremal Control	109
6.1	Introduction	109
6.2	Model predictive control vs NCO-tracking based control	112
6.2.1	MPC formulation	112
6.2.2	Neighboring extremal feedback in presence of model un- certainties	113
6.3	Results and discussions	115
6.4	Conclusions	124
7	Conclusions and Future Work	125
7.1	Conclusions	125
7.2	Suggestions for future works	128
	References	131
	Publications and Presentations	149

Summary

Control of antisolvent crystallization processes during the manufacture of Active Pharmaceutical Ingredients (APIs) is of paramount importance, as the product crystal size distribution (CSD) obtained at the end of the process has significant effect on the efficiency of other downstream operations and the efficacy of the final intended drug. Hence, the prime motive is to enable tighter control of crystallization processes for better quality in terms of product CSD. Besides, due to the complex mechanisms exhibited by the crystallization processes, traditional antisolvent flowrate control (F-control) strategies were found to be less robust in presence of process variations. Therefore, this motivated the current study on developing advanced control strategies for semi-batch antisolvent crystallization processes.

Owing to the advancements in sensor technology, direct design approaches like concentration control (C-control), which uses concentration or supersaturation measurement feedback were recently developed. This strategy was found to be more robust than F-control strategy due to its closed loop nature. However, in presence of process variations, the C-control often operates in a sub-optimal fashion with varying batch times. Moreover, in presence of high nucleation rate and shifts in solubility data, the performance of C-control strategy becomes poorer than the traditional F-control strategy. Therefore, in order to circumvent these shortcomings, a new two-staged modeling framework incorporating pattern classification and non-linear modeling tools is proposed in this study for determining the optimal setpoints for the optimal operation of the C-control strategy. Simulation results show that the

constant relative supersaturation setpoints determined using the proposed method helps in optimal operation of the semi-batch antisolvent crystallization processes in presence of variations. Based on the case studies considered during this study, the proposed methodology delivered a maximum performance improvement of 57.7% over the conventional C-control strategy.

Furthermore, inspired by the idea of model predictive controller (MPC) for real time optimal control of semi-batch antisolvent crystallization processes, a systematic approach for the adaptive concentration control strategy based on the proposed modeling framework is presented in this study. The relative supersaturation setpoint at each time instant during the batch is adjusted adaptively based on the feedback of CSD and concentration measurements. It has been shown that the adaptive C-control not only helps in providing improved robustness over the C-control strategy, but also achieves product quality values that are close to the true optimal. Based on the case studies considered during this study, the proposed methodology delivered a maximum performance improvement of 60.7% over the conventional C-control strategy. Furthermore, it has also been shown that the parameterization approach for segmenting the control vector for the relative supersaturation profile also has a significant effect on the batch end product quality.

In order to circumvent the issue concerning the computation effort during real-time optimal control schemes based on repetitive optimization, an alternative approach based on tracking the necessary conditions of optimality (NCO) is presented. Motivated to counter the pragmatic limitations of implementing the optimal control policies in presence of plant-model mismatch, measurement-based optimization (MBO) schemes that bypass the necessity of repetitive online optimization for real-time control for semi-batch antisolvent crystallization processes is explored in this study. Traditional neighboring extremal (NE) controller is employed for tracking the interior arcs resulting from the dissection of the nominal input profile. Simulation results show that the performance of the NE controller is comparable to the

MPC formulation. Furthermore, it has been shown that the NCO tracking based control adapts to shifts in solubility curves better than the C-control strategy and delivered a maximum performance improvement of 51.2% over the conventional C-control strategy. However, it still suffers from the issue concerning the change in active constraint set in presence of certain deviations in the model parameters.

Finally, understanding the shortcomings of the NCO tracking control, the feedback law of the traditional NE controller design is reformulated by incorporating the input sensitivities with respect to parameter deviations. A comparative study shows that the reformulated NE controller delivers a maximum improvement of 61.3% over the direct design C-control strategy and thus minimizes the loss in optimality to a much greater extent. Therefore, it is an attractive option for the real time optimal control of semi-batch antisolvent crystallization processes.

List of Tables

3.1	Parameters used in the model.	34
3.2	Different dynamics of the process.	48
3.3	Comparison between direct design and optimal C-control strategies.	48
3.4	Comparative study between proposed design and optimal C-control.	51
4.1	Comparison between optimal adaptive C-control strategy based on equidistant linear and geometric progression spacings.	72
4.2	Comparison between proposed design, optimal and nominal adaptive C-control strategies.	78
5.1	Case studies considered in Chapter 5.	100
5.2	Product quality (in μm) obtained by various controller design methods.	100
6.1	Product quality values (in μm).	118

List of Figures

1.1	Thesis organization.	8
2.1	Solubility diagram.	11
2.2	Nucleation mechanisms, adopted from (Mullin, 2001).	13
2.3	Factors affecting the evolution of crystal size distribution.	19
3.1	Concentration control strategy for antisolvent crystallization processes (Zhou et al., 2006).	34
3.2	Proposed integrated data-based framework.	41
3.3	Illustration of five batches of nominal process data used to construct reference database for the JITL method.	53
3.4	Illustration of ten batches of nominal process data used for validation of the JITL method.	54
3.5	Validation results for the JITL modeling method for nominal condition.	55
3.6	Validation results for the LSSVR inner relationship based MPLS model for nominal condition.	55
3.7	Performance of the proposed design, optimal, and direct design C-control for nominal conditions.	56
3.8	Performance of the proposed design, optimal, and direct design C-control for Case 1.	57

3.9	Performance of the proposed design, optimal, and direct design C-control for Case 2.	58
3.10	Performance of the proposed design, optimal, and direct design C-control for Case 3.	59
3.11	Performance of the proposed design, optimal, and direct design C-control for Case 4.	60
4.1	Adaptive concentration control strategy.	65
4.2	Advancing window MPCA.	67
4.3	Proposed data-based modeling framework for online application. . .	69
4.4	Illustration of equidistant linear and geometric progression spacing methods for CVP of relative supersaturation setpoint profile.	71
4.5	Response of geometric progression and equidistant spacing based adaptive C-control strategy for Case 1.	73
4.6	Response of geometric progression and equidistant spacing based adaptive C-control strategy for Case 2.	73
4.7	Response of geometric progression and equidistant spacing based adaptive C-control strategy for Case 3.	74
4.8	Response of geometric progression and equidistant spacing based adaptive C-control strategy for Case 4.	74
4.9	Parameters characterizing the nominal antisolvent flowrate profile. .	75
4.10	Illustration of twenty five batches of nominal process data used to construct reference database for the JITL method.	79
4.11	Illustration of eight batches of nominal process data used for validation of the JITL method.	80
4.12	Validation results for the JITL modeling method for solute concentration predictions for nominal condition.	81

4.13	Validation results for the JITL modeling method for number of crystals predictions for nominal condition.	82
4.14	Validation results for the LSSVR inner relationship based MPLS model for nominal condition.	82
4.15	Performance of the proposed design, optimal, and nominal adaptive C-control for Case 1.	83
4.16	Performance of the proposed design, optimal, and nominal adaptive C-control for Case 2.	84
4.17	Performance of the proposed design, optimal, and nominal adaptive C-control for Case 3.	85
4.18	Performance of the proposed design, optimal, and nominal adaptive C-control for Case 4.	86
5.1	Optimal antisolvent mass percent and flowrate profiles for nominal case.	98
5.2	Neighboring extremal controller gain, $K(t)$	99
5.3	Response of various control strategies for Case 1.	104
5.4	Response of various control strategies for Case 2.	104
5.5	Response of various control strategies for Case 3.	105
5.6	Response of various control strategies for Case 4.	105
5.7	Response of various control strategies for Case 5.	106
5.8	Response of various control strategies for Case 6.	106
5.9	Response of various control strategies for Case 7.	107
6.1	Neighboring extremal controller gain corresponding to state feedback, $K_x(t)$	116
6.2	Neighboring extremal controller gain corresponding to model parameter deviations, $K_\theta(t)$	117
6.3	Response of various control strategies for Case 1.	120

6.4	Response of various control strategies for Case 2.	120
6.5	Response of various control strategies for Case 3.	121
6.6	Response of various control strategies for Case 4.	121
6.7	Response of various control strategies for Case 5.	122
6.8	Response of various control strategies for Case 6.	122
6.9	Response of various control strategies for Case 7.	123

Nomenclature

a	Activity of solute in supersaturated solution
a_{eq}	Activity of solute in saturated solution
a_p, b_p, c_p	Coefficients of the parabolic distribution of the initial seed loading
α_i	Lagrange multipliers in the LSSVM formulation
$\alpha_1^k, \alpha_2^k, \beta_1^k,$	Model coefficients of the JITL based ARX model at the k th sampling instant
$\alpha_C, \alpha_n, \beta_C, \beta_n$	Model coefficients of the JITL based ARX model for predicting solute concentration and number of crystals
B	Diagonal coefficient matrix of PLS model
B	Nucleation rate, no. of particles/ m^3 s
B_{hom}	Homogenous nucleation rate, no. of particles/ m^3 s
B_0	Pre-exponential factor of the homogenous nucleation rate, no. of particles/ m^3 s
b	Nucleation order
b'	Perturbed nucleation order
C	Solute concentration, $gm_{solute}/ gm_{solvent}$
C_{sat}	Solubility, $gm_{solute}/ gm_{solvent}$
C'_{sat}	Perturbed solubility, $gm_{solute}/ gm_{solvent}$
C_k^{set}	Solute concentration setpoint at k th instant, $gm_{solute}/ gm_{solvent}$
$\hat{C}(k)$	Predicted solute concentration at k th instant, $gm_{solute}/ gm_{solvent}$

ΔC	Supersaturation, $\text{gm}_{\text{solute}} / \text{gm}_{\text{solvent}}$
d	The number of discretized points
$\delta(\cdot)$	Dirac delta function
E, F	Residual matrices
e	Error vector
F	State dynamics function
G	Growth rate, m/ s
ΔG_{crit}	Activation energy for the formation of a spherical nuclei of critical size in a supersaturated solution, J/ mol
g	Growth order
g'	Perturbed growth order
γ	Activity coefficient of solute in supersaturated solution
γ_{eq}	Activity coefficient of solute in saturated solution
γ_{sl}	Interfacial energy between solid and liquid phases, J/ mol m ²
H	Hamiltonian function
h_r	Residual vector corresponding to the inner relationship of the r th latent variable in LSSVR-based MPLS model
J	Scalar cost function
\mathcal{J}_P	Cost function in the LSSVM formulation
$K(\cdot, \cdot)$	Kernel function
$K(t)$	Neighboring extremal controller gain at time t
$K_C(t)$	Neighboring extremal controller gain corresponding to the state C at time t
$K_{\mu_0}(t)$	Neighboring extremal controller gain corresponding to the state μ_0 at time t
$K_{\mu_1}(t)$	Neighboring extremal controller gain corresponding to the state μ_1 at time t

$K_{\mu_2}(t)$	Neighboring extremal controller gain corresponding to the state μ_2 at time t
$K_{\mu_3}(t)$	Neighboring extremal controller gain corresponding to the state μ_3 at time t
$K_{\mu_4}(t)$	Neighboring extremal controller gain corresponding to the state μ_4 at time t
$K_{\theta}(t)$	Reformulated vector of neighboring extremal controller gain corresponding to the model parameter deviations at time t
$K_{\theta,b}(t)$	Reformulated neighboring extremal controller gain corresponding to the model parameter b at time t
$K_{\theta,C_{sat}}(t)$	Reformulated neighboring extremal controller gain corresponding to the model parameter C_{sat} at time t
$K_{\theta,g}(t)$	Reformulated neighboring extremal controller gain corresponding to the model parameter g at time t
$K_{\theta,k_b}(t)$	Reformulated neighboring extremal controller gain corresponding to the model parameter k_b at time t
$K_{\theta,k_g}(t)$	Reformulated neighboring extremal controller gain corresponding to the model parameter k_g at time t
$K_x(t)$	Reformulated vector of neighboring extremal controller gain corresponding to the state deviations at time t
$K_{x,C}(t)$	Reformulated neighboring extremal controller gain corresponding to the state C at time t
$K_{x,\mu_0}(t)$	Reformulated neighboring extremal controller gain corresponding to the state μ_0 at time t
$K_{x,\mu_1}(t)$	Reformulated neighboring extremal controller gain corresponding to the state μ_1 at time t
$K_{x,\mu_2}(t)$	Reformulated neighboring extremal controller gain

	corresponding to the state μ_2 at time t
$K_{x,\mu_3}(t)$	Reformulated neighboring extremal controller gain corresponding to the state μ_3 at time t
$K_{x,\mu_4}(t)$	Reformulated neighboring extremal controller gain corresponding to the state μ_4 at time t
k_b	Nucleation constant, no. of particles/ $\text{m}^3 \text{ s}$
k'_b	Perturbed nucleation constant, no. of particles/ $\text{m}^3 \text{ s}$
k_g	Growth constant, m/ s
k'_g	Perturbed growth constant, m/ s
k_{min}, k_{max}	Minimum and maximum number of relevant data
k_v	Shape factor
κ	Weight parameter
L	Integral cost function
L, L_0, L_s	Characteristic length of the solute, nuclei and seed crystals, m
L_j	The j th characteristic length of the solute crystals, m
$L_{s,initial}, L_{s,final}$	Minimum and maximum sizes of the seeds, m
$L_{s,mean}, L_{s,s.d}$	Mean and standard deviation of seed crystal size distribution, m
λ	Adjoint state vector
Λ^{set}	Relative supersaturation setpoint
M_{seed}	Seed mass, gm
$M_{solvent}$	Solvent mass, gm
$M_{solute,k}, M_{w,k}$	Mass of solute and antisolvent at k th sampling instant, gm
$\dot{M}_{w,k}$	Antisolvent flowrate at k th sampling instant, gm/ s
m_w	Antisolvent mass percent in the crystallizer
$m_{w,k}$	Antisolvent mass percent setpoint at k th sampling instant
μ_i	The i th moment of the crystal size distribution
μ_l	Chemical potential of the dissolved component to be

	precipitated from the solution, J/ mol
μ_s	Chemical potential of solid phase, J/ mol
μ^L, μ^U	Lagrange multipliers
$\Delta\mu$	Difference in chemical potential, J/ mol
n	Number density of the solute crystals, no. of particles/ m ³ m
n_c, \hat{n}_c	Actual and predicted number of the solute crystals, no. of particles
$n_{c,max}$	Maximum number of the solute crystals, no. of particles
np	Number of principal components
P, Q	Loading matrices
P	Product quality vector
P_{yield}	Product quality in terms of product yield
P_{size}	Product quality in terms of volume weighted mean size of product crystals, μm
\hat{P}	Predicted product quality vector using LSSVR-MPLS model
p_r	r th loading vector
Φ	Terminal cost function
Ψ	Least squares support vector regression inner relationship based multiway partial least squares model
R	Number of latent variables retained in the MPLS model
r_c	Radius of the critical nucleus, m
ρ_c	Crystal density, kg/ m ³
$S_r(\cdot)$	LSSVR model corresponding to the inner relationship of the r th latent variable
s_i	Similarity measure
σ	Scaling constant in RBF kernel function

\mathbf{T}, \mathbf{U}	Score matrices
T	Temperature of the solution, K
t_f	Final batch time, s
t_r, u_r	Vector of r th latent variable in the MPLS model
t_s	Sampling time, s
$t_{s,i}$	The i th switching time, s
θ_b, θ_g	Nucleation and growth kinetic parameters of solute crystals
$\Delta\theta_i$	Perturbation in the i th model parameter
$\Delta\theta_6$	Perturbation in the initial conditions of the states
$\delta\theta_i$	Deviation in the i th model parameters
u^L, u^U	Lower and upper bounds for process inputs
u_k	Process inputs at the k th sampling instant
$u^*(t), x^*(t), \lambda^*(t)$	Nominal input, state and adjoint state vectors at time t
$\delta u(t)$	Correction in the input from its nominal value at time t
$V(t)$	Volume of the solution in the crystallizer at time t , ml
V_m	Molar volume of the solute, m ³ /mol
V_{max}	Maximum volume of the crystallizer, ml
w, α_i, b	Parameters of the LSSVR model
X, Y	Process variable and product quality data matrices
X_p	Input vector to the LSSVR-MPLS model
$\mathbf{x}_k, \mathbf{x}_q$	Regression and query vector for the ARX model
x_k	System states at the k th sampling instant
$x_{f,new}, x_{p,new}$	Vector of future and past proces data for the new batch
$\delta x(t)$	Deviation in the states from the nominal values at time t
Y_{class}	Output data matrices for multi-class classification
y_k	Process variable at the k th sampling instant
\hat{y}_k	Predicted process variable at the k th sampling instant

Abbreviations

API	Active pharmaceutical ingredient
ARX	Autoregressive model with exogenous inputs
ATR-FTIR	Attenuated total reflectance fourier transform infrared
BVI	Bulk video imaging
C-control	Concentration control
CLD	Chord length distribution
CMR	Conditional mean replacement
CSD	Crystal size distribution
CVP	Control vector parameterization
DoDE	Design of dynamic experiments
DoE	Design of experiments
FBRM	Focused beam reflectance measurement
F-control	Flowrate control
JITL	Just in time learning
KKT	Karush-Kuhn-Tucker
<i>k</i> -NN	<i>k</i> -Nearest neighborhood
LSSVM	Least squares support vector model
LSSVR	Least squares support vector regression
LSSVR-MPLS	Least squares support vector regression based multiway partial least squares
MPC	Model predictive control

MPCA	Multiway principal component analysis
MPLS	Multiway partial least squares
MSZW	Metastable zone width
NCO	Necessary conditions of optimality
NE	Neighboring extremal
ODE	Ordinary differential equation
PBE	Population balance equation
PCA	Principal component analysis
PCR	Principal component regression
PD	Proportional-derivative
PDE	Partial differential equation
PLS	Partial least squares
PMP	Projection to the model plane
PVM	Particle vision and measurement
RBF	Radial basis function
RMSE	Root mean squared error
RS	Relative supersaturation
SCP	Single component projection
SPC	Statistical process control
SS	Supersaturation

Chapter 1

Introduction

1.1 Motivation

Crystallization is one of the oldest unit operations known to mankind and finds its utilization in the industries for production, purification and recovery of solid material. It is the process of formation of orderly repeating three dimensional molecular array called solid phase crystals, when an ensemble of randomly organized atoms, molecules, or ions in the liquid phase come together (Mullin, 2001). In the production of active pharmaceutical ingredients (APIs), (semi-)batch crystallization operations are widely employed to facilitate the purification of slurry by solid-liquid separation technique and isolation of chemical species from mixtures of reaction products.

Antisolvent crystallization, also referred as salting out or drowning out crystallization, is one of the modes of operating the crystallization process. Other common modes include temperature cooling, reactive, pH shift, evaporative, and some hybrid methods like combined cooling and antisolvent modes. Antisolvent crystallization draws significant importance in pharmaceutical manufacture, as majority of the APIs are thermally labile. Furthermore, as cooling mode is often inadequate to generate high supersaturation that is required for crystal formation, antisolvent

addition is a preferred mode of pharmaceutical crystallization. However, in the absence of tight control, the obvious disadvantage of this process is the necessity to introduce additional solvent(s), which reduces the volumetric productivity and creating a solvent mixture requiring additional separation for solvent recovery (Tung et al., 2009). Thus, the scope and necessity of providing better control for antisolvent addition mode strongly motivates the current research work.

During the crystallization process, control of final crystal size distribution (CSD) becomes critical as it determines the operational efficiency of the other downstream operations like drying, filtration and milling. Furthermore, the product quality, signified by CSD, morphology, purity, crystal habit and surface structure, also influence the flow behavior, particle adsorption, shelf-life of the final product, bioavailability and the controlled drug delivery mechanism (Higuchi and Hiestand, 1963, Kim et al., 2005, Shekunov et al., 2007). Often, the product CSD is directly linked to the efficiency and profitability of the process. Hence, given its widespread use in the industries, better monitoring and optimal control of crystallization processes is of paramount importance.

Consistency in the product specifications is very important to be controlled as it dictates the bioperformance and the suitability of the manufactured drug for its intended use. In the pioneering work on control of batch crystallizers, it has been shown that keeping the supersaturation constant and operating below the metastable zone limit during a crystallization operation is arguably optimal (Mullin and Nyvlt, 1971, Jones, 1974, Nyvlt, 1992). However, until the recent past, much of the industrial semi-batch crystallization operations were recipe-based, where the initial seed loading and the antisolvent addition policies were determined using either trial-and-error procedure or optimizing certain objective function using an offline model. The resulting policies were then implemented using time dependent setpoints for the entire batch duration of the *real process*. This method is not only time consuming and computationally expensive in certain situations, but also very sensitive to modeling

errors.

Thus, recognizing the dearth and importance of efficient and innovative approaches for pharmaceutical development, manufacturing and quality assurance in the industries, the United States Food and Drug Administration (FDA) designed a regulatory framework Process Analytical Technology (PAT) for helping the manufacturers in providing guidance concerning anticipated technical and regulatory issues (FDA, 2004). With recent developments in the sensor technology enabling *in situ* process measurements relevant to online monitoring and control of pharmaceutical processes, application of PAT tools are drawing attention both in industrial and academic research (Togkalidou et al., 2001b, Yu et al., 2004, Howard et al., 2009, Simon et al., 2009a, 2010). For instance, model-free direct design approaches like supersaturation/ concentration control (C-control) and direct nucleation control strategies, which use solute concentration and *in situ* chord length distribution, respectively, as feedback variable have been developed (Patience and Rawlings, 2001, Woo et al., 2009). These approaches were found to be less sensitive to process disturbances and variations due to their closed-loop nature. However, the direct design approaches suffer from being operated at the sub-optimal regions, as they completely rely on process understanding and finding reference signals by trial-and-error (Zhou et al., 2006). Furthermore, these strategies have varying batch times, which may sometimes pose as a bottleneck for the smooth large-scale operations and even lead to batch-to-batch variability, if not adapted after each run. In the case of C-control strategy, even though the process is operated in a robust fashion, the control actions are based on solute concentration measurements. However, the true process variable to be controlled during the process is the CSD. Hence, optimal control strategies based on the feedback of CSD measurements are important as they steer the process to obtain the desired product specifications (Patience and Rawlings, 2001, Zhou et al., 2006).

Hojjati et al. (2007) and Sheikhzadeh et al. (2008a) demonstrated the applica-

tion of multivariable feedback controllers using fuzzy logic, rigid logic, and neuro-fuzzy techniques and *in situ* measurements of supersaturation and difference in chord lengths of fine particles for real-time control of semi-batch antisolvent crystallization processes. However, tuning the rules and membership functions for the fuzzy and neuro-fuzzy controllers could be tedious. Moreover, analysis on the robustness of these studies under the presence of process variations and disturbances were lacking. Real-time optimal control of semi-batch antisolvent crystallization process has been recently demonstrated through experimental implementation (Sheikhzadeh et al., 2008b). However, the required computational effort is demanding because it involves repetitively solving the optimal control formulation, which renders being unattractive for control of (semi-)batch processes.

As can be inferred, despite many efforts to address the control of pharmaceutical (semi-)batch crystallization processes, there still remains room for improvement in terms of better control strategies that are robust towards process variations (Nagy et al., 2008a). Besides, due to its nature of being both thermodynamically and kinetically dependent, crystallization process has been posing challenging and interesting problems that gained considerable interest among process design and control engineers over the past decade (Rohani et al., 2005a,b). Moreover, with less awareness about the process in industrial practice and prohibitively compromised application of control techniques for the highly complex process, the issues with the control of crystallization processes for obtaining optimal product CSD are not yet addressed effectively. Thus, motivated to circumvent these issues, the following contributions are made through this thesis.

1.2 Contributions

Recognizing the necessity of control strategies that ensure optimal product quality even in presence of process variations and disturbances in semi-batch antisolvent

crystallization processes, this thesis aims to provide solutions using the principles of process systems engineering. The key contributions of this thesis are summarized as follows:

1. Although direct design approaches were found to be relatively less sensitive to process variations due to their closed-loop nature, they suffer from being operated in sub-optimal manner because the relevant design parameters, for example supersaturation setpoints for C-control are determined by trial-and-error procedure from the plant tests which require considerable engineering efforts. Hence, development of alternative methods based on the available historical process data to determine the supersaturation setpoints for optimal control of antisolvent crystallization processes is crucial to steer the process to obtain the desired product specifications (Zhou et al., 2006, Woo et al., 2009, Nagy and Braatz, 2012). Thus, in order to alleviate the aforementioned limitations, a new modeling framework that integrates pattern classification and nonlinear process modeling methods is developed in this study. To the authors' knowledge, the idea of integrating pattern classification and nonlinear process modeling for determining setpoint values for optimal operation has not been considered in the literature for the application of crystallization processes. Moreover, the study tries to bring in the tools from machine learning concepts that work efficiently even when the available data is limited.
2. As discussed in the previous section, the cascade control strategy is robust towards shifts in the solubility curve. However, longer batch time is often required to meet the pre-specified control objective, for example batch time is extended from two hours to almost seven hours (Woo et al., 2009). Hence, implementing this strategy could possibly pose as a bottleneck in the smooth operation of the downstream processing. To lessen this drawback, the integrated modeling framework developed in the previous study is used

to adaptively tune the relative supersaturation setpoints based on the online solute concentration and CSD measurements. Therefore, inspired by the idea of model predictive control for real-time optimal control of semi-batch antisolvent crystallization processes, the current study develops a systematic approach for the adaptive C-control strategy to achieve better control performance.

3. Measurement based optimization schemes for real-time control of the semi-batch antisolvent crystallization processes is developed in this thesis. Specifically, a NCO tracking based control strategy is employed for optimal operation of this process even in presence of plant-model mismatch. In order to track the interior (sensitivity seeking) arcs, a Neighboring Extremal (NE) controller is designed. To evaluate control performance of proposed design, a comparative study is presented to illustrate that NCO tracking based control delivers better performance than those obtained by the nominal optimal control, C-control, and model predictive control strategies.
4. Model Predictive Control (MPC) and its first order approximation, the Neighboring Extremals (NE), have been used for real-time optimal control in presence of model uncertainties. Traditionally, both MPC and NE would only correct for deviations in states considering the underlying model to be nominal – a procedure that is valid for additive disturbances. However, in presence of model uncertainties, it has been shown that MPC scheme or NE controller could cause corrections in the wrong direction, thereby deteriorating the performance. This finding motivated the proposed research to address the reformulation of NE feedback by considering sensitivities with respect to the model parameters. The feedback then has two components – one based on state deviations and the other based on parameter deviations. Simulation results shows the efficacy of this approach and the importance of incorporating

the knowledge of parameter variations in real-time optimal control.

1.3 Thesis organization

The thesis is organized as follows. Chapter 2 provides the background information on the fundamentals of crystallization and literature review on the recent developments in the control of semi-batch antisolvent crystallization processes. Chapter 3 presents the proposed integrated data-based methodology, which is incorporated into the existing C-control strategy to achieve better control performance. The adaptive C-control strategy is then discussed in Chapter 4. The measurement based optimal control strategies for semi-batch antisolvent crystallization processes using Necessary Conditions of Optimality based tracking control, along with the design and application of neighboring extremal control are discussed in chapters 5 and 6. Figure 1.1 presents the schematic representation of the control strategies developed in the thesis. Finally, the conclusion and potential topics that warrant further research are briefly discussed in Chapter 7.

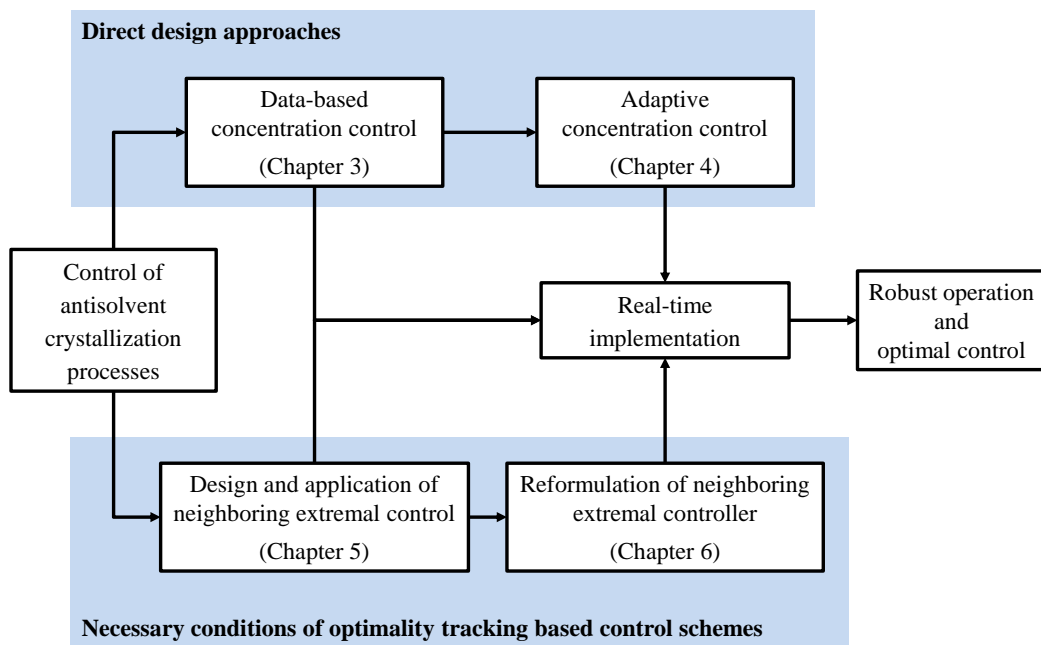


Figure 1.1 Thesis organization.

Chapter 2

Literature Review

This chapter presents a brief review on the fundamentals of crystallization process, including the definition for supersaturation, kinetic mechanism and rates, and crystal size distribution. Subsequently, recent developments on the control of semi-batch antisolvent crystallization processes are reviewed.

2.1 Fundamentals of crystallization

Solution crystallization is the process of formation of orderly repeating three dimensional molecular array called solid phase crystals, when an ensemble of randomly organized atoms, molecules, or ions in the liquid phase come together. Crystallization is one of the oldest unit operations known to mankind and finds its utilization in the industries for production, purification and recovery of solid material. During the drug manufacture, crystallization is not only used for the purification and separation of the drug molecules from the solution, but also helps in providing a product with many desirable properties, which ultimately determine the efficiency of other downstream operations and the efficacy of the drug (Shekunov and York, 2000, Mullin, 2001).

For a better understanding of the crystallization process, the key elements which

influence the crystallization process are discussed in the following sections.

2.1.1 Driving force for crystallization

Crystallization, like any chemical rate process, is kinetically driven by the concentration. However, the concentration range over which the process occurs is limited by the equilibrium behavior of the system corresponding to the chosen conditions. In thermodynamic viewpoint, crystallization takes place only if the chemical potential of the solid phase μ_s is less than that of the dissolved component to be precipitated from the solution μ_l , making the difference in the chemical potential $\Delta\mu$ the true driving force for the process.

$$\Delta\mu = \mu_l - \mu_s = kT \ln \frac{a}{a_{eq}} = kT \ln \frac{\gamma C}{\gamma_{eq} C_{sat}}, \quad (2.1)$$

where T represents temperature of the solution, a and a_{eq} represent the activities in supersaturated and saturated solution, C and C_{sat} represent solute concentration, and solubility, and γ/γ_{eq} represent the activity coefficient ratio. However, the most common representation for the driving force for crystallization is considered to be supersaturation, SS , defined as

$$SS = \Delta C = C - C_{sat}, \quad (2.2)$$

or, the relative supersaturation, RS , given by

$$RS = \frac{C - C_{sat}}{C_{sat}} = \frac{\Delta C}{C_{sat}}, \quad (2.3)$$

where ΔC represents supersaturation.

Figure 2.1 shows a hypothetical solubility curve for a solute in solvent-antisolvent mixture. The most fundamental knowledge and indispensable requirement for understanding the crystallization process of any compound is its solubility behavior

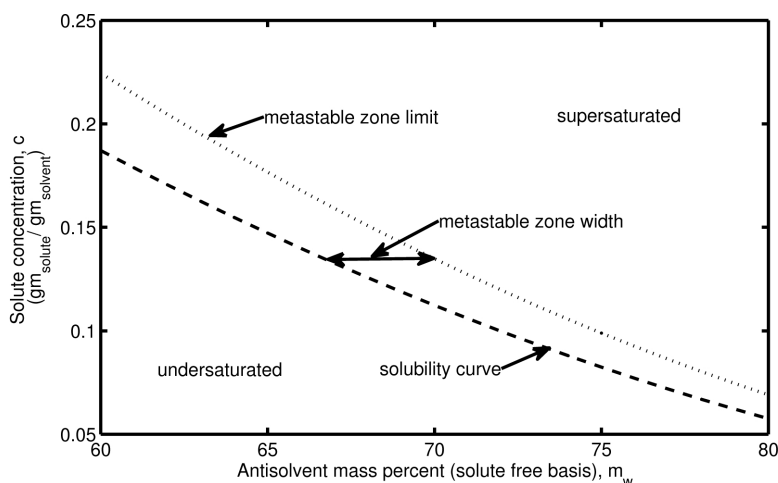


Figure 2.1 Solubility diagram.

in the solvent mixture. Often, it is also termed as saturation or equilibrium concentration. The regions above and below the saturation concentration are termed as supersaturation and undersaturation respectively. If the solution is supersaturated, .i.e. the amount of dissolved solute in the solution is greater than the saturation concentration, then the crystals can nucleate and grow. Hence, generation of supersaturation is mandate for crystallization.

In general, supersaturation can be generated in different ways such as temperature cooling, antisolvent addition, reaction, evaporation, pH shift and also by some hybrid modes*. Usually, but not limited only to the control of the process, these modes of supersaturation generation have their own unique advantages and limitations. For a given system, the degree of supersaturation generated during the process and the product quality towards the end of the batch depend largely on the specific mode as it influences both the thermodynamic and kinetics relationships of the process. This means, for instance during antisolvent crystallization, the solubility and the kinetics of crystal nucleation and growth are highly complex functions of both antisolvent mass percent (on solute free basis) and supersaturation.

The region above the solubility curve is known as the metastable zone. In this

*Combined cooling and antisolvent addition mode has received attention recently.

region, growth of the existing crystals is usually observed, but the nucleation of the solute crystals is difficult to occur in this condition. However, spontaneous nucleation takes place once the solute concentration exceeds the metastable limit. The time elapsed between the creation of supersaturation and formation of a new detectable solid phase is called induction time. Induction time measurements are important in elucidating the possible nucleation and growth mechanisms. As the prime motivation for most of the studies on the crystallization of various compound systems is to obtain consistent and uniform CSD, understanding the underlying mechanisms of nuclei formation and its growth is critical.

2.1.2 Nucleation

Nucleation is defined as the process of creating a new solid phase from supersaturated homogeneous phase. Supersaturation alone forms only a part of the necessary condition for a system to begin to crystallize. Before crystals can develop, a number of minute solid bodies, embryos, nuclei or seeds must exist in the solution which act as potential sites for crystallization and growth. Depending on the source of the nuclei formation, the nucleation mechanisms for the generation of these active sites can be classified into two main categories as primary and secondary nucleation as shown in Figure 2.2. The term primary nucleation describes the formation of new crystals directly from the homogeneous liquid phase, while secondary nucleation requires the presence of suspended solute crystals. Primary nucleation occurs usually at elevated supersaturation levels and is generally further classified as homogeneous, which occurs in pure bulk solution, and heterogeneous, which is induced due to the presence of foreign particles. Extensive studies and reviews on nucleation mechanism of different inorganic and organic compounds have been carried out during the past (Mahajan and Kirwan, 1994, Nyvlt, 1985).

Classical theory of homogeneous nucleation stems from the work of Gibbs

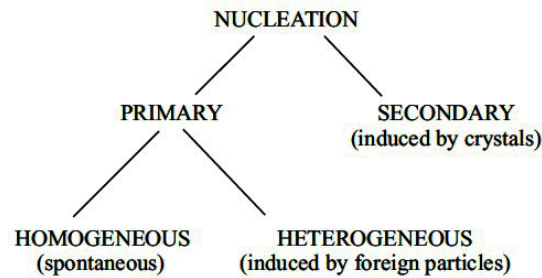


Figure 2.2 Nucleation mechanisms, adopted from (Mullin, 2001).

(1948), Volmer (1939), Becker and Döring (1935) and others, which states that if a solution is supersaturated, clusters of solute molecules are formed in the solution by an addition mechanism that may continue until a critical size is reached (Mullin, 2001), during which the free energy reaches maximum. Once the size of the cluster exceeds the critical size, the free energy decreases with further growth, leading to spontaneous nucleation. However, under industrial conditions, the formation of nuclei through homogeneous nucleation mechanism is highly unlikely due to the high supersaturation levels required.

Presence of impurities can act as both nucleation inhibitor and accelerator. The heterogeneous nucleation can occur at supersaturation level lower than that required for homogeneous nucleation and is, therefore, the dominant mechanism of primary nucleation when impurities are present. Classical theory suggests that primary heterogeneous nucleation is characterized by a process that is either starved of nuclei or overwhelmed by a burst of new crystals, making the CSD control difficult (Nyvlt, 1985).

The rate of formation of nuclei by primary nucleation mechanism is given by an Arrhenius-type relation as,

$$B_{hom} = B_0 \exp\left(-\frac{\Delta G_{crit}}{kT}\right), \quad (2.4)$$

where B_0 is called the pre-exponential factor and ΔG_{crit} is the activation energy

for nucleation associated with the formation of a spherical nuclei in a supersaturated solution defined as

$$\Delta G_{crit} = \frac{4\pi r_c^2 \gamma_{sl}}{3}, \quad (2.5)$$

where r_c is the radius of the critical nucleus and the γ_{sl} is the interfacial energy between the solid and liquid. The Kelvin equation gives the relation between the critical size and the prevailing supersaturation as

$$r_c = \frac{2\gamma_{sl}V_m}{\Delta\mu}, \quad (2.6)$$

where V_m is the molar volume of the solute.

Thus, assuming spherical nuclei are formed and combining Eqs. (2.1), (2.4), (2.5) and (2.6), the equation for the rate of nucleation is given as

$$B_{hom} = B_0 \exp \left[\frac{-16\pi\gamma_{sl}^3 V_m^2}{3k^3 T^3 \ln^2(a/a_{eq})} \right]. \quad (2.7)$$

Nevertheless, for most of the engineering applications the following semi-empirical power law is commonly used for describing the rate of primary nucleation.

$$B = k_b \Delta C^b, \quad (2.8)$$

where k_b and b represent the nucleation kinetic parameters.

Secondary nucleation takes place because of the suspended solute particles in the solution. Among the many possible mechanisms described under the class of secondary nucleation, the three main categories include, "apparent", "true" and "contact". Apparent secondary nucleation refers to small fragments washed from the surface of seeds when they are introduced into the crystallizer. True secondary nucleation occurs when the current level of supersaturation is higher than the critical level for the solute particles present in solution. Contact secondary nucleation

occurs when a growing particle contacts the walls of the container, the stirrer, the pump impeller, or other particles thus leaving behind residual solute particles. However, the contact secondary nucleation is the most common mechanism experienced in industrial practice (Dirksen and Ring, 1991, Myerson, 2002).

2.1.3 Crystal growth

Soon after the size of the nuclei crosses the critical radius in the supersaturated solution, they begin to grow into crystals of visible size. The mechanism of crystal growth from solution involves two critical successive steps – diffusional step, during which the solute particle migrates across the surface to find energetically favorable incorporation sites, followed by the surface integration step, during which the desolvation, surface diffusion over the crystal surface and sequential addition of units takes place (Randolph and Larson, 1971, Granberg and Rasmuson, 2005). Thus, surface adsorption and diffusion determine whether an incoming solute molecule is incorporated into the crystal or returns to the bulk phase (Rawlings et al., 1993).

Several attempts have been made to explain the mechanisms and rate of crystal growth and are classified broadly into three categories as:

1. Surface energy theory (Gibbs, 1878 and Curie, 1885)
2. Diffusion theory (Noyes and Whitney, 1897 and Nernst, 1904)
3. Adsorption layer theory (Volmer, 1922)

Based on the surface energy theory, a growing crystal assumes the shape which has minimum surface energy. Though not completely abandoned, this theory has largely fallen into disuse. The diffusion theory postulates that the matter is deposited continuously on crystal face at a rate proportional to the concentration gradient between the point of deposition and bulk of the solution. The adsorption layer theory

suggests that the crystal growth is a discontinuous process, taking place layer-by-layer through adsorption on the crystal surface (Mullin, 2001).

Most of the literature treats the growth kinetics with a semi empirical power law, which has now become the standard representation.

$$G = k_g \Delta C^g, \quad (2.9)$$

where k_g and g represent the growth kinetic parameters.

2.1.4 Role of solvent composition on the precipitation kinetics

Earlier works on salting out crystallization suggested the dependence of the kinetic parameters on the solvent composition (Nyvlt, 1992), which was further substantiated by several other researchers (Granberg et al., 2001, Nowee et al., 2008a, Trifkovic et al., 2008). Based on the interfacial energy, which is the work required in forming a new interface between a solid and a liquid, two theories were postulated in the pursuit of elucidating the role of solvent in precipitation kinetics (Nyvlt, 1985, Davey, 1986, Granberg et al., 2001, Mohan and Myerson, 2002).

The first theory is based on *solid-liquid interactions*, which states that favorable interactions between solute and solvent molecules on specific faces lead to reduced solid-liquid interfacial energy, thereby promoting the rate of nucleation by reducing the activation energy. Besides, roughness of the growing surface is significantly influenced by the solvent composition. Thus, an increase in the solubility leads to enhanced roughness of the crystal surface and thus results in rapid growth.

The second theory that is based on *solute-solvent dissociation* states that, at constant supersaturation, the rate of dissociation of the strongly bound solvent molecules to the surface of the solute molecule determines the nucleation rate due to the strong dependency of the solubility on the interfacial energy. On the other hand, the crystal growth rates are influenced by the specific adsorption of the solvent molecules

at the growing crystal surface and may result in lower growth rates despite a higher solubility.

For antisolvent crystallization of paracetamol in acetone-water mixture system, that is investigated in this thesis, at constant supersaturation, with increasing water composition the nucleation rate decreases due to increasing interfacial energy. Also, the estimated interfacial energy being in the range 1–3 mJ/m², which is much lower than the values predicted for many inorganic compounds, the free energy difference between the crystal surface at the interface to the solution and the crystalline structure in the interior of the crystal is quite low (Granberg et al., 2001). Thus, recognizing the effect of solvent composition, the parameters of the kinetic models for both nucleation and growth rate (k_b , b , k_g and g) are considered to be polynomial functions of antisolvent mass-percent (on solute-free basis).

2.1.5 Crystal size distribution

A vast majority of the APIs manufactured in the pharmaceutical industries are generally crystalline in their form. Typically, during the crystallization process, the size of the solute crystals vary over a wide range and are generally characterized by their crystal size distribution (CSD). The CSD is one of the key specifications, as it affects bulk density, agglomeration, flow/ rheology, and compaction of the product crystals. These physical properties have a direct influence on the efficiency of other downstream processes like filtration, drying and milling operations, that may consequently affect the bioavailability, tablet stability and shelf life of the drug. Hence, the objective of industrial crystallization processes is to meet the specifications on size, shape, purity, and yield of the product crystals, as they determine both the efficiency of the API manufacturing processes and the efficacy of the final intended drug. Thus, CSD has a direct effect on both productivity and profitability of API manufacturing processes (Randolph and Larson, 1971, Rawlings et al., 1992, Yu

et al., 2007).

In presence of supersaturation, the nucleation rate influences the number of newly born crystals, while the growth rate influences the length of the existing crystals. Thus, the evolution of the CSD during the crystallization processes is fueled by the generation of supersaturation. Usually, generation of high supersaturation levels at the inception of the crystallization process is required to generate large number of nuclei through homogenous nucleation, that are then grown to the required size by lowering the supersaturation levels (Randolph and Larson, 1971). However, the size of the nuclei can considerably vary over a wide range when generated through homogenous nucleation and this may have an undesirable effect of the product CSD. Hence, seeded operations have become more popular, where the process is initiated through the addition of fine crystals, called the seeds, that usually have a small variation in their size with a characteristic unimodal distribution (Chung et al., 1999, Hu et al., 2005). Evidently, these operation do not require the generation of high supersaturation and thus can suppress the undesirable nucleation events significantly and promote the growth of existing crystals. Ideally, the product CSD is expected to retain the variance of the seed CSD and only increase in the mean size value. However, formation of fine crystals through heterogenous and secondary nucleation events and the length dependant growth rates can affect the product CSD, which leads to higher variance and in certain scenarios, even to bimodal distribution (Randolph and Larson, 1971, Rawlings et al., 1992). Furthermore, some of the studies have also shown that the CSD of the initial seeds has significant influence on the product CSD (Chung et al., 1999, Hu et al., 2005, Nagy, 2009). Besides, additional factors like breakage, aggregation, agglomeration and fines dissolution also affect the product CSD for certain solute-solvent systems. Figure 2.3 demonstrates the complex interaction of the crystal kinetics with the CSD in the case of antisolvent crystallization processes.

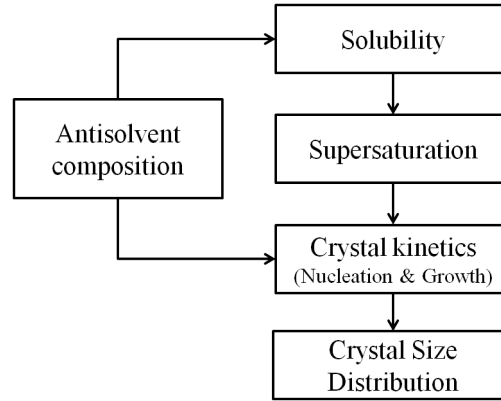


Figure 2.3 Factors affecting the evolution of crystal size distribution.

2.2 Modeling of antisolvent crystallization processes

For the purposes of modeling and control of the crystallization processes, the most common way of representing the process is by using the population balance equation that accounts for the distribution of the crystals of different sizes during the process as function of both time and the characteristic length in different dimensions of the crystal. For the purpose of simplification, crystal agglomeration, growth dispersion, and breakage phenomena are neglected (Qamar et al., 2006). A simplified population balance equation for constant shape factor case is represented as:

$$\frac{\partial n}{\partial t} + \sum_{j=1}^d \frac{\partial}{\partial L_j} G(L_j, C, m_w; \theta_g) n = B(n, C, m_w; \theta_b) \prod_{j=1}^d \delta(L_j), \quad (2.10)$$

where m_w represents the antisolvent mass percent, C represents the solute concentration, n represents the number density of the crystals, L_j is the j^{th} characteristic size of the solute crystal, G is the growth kinetics, B is the nucleation kinetics, δ is the Dirac delta function, while θ_g and θ_b represent the growth and nucleation kinetic parameters respectively.

Further simplification is done by avoiding both the length dependency of the growth kinetics and also the formation of new nuclei by secondary nucleation mechanisms. Thus, in the seeded batch operations, one-dimensional population balance

equation is represented by

$$\frac{\partial n(L, t)}{\partial t} + G(t) \frac{\partial n(L, t)}{\partial L} = B\delta(L). \quad (2.11)$$

The initial seed loading is described using a parabolic distribution given by

$$n(L)|_{t=0} = n(L_s, 0) = \begin{cases} a_p L_s^2 + b_p L_s + c_p, & L_{s,initial} \leq L_s \leq L_{s,final} \\ 0, & \text{otherwise} \end{cases}, \quad (2.12)$$

$$\begin{aligned} L_{s,initial} &= L_{s,mean}(1 - L_{s,s.d}), \\ L_{s,final} &= L_{s,mean}(1 + L_{s,s.d}), \end{aligned} \quad (2.13)$$

where $L_{s,mean}$ is the mean size of the seeds, $L_{s,s.d}$ is the standard deviation in the seed distribution and the coefficients a_p , b_p and c_p are determined based on the seed mass M_{seed} . The method of moments transforms the hyperbolic partial differential equation represented by the population balance equation in Eq. (2.11) into a set of ordinary differential equations called the moment equations. Given L_0 to be the crystal size at nucleation, the moment equations defined on a per mass of solvent basis are obtained as follows (Hulburt and Katz, 1964)

$$\frac{d\mu_i}{dt} = iG\mu_i + BL_0^i, \quad i = 0, 1, 2, \dots \quad (2.14)$$

where μ_i denotes the i th moment of the CSD defined as

$$\mu_i = \int_0^{\infty} L^i n(L, t) dL, \quad i = 0, 1, 2, \dots \quad (2.15)$$

The mass balance equation for obtaining the solute concentration is given as

$$\frac{dC}{dt} = -3\rho_c k_v G(t) \mu_2(t) - \rho_c k_v B(t) L_0^3, \quad (2.16)$$

where ρ_c is the crystal density and k_v is the shape factor of the crystals.

In seeded operations, with the consideration that the nucleation takes place at negligible crystal size, i.e., $L_0 \lll L_{s,mean}$, Eq. (2.14) reduces to the following set of equations.

$$\begin{aligned}\frac{d\mu_0}{dt} &= B, \\ \frac{d\mu_i}{dt} &= iG\mu_{i-1}, \quad i = 1, 2, \dots \\ \frac{dC}{dt} &= -3\rho_c k_v G(t) \mu_2(t).\end{aligned}\tag{2.17}$$

Therefore, by integrating the above set of ordinary differential equations over time, the corresponding moments of the CSD throughout the batch time are obtained.

2.3 Recent advances in control of antisolvent crystallization processes

To achieve a better control of the crystallization process, a clear understanding of the solubility behavior, nucleation and growth mechanisms of the given system is fundamentally necessary. Hence, there have been studies carried out on a wide range of topics, specifically on crystal growth and nucleation mechanisms of various organic and inorganic molecules (Nyvlt, 1968, 1985). In the case of antisolvent crystallization, the effect of solvent composition on these kinetics and solubility behavior are however less pronounced in the literature. Moreover, apart from these kinetics, the agglomeration and aggregation mechanisms also affect the content uniformity and stability of the final product (Alander and Rasmuson, 2005, Yu et al., 2005). Furthermore, the other subsidiary mechanisms like fines dissolution, growth dispersion, and crystal breakage effects aggravate the issues concerning the control of final CSD. However, these mechanisms are often less understood and the mathe-

mathematical models developed are mostly empirical in nature due to the lack of sensors that provide accurate measurements of certain properties like induction time, degree of agglomeration, and characterizing the metastable zone. Presence of impurities also plays a major role during the (semi-)batch crystallization operations as they influence the primary heterogeneous and secondary nucleation mechanisms (Glennon et al., 2007). Hence, the kinetic models developed at a laboratory-scale always accompany a certain degree of uncertainty in the estimated parameters. Therefore, model based control strategies that are robust towards these uncertainties are necessary for obtaining the desired product specifications.

In the pioneering work on control of batch crystallization processes, programmed cooling has been carried out for optimal operation of cooling crystallizers by operating within the metastable zone width (MSZW) with a constant supersaturation trajectory (Hulburt and Katz, 1964). This approach has been extended to salting-out crystallization processes as well by determining the optimum rate of addition of the second solvent during the process (Nyvlt, 1992). Though it seems that the application of the control strategies developed for batch cooling crystallization can be applied to semi-batch antisolvent crystallization processes straightforwardly, it is often restricted due to the input constraint resulting from the maximum permissible volume and level of supersaturation developed during antisolvent addition. Also, as simultaneous addition of both solvent and antisolvent leads to lesser volume productivity, synonymous application of techniques like temperature cycling used for the cooling mode (Abu Bakar et al., 2009a, 2010) leads to inefficient process design in terms of yield when applied to antisolvent crystallization processes.

In the early stages of development, the pre-determined optimal setpoint trajectory for the antisolvent flowrate is obtained by optimizing a desired product quality based on a nominal first-principles model. Also, the seed loading has been shown to considerably influence the final CSD and hence, sometimes the parameters representing the seed distribution are also considered along with the input profile in

the dynamic programming formulation to design optimal recipes for the control of crystallization processes (Chung et al., 1999, Aamir et al., 2010). However, this approach was found to be sensitive to process disturbances, and model uncertainties and during some worst scenarios, might even upset the process. Consequently, this motivated the interest towards designing robust control strategies by taking into account modeling uncertainties (Ma et al., 1999). However, owing to the conservative design philosophy of the robust control strategies, the issues with the control of batch crystallization processes are not yet addressed completely (Nagy and Braatz, 2004). Besides, run-to-run control strategies that combine parameter estimation and recipe optimization for better control of final product quality were explored (Lee et al., 2002a). Meanwhile, some researchers focused on developing robust control strategies for optimal operation through inferential modeling of the true objective *i.e.*, average cake resistance during filtration and filtration time, by developing empirical relations among key variables such as seed loading, temperature, solvent ratio, and agitation intensity in the case of batch cooling crystallizers (Togkalidou et al., 2001a). Model-based optimal recipes for product CSD control for antisolvent crystallization processes were developed together with their sensitivity to initial feed concentration and antisolvent concentration (Nowee et al., 2008b).

Owing to the recent developments in the sensor technology, concentration or supersaturation control strategy for seeded antisolvent crystallization processes using the feedback of concentration measurements from ATR-FTIR were shown to give encouraging results experimentally (Liotta and Sabesan, 2004, Yu et al., 2006a,b, Zhou et al., 2006). Besides, instead of using expensive instruments like ATR-FTIR for measuring solute concentration, alternative tools like conductivity meter have been explored recently. Although this method has shown to perform very close to standard C-control with the use of ATR-FTIR, it can only be applicable for inorganic compounds (Hermanto et al., 2013). However, the implementation of existing direct design approaches is carried out by trial-and-error procedure,

leading to sub-optimal operation of crystallization processes. Besides, even though the C-control strategy is less sensitive to variations in the kinetic parameters, it may fail when variations in the solubility data and the nucleation kinetics occur (Woo et al., 2009). Moreover, as this strategy relies on the feedback of the solute concentration measurements, it only helps in avoiding the occurrence of nucleation events by restricting the concentration profile go beyond beyond the metastable zone limit. Furthermore, characterizing the hypothetical MSZW is often subjective to the experimenters' observations, as there are no standard protocols for determining the MSZW yet, as it varies with many process parameters like antisolvent addition rate, solvent composition, mixing intensity, agitation rate, initial seed loading, temperature and presence of impurities (Karpinski and Nyvlt, 1983, Barrett and Glennon, 2002, Glennon et al., 2007).

On the other hand, nucleation control strategies based on *indirect* measurements of CSD information using focused beam reflectance measurement (FBRM) have also gained importance. By suppressing the occurrence of nucleation events during the crystallization, the true performance measure of the process, the product CSD is controlled directly (Patience and Rawlings, 2001, Abu Bakar et al., 2009b, Hermanto et al., 2010). FBRM probe provides online measurements of *in situ* chord length distribution (CLD) of the crystals in dispersion and requires a model in order to transform the CLD measurements into CSD (Ruf et al., 2000). However, the applicability of FBRM for CSD measurements is typically dependent on the solute-solvent system under consideration. For instance, in order to measure the size of needle-shaped L-Glutamic crystals, the use of FBRM may not be suitable as the probability of the laser beam to be in alignment with the length of the crystal is usually very low and also the transformation of the CLD to the CSD is not a trivial task. Thus, FBRM can provide reliable measurements of the particle counts than the entire CSD. Therefore, alternative approaches like the use of online microscopy systems (Wang et al., 2007), bulk video imaging (BVI) (Simon et al., 2009b) and

particle vision and measurement (PVM) (Zhou et al., 2009) techniques coupled with image processing and analysis have received considerable attention. However, very few control studies that make use of CSD measurement feedback are reported in the literature (Randolph et al., 1987, Abu Bakar et al., 2009b, Hermanto et al., 2010).

The direct design C-control strategy helps in mitigating the occurrence of the spontaneous nucleation events by choosing an appropriate supersaturation setpoint value based on the trial experiments. However, due to the unavailability of feedback information regarding the evolution of CSD during the batch, this strategy may not always provide better product quality in terms of mean size or any desired specifications in terms of the product CSD (Zhou et al., 2006). Thus, this issue becomes critical when the *real* process exhibits variations in the crystal kinetics or the solubility data. Moreover, as the true objective of controlling the process is to obtain uniform crystals with narrow CSD, control strategies based on crystal size measurements along with concentration measurements should be employed to achieve desired product specifications (Nagy et al., 2011a). A recent study considered a cascaded control strategy with the master controller giving supersaturation setpoints to slave controller based on the number of particle count per second measurements made by FBRM. The slave controller subsequently determines the antisolvent mass percent setpoints given to the flow controller based on the supersaturation measurements made by ATR-FTIR (Woo et al., 2009). However, a systematic approach in appropriately choosing the setpoints such that the optimal product quality is obtained towards the end of the batch is still lacking and hence it warrants further investigation.

Multivariable feedback controllers using fuzzy logic, rigid logic, and neuro-fuzzy techniques and *in situ* measurements of supersaturation and difference in chord lengths of fine particles (1 - 50 μm) were implemented for real-time control of semi-batch antisolvent crystallization processes (Hojjati et al., 2007, Sheikhzadeh et al., 2008a,c). However, tuning the rules and membership functions for the fuzzy

and neuro-fuzzy controllers could be tedious. Moreover, analysis on the robustness of these studies under the presence of process variations and disturbances were lacking.

Understanding the necessity of real time optimal control schemes for batch crystallization processes, the application of model predictive control (MPC) has received interest in the recent past (Nagy and Braatz, 2003, 2004, Shi et al., 2006, Hermanto et al., 2009, Mesbah et al., 2011). Moreover, better robustness towards process variations is ensured through repetitive optimization using the feedback of online measurements and state estimation (Eaton and Rawlings, 1990, Nagy and Braatz, 2012). Besides, real-time dynamic optimal control of semi-batch antisolvent crystallization process has been recently demonstrated through experimental implementation (Sheikhzadeh et al., 2008b). Even though, MPC is a proven technology in process industries, the computation cost involved in solving the real-time nonlinear formulation makes it unattractive for the control of (semi-)batch crystallization processes. Thus, instead of tracking an optimal trajectory or using repetitive optimization based on an offline model, measurement based schemes that track the NCO have been developed (Srinivasan et al., 2003a). However, these approaches require the characterization of the nominal solution using boundary and interior arcs that are necessarily invariant even in presence of uncertainty and disturbances.

From the literature review, it can be concluded that despite the long history of control of crystallization processes, all the strategies developed till date suffer from at least one of the following limitations, (i) open loop in nature and thus sensitive to modeling uncertainty and process disturbances; (ii) sub-optimal operation in presence of process variations; and (iii) high computational effort in real-time optimization. Therefore, the aforementioned issues motivate the contributions of this thesis.

Chapter 3

Improved Operation of C-control for Antisolvent Crystallization Processes

Concentration control (C-control) strategy for semi-batch antisolvent crystallization processes has been recently developed with the aid of new sensors that measure *in situ* process variables. This control strategy gives better robustness over the traditional flowrate control in presence of process variations. However, the setpoints for the existing C-control is determined through trial-and-error procedure and hence gives sub-optimal product quality in most cases. This motivates the development of a modeling framework by integrating pattern classification and nonlinear process modeling for determining setpoints for optimal operation of C-control strategy. In this chapter, the details of the proposed modeling framework are presented along with case studies to show its performance.

3.1 Introduction

For many years, control of batch crystallization processes was believed to be an art rather than science. This notion existed primarily due to limited knowledge of the crystallization process and lack of instrumentation in operation. However, during

the past decade, due to the necessity of quality assurance in pharmaceutical manufacturing through the use of Process Analytical Technology (PAT), novel control strategies were developed for (semi-)batch crystallization processes. Product crystal size distribution (CSD), crystal shape, polymorphic transformation, purity, and yield form the critical parameters to be controlled as they determine the efficiency of the other downstream processes and bio-performance of the final drug. Hence, the necessity for robust control strategies that ensure consistent product quality with less batch-to-batch variability and improved efficiency through optimal operation have received research interest in both academics and industrial sectors in the past decade.

Traditionally, control of semi-batch antisolvent crystallization processes is based on tracking the optimal antisolvent addition rate profile, which is obtained from an offline process model. However, this approach has been found to be highly sensitive to process variations in kinetics and shifts in solubility curve due to the presence of foreign contaminants, inhibitors, inorganic salts, and admixtures in the solvent (Nagy et al., 2008a). With the recent advancements in sensor technology, online process monitoring and control of pharmaceutical processes has become possible. To this end, model-free direct design approaches like concentration control (C-control) and direct nucleation control strategies, which use solute concentration and *in situ* chord length distribution, respectively, as feedback have been developed (Patience and Rawlings, 2001, Woo et al., 2009). These approaches were found to be relatively less sensitive to process variations due to their closed-loop nature. However, direct design approaches suffer from being operated in sub-optimal manner because the relevant design parameters, for example supersaturation setpoints for C-control are determined by trial-and-error procedure from the plant tests which require considerable engineering efforts. Hence, development of alternative methods to determine the supersaturation setpoints for optimal control of antisolvent crystallization processes is crucial to steer the process to obtain the desired

product specifications (Zhou et al., 2006, Woo et al., 2009, Nagy and Braatz, 2012). Thus, in order to alleviate the aforementioned limitations, a new modeling framework that integrates pattern classification and nonlinear process modeling method is developed in this chapter.

In presence of process variations, reliable methods for pattern classification are necessary in order to characterize the specific dynamics of batch process data in order to determine the supersaturation setpoints for C-control that give optimal product quality. During the late 1990's, support vector machines (SVM) have been developed (Vapnik, 1999, Muller et al., 2001) and were extensively applied for fault detection and diagnosis, because they have shown improved performance even when the availability of process data is limited. This makes it an attractive choice when expensive PAT tools are employed for control of batch crystallization processes. Through rigorous simulation based studies on different process data, much of the literature substantiate that Least Squares Support Vector Machine (LSSVM) gives good generalization performance over competing techniques like artificial neural networks (Jain et al., 2000). Consequently, the current study exploits the advantage of the LSSVM for pattern classification in the proposed modeling framework.

On the other hand, Just-In-Time-Learning (JITL) modeling technique (Aha et al., 1991, Atkeson et al., 1997, Rhodes et al., 1997, Bontempi et al., 2001, Cheng and Chiu, 2004, Fujiwara et al., 2009, Ge and Song, 2010) for predicting the solute concentrations during the batch time and the nonlinear Multiway Partial Least Squares (MPLS) algorithm which makes use of Least Squares Support Vector Regression (LSSVR) based inner relationship between the scores (Li et al., 2006) for predicting the product quality at the batch end are developed in this paper. Thus, by integrating the pattern classification and the nonlinear modeling techniques, the proposed modeling framework is incorporated into the C-control strategy to determine the supersaturation setpoints resulting in optimal product quality at the batch end even in

presence of process variations. Therefore, the proposed C-control strategy is able to retain the simple design philosophy of existing C-control strategy, while achieving comparable control performance to that obtained by the existing C-control without resorting to tedious plant tests or an accurate process model at the expense of considerable engineering efforts. Simulation results based on a case study of antisolvent crystallization process of paracetamol in acetone-water mixture confirms that the performance of the proposed C-control strategy is comparable to the best achievable performance of C-control strategy obtained by assuming the availability of precisely known process models.

To the authors knowledge, the idea of integrating pattern recognition and nonlinear process modeling tools for determining setpoint values for optimal operation has not been considered in the literature for the application of semi-batch crystallization processes. Moreover, the study tries to bring in the tools from machine learning concepts that work efficiently even when the available data is limited. The rest of the paper is organized as follows. Section 3.2 introduces the antisolvent crystallization process and discusses the implementation procedure for the C-control strategy. Section 3.3 presents the necessary background for the methods and tools used in this study. Finally, Section 3.4 presents the results and discussions regarding the application of the proposed modeling framework for optimal product quality control in presence of process variations for semi-batch antisolvent crystallization process.

3.2 Concentration control of semi-batch antisolvent crystallization processes

3.2.1 Process model

For the purposes of modeling and control of the crystallization processes, the most common way of representing the process is by using the population balance equa-

tion that accounts for the distribution of the crystals of different sizes during the process as function of both time and the characteristic length in different dimensions of the crystal. Furthermore, crystal agglomeration, growth dispersion, length dependency of the growth kinetics, and breakage phenomena are often neglected in most of the literature on batch crystallization processes (Qamar et al., 2006). In the seeded operation, population balance equation is represented by

$$\frac{\partial n(L, t)}{\partial t} + G(t) \frac{\partial n(L, t)}{\partial L} = B\delta(L), \quad (3.1)$$

where n represents the number density of the crystals, L is the characteristic size of the solute crystal, G is the length independent growth rate, B is the nucleation rate, and δ is the Dirac delta function. The initial seed loading is described using a parabolic distribution given by

$$\begin{aligned} n(L)|_{t=0} &= n(L_s, 0) \\ &= \begin{cases} a_p L_s^2 + b_p L_s + c_p, & L_{s,initial} \leq L_s \leq L_{s,final} \\ 0, & \text{otherwise} \end{cases}, \quad (3.2) \end{aligned}$$

$$L_{s,initial} = L_{s,mean}(1 - L_{s,s.d}), \quad (3.3a)$$

$$L_{s,final} = L_{s,mean}(1 + L_{s,s.d}), \quad (3.3b)$$

where $L_{s,mean}$ is the mean size of the seeds, $L_{s,s.d}$ is the standard deviation in the seed distribution, and the coefficients a_p , b_p , and c_p are determined based on the seed mass, M_{seed} . The method of moments transforms the hyperbolic partial differential equation represented by the population balance equation in Eq. (3.1) into a set of ordinary differential equations called the moment equations. Given L_0 to be the crystal size at nucleation, the moment equations defined on a per mass of solvent

basis are obtained as follows (Hulburt and Katz, 1964)

$$\frac{d\mu_i}{dt} = iG\mu_i + BL_0^i, \quad i = 0, 1, 2, \dots \quad (3.4)$$

where μ_i denotes the i th moment of the CSD defined by

$$\mu_i = \int_0^{\infty} L^i n(L, t) dL, \quad i = 0, 1, 2, \dots \quad (3.5)$$

The mass balance equation for obtaining the solute concentration is given as

$$\frac{dC}{dt} = -3\rho_c k_v G(t)\mu_2(t) - \rho_c k_v B(t)L_0^3, \quad (3.6)$$

where C represents the solute concentration, ρ_c is the crystal density, and k_v is the shape factor of the crystals.

In seeded operations, with the consideration that the nucleation takes place at negligible crystal size, i.e., $L_0 \lll L_{s,mean}$, Eq. (3.4) reduces to the following set of equations

$$\begin{aligned} \frac{d\mu_0}{dt} &= B, \\ \frac{d\mu_i}{dt} &= iG\mu_{i-1}, \quad i = 1, 2, \dots \\ \frac{dC}{dt} &= -3\rho_c k_v G(t)\mu_2(t). \end{aligned} \quad (3.7)$$

In this study, a laboratory-scale, semi-batch, seeded antisolvent crystallization process model for paracetamol in acetone-water mixture is considered (Granberg and Rasmuson, 2000, Granberg et al., 2001, Granberg and Rasmuson, 2005, Woo et al., 2009). The corresponding expressions for the crystal kinetics and solubility

are summarized as follows:

$$B = k_b \Delta C^b, \quad (3.8)$$

$$G = k_g \Delta C^g, \quad (3.9)$$

where k_b and b represent the nucleation kinetic parameters, k_g and g represent the growth kinetics parameters, $\Delta C (= C - C_{sat})$ represents supersaturation*, and C_{sat} is the saturation concentration (solubility) represented as a function of antisolvent mass percent on solute-free basis, m_w ,

$$\begin{aligned} C_{sat} &= 1.0559 - 2.048 \times 10^{-2}m_w + 1 \times 10^{-4}m_w^2, \quad (60\% \leq m_w \leq 80\%) \\ k_b &= 4.338 \times 10^{58} \exp(-1.374m_w), \\ b &= 1.997 \times 10^{-3}m_w^2 - 6.237 \times 10^{-1}m_w + 40.42, \\ k_g &= -9.63 \times 10^{-11}m_w^3 + 3.3558 \times 10^{-8}m_w^2 - 1.2606 \times 10^{-6}m_w \\ &\quad + 3.6852 \times 10^{-5}, \\ g &= -1.108 \times 10^{-4}m_w^2 + 1.024 \times 10^{-2}m_w + 1.427. \end{aligned} \quad (3.10)$$

Table 3.1 lists the corresponding model parameters and initial operating conditions for the antisolvent crystallization process of paracetamol in acetone-water mixture. The product quality considered in this study is defined in terms of the volume-weighted mean size of the product crystals (in μm) and product yield (in %) as shown in Eqs (3.11) and (3.12), respectively.

$$P_{size}(t_f) = \left(\frac{\mu_4}{\mu_3} \right) \Big|_{t_f}, \quad (3.11)$$

$$P_{yield}(t_f) = 100 \left(1 - \frac{C_{t_f}}{C_0} \right), \quad (3.12)$$

*The units of C , C_{sat} and ΔC are ($\text{gm}_{solute}/\text{gm}_{solvent}$). k_b and k_g have the same units as B (no. of particles/ $\text{m}^3 \text{ s}$) and G (m/s) respectively, while b and g are dimensionless.

where t_f is the total batch time, C_0 and C_{t_f} are the solute concentrations at the start and end of the batch, respectively.

Table 3.1 Parameters used in the model.

$k_v = 0.7465$	$M_{solvent} = 120 \text{ gm}$
$\rho_c = 1293 \text{ kg/m}^3$	$M_{seed} = 0.4986 \text{ gm}$
$L_{s,s.d} = 0.27368$	$L_{s,mean} = 187.5 \text{ }\mu\text{m}$
$C_0 = 0.1871 \text{ gm/gm}$	$m_{w,initial} = 60$

3.2.2 C-control strategy

Recent studies on the C-control of batch crystallization processes have tried to determine ways to operate in order to obtain optimal product quality by choosing the constant absolute supersaturation and constant relative supersaturation setpoints within the metastable limits (Yu et al., 2006b, Zhou et al., 2006, Woo et al., 2009). Besides, in order to obtain optimal volume-weighted mean size of the product crystals for the antisolvent crystallization of paracetamol in acetone-water mixture, the constant relative supersaturation setpoint has been found to give better results, as the absolute supersaturation becomes low towards the end of the batch, thereby avoiding the formation of new nuclei (Zhou et al., 2006, Woo et al., 2009). Figure 3.1 depicts the implementation of the C-control strategy.

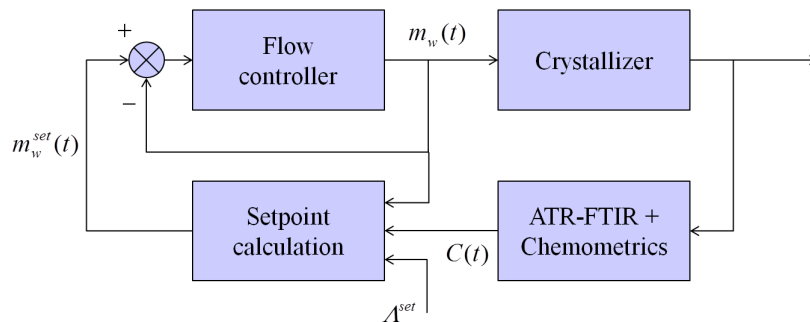


Figure 3.1 Concentration control strategy for antisolvent crystallization processes (Zhou et al., 2006).

The solute concentration C_k at k th sampling instant is given by,

$$C_k = \frac{M_{solute,k}}{M_{solvent} + M_{w,k}}, \quad (3.13)$$

where $M_{solute,k}$ and $M_{w,k}$ represent the mass of the solute and antisolvent, respectively, at the k th sampling instant, and $M_{solvent}$ is the mass of solvent.

Suppose that the sampling time is very small compared with the batch time, the mass of solute at the $(k+1)$ th sampling instant can then be approximated by $M_{solute,k}$. Hence,

$$C_{k+1} = \frac{M_{solute,k}}{M_{solvent} + M_{w,k} + t_s \dot{M}_{w,k+1}}, \quad (3.14)$$

where $\dot{M}_{w,k+1}$ is the antisolvent flowrate to be implemented at the $(k+1)$ th sampling instant, and t_s is the sampling time[†].

In C-control strategy, the relative supersaturation setpoint (Λ^{set}) is defined as follows (Zhou et al., 2006, Woo et al., 2009):

$$\Lambda^{set} = \frac{C_{k+1}^{set}}{C_{sat}(m_{w,k+1}^{set})} - 1, \quad k = 0, 1, 2, 3, \dots \quad (3.15)$$

where

$$m_{w,k+1}^{set} = 100 \left(\frac{M_{w,k} + t_s \dot{M}_{w,k+1}}{M_{solvent} + M_{w,k} + t_s \dot{M}_{w,k+1}} \right), \quad (3.16)$$

where the superscript "set" denotes the setpoint. Thus, for a specified value of Λ^{set} , the setpoint of antisolvent mass percent at the $(k+1)$ th sampling instant is obtained by solving the following equation.

$$C_{k+1}^{set} - (1 + \Lambda^{set})C_{sat}(m_{w,k+1}^{set}) = 0. \quad (3.17)$$

As the objective of C-control strategy is to determine the control action, $\dot{M}_{w,k+1}$, such that the solute concentration at the next sampling instant, C_{k+1} , is equal to

[†]Sampling time for the concentration measurements in this study is considered to be 30 secs.

C_{k+1}^{set} , $\dot{M}_{w,k+1}$ is obtained by solving Eqs. (3.16) and (3.18) simultaneously, where the latter is given by

$$(1 + \Lambda^{set})C_{sat}(m_{w,k+1}^{set}) + \frac{M_{solute,k}}{M_{solvent}} \left(\frac{m_{w,k+1}^{set}}{100} - 1 \right) = 0. \quad (3.18)$$

It has been shown in the literature that direct design C-control strategy provides improved robustness over the traditional F-control for most of the process variations (Zhou et al., 2006). However, it fails to adapt during shifts in solubility data and process variations leading to high nucleation and low growth rates (Nagy et al., 2008a, Woo et al., 2009). This will also be highlighted through the case studies discussed in the subsequent sections. Thus, the current study is motivated towards finding alternate methods based on historical data of the process to determine the suitable setpoint value that ensures optimal operation of antisolvent crystallization process even in presence of aforementioned process variations.

3.3 Proposed integrated modeling framework

In the case of batch crystallization processes, most dynamics are highly nonlinear in nature. Hence, an integrated modeling framework by combining pattern classification and nonlinear process modeling methods is proposed to predict solute concentrations during the batch time and the product quality at batch end, which play a crucial role in the development of the proposed modeling framework.

3.3.1 Overview of LSSVM for multiclass classification

Typically, multiclass problem with M classes is solved by reformulating it into a set of L binary classification problems (van Gestel et al., 2004). In this respect, the methodology of binary classification using LSSVM is briefly discussed here to facilitate the ensuing discussions.

LSSVM for binary classification:

The LSSVM algorithm proposed by (Suykens and Vandewalle, 1999) is used in this study. Consider a model in the primal weight space given by:

$$y_b(x) = \text{sign}[w^T \varphi(x) + b]. \quad (3.19)$$

Given a set of N training samples $\{x_k, y_{b,k}\}_{k=1}^N$, where $x_k \in \mathbb{R}^p$ is the k th input and $y_{b,k} \in \{-1, +1\}$ is the corresponding class labels, the LSSVM classifier satisfies the following conditions:

$$\begin{cases} w^T \varphi(x_k) + b \geq +1, & \text{if } y_k = +1 \\ w^T \varphi(x_k) + b \leq -1, & \text{if } y_k = -1 \end{cases} \quad (3.20)$$

which is equivalent to

$$y_{b,k}[w^T \varphi(x_k) + b] \geq 1, \quad (3.21)$$

where the nonlinear function $\varphi(\cdot)$ maps the input x to a high dimensional feature space. However, in order to evaluate $y_b(x)$ using Eq. (3.19), the parameters w and b must be obtained. Hence, an optimization problem is formulated as given in Eq. (3.22).

$$\min_{w,b,e} \mathcal{J}_P(w, b, e) = \frac{1}{2} w^T w + \frac{\gamma}{2} \sum_{k=1}^N e_k^2, \quad (3.22)$$

subject to the equality constraints

$$y_{b,k}[w^T \varphi(x_k) + b] = 1 - e_k, \quad k = 1, \dots, N. \quad (3.23)$$

The solution of Eq. (3.22) is obtained through the Lagrangian:

$$\mathcal{L}(w, b, e; \alpha) = \mathcal{J}_P(w, b, e) - \sum_{k=1}^N \alpha_k \{y_{b,k}[w^T \varphi(x_k) + b] - 1 + e_k\}, \quad (3.24)$$

where $\alpha_k \in \mathbb{R}$ are the Lagrange multipliers that can be either positive or negative in

the LSSVM formulation.

From the conditions for optimality, the Karush-Kuhn-Tucker (KKT) system of equations leads to the elimination of w and e to obtain

$$\left[\begin{array}{c|c} 0 & y_b^T \\ \hline y_b & \Omega + \gamma^{-1}I \end{array} \right] \left[\begin{array}{c} b \\ \alpha \end{array} \right] = \left[\begin{array}{c} 0 \\ 1_v \end{array} \right], \quad (3.25)$$

where $y_b = [y_{b,1}, \dots, y_{b,N}]$, $1_v = [1, \dots, 1]$, $e = [e_1, \dots, e_N]$, $\alpha = [\alpha_1, \dots, \alpha_N]$.

Thus, by applying the Mercer's condition within the Ω matrix, we get

$$\Omega_{ij} = y_{b,i}y_{b,j}\varphi(x_i)^T\varphi(x_j) = y_{b,i}y_{b,j}K(x_i, x_j), \quad (3.26)$$

where the kernel function $K(\cdot, \cdot)$ used in this study is the Radial Basis Function (RBF) kernel given below.

$$K(x, x_k) = \exp\left(-\frac{\|x - x_k\|_2^2}{\sigma^2}\right), \quad (3.27)$$

where σ is a constant used for the scaling of inputs in the RBF kernel function. As shown in Eq. (3.25), the set of linear equations is solved in the dual space (large scale algorithm) in order to obtain the parameters of the LSSVM classifier shown below in Eq. (3.28).

$$y_b(x) = \text{sign} \left[\sum_{k=1}^N \alpha_k y_{b,k} K(x, x_k) + b \right] \quad (3.28)$$

Now, using this scheme for the binary classification, the multiclass classification problem is solved. Thus, to each class \mathcal{C}_m , a unique codeword $c_m = [y_m^{(1)}, y_m^{(2)}, \dots, y_m^{(L)}] \in \{-1, 0, +1\}^L$ is assigned, where each binary classifier $f^{(l)}(x)$, $l = 1, \dots, L$, discriminates between the corresponding output bit y_l .

There exists different approaches to construct the set of binary classifiers. In this

study, one-versus-one (1-vs-1) output coding approach is used, during which $L = M(M - 1)/2$ binary classifiers are plugged in, where each of which discriminates between two opposing classes. Each binary classifier is inferred on the training set $D^{(l)} = \{(x_k, y_k^{(l)}) | k = 1, \dots, N \text{ and } y_k^{(l)} \in \{-1, +1\}\}$, consisting of $N^{(l)} \leq N$ training points, by solving

$$\left[\begin{array}{c|c} 0 & y^{(l)\text{T}} \\ \hline y^{(l)} & \Omega^{(l)} + \gamma^{(l)-1} I \end{array} \right] \left[\begin{array}{c} b^{(l)} \\ \alpha^{(l)} \end{array} \right] = \left[\begin{array}{c} 0 \\ 1_v \end{array} \right], \quad (3.29)$$

where $\Omega_{ij,l} = K_l(x_i, x_j)$. The binary classifier is then obtained as follows

$$f^{(l)}(x) = \text{sign} \left[\sum_{k=1}^{N^{(l)}} y_k^{(l)} \alpha_k^{(l)} K^{(l)}(x, x_k) + b^{(l)} \right]. \quad (3.30)$$

Thus, each of these L classifiers assign an output bit $y^{(l)} = \text{sign}[f^{(l)}(x)]$, such that the unique codeword c to a new input vector x can be reconstructed to predict its corresponding class (van Gestel et al., 2004).

In this study, LS-SVMlab: a MATLAB/C toolbox is used for implementing the LSSVM algorithms (Pelckmans et al., 2002) with a slight modification by replacing the existing LSSVM method by a k -nearest neighborhood based LSSVM (k -NN LSSVM) algorithm in order to improve the computational efficiency.

The batch data to be classified is preprocessed using Multiway Principal Component Analysis (MPCA) to reduce the dimensionality of the variables (Nomikos and MacGregor, 1994). To this end, the input data X should be unfolded by treating each of the variable value at each sampling instant as a separate variable as given

below.

$$X = \begin{bmatrix} \overbrace{x_1 x_2 \cdots x_J}^{i=1,k=1} & \overbrace{x_1 x_2 \cdots x_J}^{i=1,k=2} & \cdots & \overbrace{x_1 x_2 \cdots x_J}^{i=1,k=K} \\ \overbrace{x_1 x_2 \cdots x_J}^{i=2,k=1} & \overbrace{x_1 x_2 \cdots x_J}^{i=2,k=2} & \cdots & \overbrace{x_1 x_2 \cdots x_J}^{i=2,k=K} \\ \vdots & \vdots & \ddots & \vdots \\ \overbrace{x_1 x_2 \cdots x_J}^{i=I,k=1} & \overbrace{x_1 x_2 \cdots x_J}^{i=I,k=2} & \cdots & \overbrace{x_1 x_2 \cdots x_J}^{i=I,k=K} \end{bmatrix} \quad (3.31)$$

Now, these JK variables in each row of X are treated as independent variables and are autoscaled using the corresponding values of mean and standard deviation. Based on the variance captured, the first np principal components are retained in the lower dimensional space of the MPCA model as shown in Eq.(3.32).

$$X = \sum_{r=1}^{r=np} t_r p_r^T + \mathbf{E}, \quad (3.32)$$

where p_r is the r th loading vector, t_r is score vector of r th latent variable, and \mathbf{E} is the residual.

The training data set for the pattern classification algorithm is obtained for the I batches whose input data consists of the first np scores, while the output Y_{class} is the vector containing the information regarding the specific class of dynamics to which each of these I batches belong. For any new incoming batch data, which consists of the input variables as a $(1 \times JK)$ row vector is autoscaled using the mean and standard deviation values determined earlier and projected onto the lower dimensional space. The corresponding scores obtained for this batch are treated as the corresponding query vector. Thus, the LSSVM based pattern classifier is trained using the training data and subsequently used to determine the specific dynamics of the query vector.

3.3.2 Nonlinear dynamic modeling

In the proposed modeling framework as shown in Figure 3.2, the pattern classifier selects the relevant samples from the database for prediction of the process variables during the batch and the product quality prediction at the batch end.

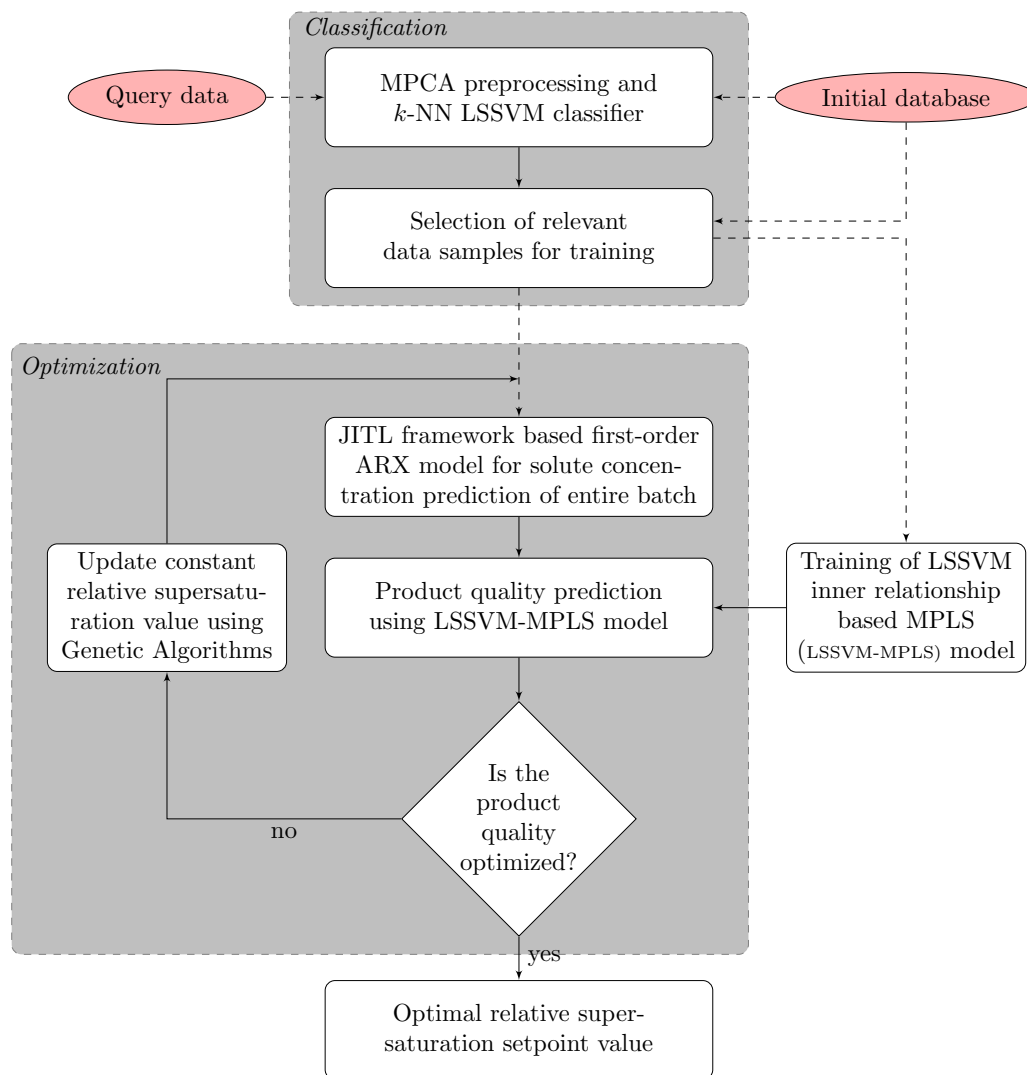


Figure 3.2 Proposed integrated data-based framework.

Traditionally, dynamic modeling of batch processes focus on global approaches, such as neural networks, fuzzy set, and other kinds of nonlinear parametric models. However, these approaches suffer from the drawbacks arising due to either the necessity of specifying the model structure *a priori* or ultimately the complexity

associated with the highly non-convex optimization problems. Besides, the training of these models is often computationally demanding and thus becomes difficult to be trained online when the process dynamics move away from the nominal operating region. To alleviate these drawbacks of the global modeling approaches, local modeling approaches like T–S fuzzy model (Takagi and Sugeno, 1985) and neuro-fuzzy network model (Jang and Sun, 1995) were developed. In this work, the just-in-time learning (JITL) framework is explored owing to its three main characteristics. Firstly, the model building is postponed until an output for a given query data is requested. Secondly, the predicted output for the query data is computed by exploiting the stored data in the database. Finally, after the output predictions are obtained, the local model constructed is discarded (Aha et al., 1991, Atkeson et al., 1997, Rhodes et al., 1997, Bontempi et al., 2001, Cheng and Chiu, 2004, Fujiwara et al., 2009, Ge and Song, 2010). In this modeling framework, the nonlinear dynamics of the batch process is approximated using a linear ARX model at each sampling time. There are three main steps in JITL to predict the model output corresponding to the query data: (i) the most relevant data samples from the database are selected based on the similarity criteria applied to the query data and the database; (ii) a local model built using the most relevant data; (iii) model output is calculated based on the local model and current query data.

As a simple low-order model is usually employed by the JITL, without the loss of generality, consider the following second-order ARX model:

$$\hat{y}(k) = \alpha_1^k y(k-1) + \alpha_2^k y(k-2) + \beta_1^k u(k-1), \quad (3.33)$$

where $\hat{y}(k)$ is the predicted output by the JITL model at the k th sampling time, $y(k-1)$ and $u(k-1)$ are the output and input variables at the $(k-1)$ th sampling time, respectively, and α_1^k , α_2^k and β_1^k are the model coefficients at the k th sampling time.

Define regression vector for the ARX model given in Eq. (3.33) as

$$\mathbf{x}_k = \begin{bmatrix} y(k-1) & y(k-2) & u(k-1) \end{bmatrix}. \quad (3.34)$$

Suppose that the present database consists of N_1 process data $(y_i, \mathbf{x}_i)_{i=1 \sim N_1}$, given a query data \mathbf{x}_q , the objective of JITL is to obtain the local ARX model of the nonlinear systems by focusing on the relevant region around the current operating condition. The first step is to select the relevant regression vectors from the database that resemble the query data closely. To do so, the following similarity measure, s_i , is considered.

$$s_i = \kappa \sqrt{e^{-\|\mathbf{x}_q - \mathbf{x}_i\|^2} + (1 - \kappa) \cos(\theta_i)}, \quad \text{if } \cos(\theta_i) \geq 0 \quad (3.35)$$

where κ is a weight parameter constrained between 0 and 1, and θ_i is the angle between $\Delta \mathbf{x}_q$ and $\Delta \mathbf{x}_i$, where $\Delta \mathbf{x}_q = \mathbf{x}_q - \mathbf{x}_{q-1}$ and $\Delta \mathbf{x}_i = \mathbf{x}_i - \mathbf{x}_{i-1}$. The value of s_i is bounded between 0 and 1. When s_i approaches to 1, it indicates that \mathbf{x}_i resembles \mathbf{x}_q closely.

After all s_i are computed by Eq. (3.35), for each $l \in [k_{min} \ k_{max}]$, where k_{min} and k_{max} are the pre-specified minimum and maximum number of relevant data, the relevant data set (y_l, Φ_l) is constructed by selecting the l most relevant data (y_i, \mathbf{x}_i) corresponding to the largest s_i to the l -th largest s_i . The leave-one-out cross validation test is then conducted and the validation error is calculated. Thus, based on the relevant data that gives the smallest validation error, the optimal number of relevant data, l^* , is determined. Subsequently, the predicted output for the query data is calculated as, $\hat{y}_q = \mathbf{x}_q^T (P_{l^*}^T P_{l^*})^{-1} P_{l^*}^T W_{l^*} y_{l^*}$, where $P_{l^*}^T = W_{l^*} \Phi_{l^*}$ and W_{l^*} is a diagonal matrix with entries being the first l^* entries of s_i .

3.3.3 Nonlinear product quality modeling of batch processes

The important attributes that define the efficient control of batch processes is dictated by the batch end product qualities. However, these values are obtained only towards the end of the batch. Usually, the product quality of semi-batch crystallization processes is characterized based on the yield, product crystal size distribution, and mean size of the product crystals. Thus, methods for online prediction of these attributes based on the real-time measurements from various PAT tools play a very important role for both process monitoring and subsequent control (Sheikhzadeh et al., 2008b, Trifkovic et al., 2009, Hermanto et al., 2009). Besides, in the absence of exhaustive first-principles models, the traditional statistical process control (SPC) approaches based on multivariate statistical tools are used for process monitoring and inferential control (Nomikos and MacGregor, 1994, Togkalidou et al., 2001a, Pollanen et al., 2006, Hermanto et al., 2011).

For product quality predictions, multivariate statistical models like PLS models are used during batch processes modeling. Specifically, nonlinear PLS modeling techniques have been explored by considering different nonlinear inner relationship between the scores of the inputs and the outputs like quadratic regression models (Wold et al., 1989) and artificial neural networks (Qin and McAvoy, 1992). In this study, a new nonlinear version of MPLS is developed, where the inner relationship of the input-output scores is modeled using a series of LSSVR models.

Prior to the construction of the nonlinear PLS models, the historical data of the process variables collected at each sampling instant for all the batches were used to form the 3-D matrix of the form X (I batches \times J variables \times K sampling instances). Also, the information regarding the corresponding product quality data Y (I batches \times M product qualities) for each batch are also collected. Thus, MPLS model, that is often used in the literature for online monitoring of the batch process, is used for predicting the product quality values during this study (Nomikos and

MacGregor, 1995a, Russell et al., 1998, Li et al., 2006).

Unlike its usual application for online monitoring of the process variables using the partial information of the batch data, the MPLS model developed during this study uses the entire batch data for the prediction of the product qualities. This requires, for any given value of the constant relative setpoint and the initial conditions of the batch, the process variables of the entire batch is obtained from the JITL based modeling framework, as discussed earlier.

The MPLS is equivalent to performing the standard PLS on the two dimensional measurement data of process variables \mathbf{X} and product quality data \mathbf{Y} . Similar to MPCA, the MPLS model requires the unfolding of the measurement data in the multiway fashion as described in Section 3.3.1.

For example, MPLS decomposes the matrices \mathbf{X} and \mathbf{Y} into a linear combination of scores matrices \mathbf{T} and \mathbf{U} , loading matrices \mathbf{P} and \mathbf{Q} , along with the residual matrices \mathbf{E} and \mathbf{F} .

$$X = \sum_{r=1}^R t_r p_r + E = TP^T + E, \quad (3.36)$$

$$Y = \sum_{r=1}^R u_r q_r + F = UQ^T + F, \quad (3.37)$$

where vectors t_r and u_r represent the r th latent variables, R is the number of latent variables retained in the model. For the standard linear PLS model, the inner relationship between the latent variable matrices \mathbf{U} and \mathbf{T} is modeled using a linear function as, $\mathbf{U} = \mathbf{T}\mathbf{B}$, where \mathbf{B} is a diagonal coefficient matrix. The LSSVM based MPLS model proposed in this study replaces the linear inner relationship of the input-output score matrices using a series of single-input-single-output LSSVR models as

$$u_r = S_r(t_r) + h_r, \quad (3.38)$$

where $S_r(\cdot)$ represents the LSSVR model corresponding to the inner relationship of

the r th latent variable, and h_r is the corresponding residual. Thus, LSSVR is not only used for multiclass classification as discussed earlier in the section 3.3.1, but also for nonlinear regression in this study. The approach is very similar as explained earlier, however the model in the primal weight space will be now of the form shown in Eq. (3.39) or it can be rewritten as shown in Eq. (3.40).

$$\hat{u}_r(t_r) = w^T \varphi(t_r) + b, \quad (3.39)$$

$$\hat{u}_r = \left[\sum_{i=1}^I \alpha_i K(t_r, t_{r,i}) + b \right], \quad (3.40)$$

where $K(\cdot)$ is the kernel function, I is the number of reference batches in total, and the parameters α_i and b are determined through the solution of the resultant optimization problem of the LSSVM formulation as described below.

$$\min_{w,b,e} \mathcal{J}_P(w, b, e) = \frac{1}{2} w^T w + \frac{\gamma}{2} \sum_{i=1}^I e_i^2, \quad (3.41)$$

subject to

$$u_{r,i} = w^T \varphi(t_{r,i}) + b + e_i, \quad i = 1, \dots, I \quad (3.42)$$

Therefore, during the implementation of the concentration control strategy, the LSSVM based pattern classifier recognizes the specific dynamics of the current processes online based on the historical process data. Thus, a subset of the complete database is selected as the relevant database for the prediction of solute concentration (using JITL framework) and product quality values (using nonlinear MPLS model). In the Section 3.4, the application of the developed framework on anti-solvent crystallization processes is illustrated to show that the selection of optimal setpoints for concentration control is enabled using the proposed methodology.

3.4 Results and discussions

As a case study, process data for five different dynamics were considered by introducing perturbations in the nucleation and growth kinetic parameters, along with shifts in solubility data, meaning that the concerned parameters in the Eqs. (3.8) to (3.10) are given by

$$\begin{aligned}
 g' &= g(1 + \Delta\theta_1), \\
 k'_g &= k_g(1 + \Delta\theta_2), \\
 b' &= b(1 + \Delta\theta_3), \\
 k'_b &= k_b(1 + \Delta\theta_4), \\
 C'_{sat} &= C_{sat}(1 + \Delta\theta_5),
 \end{aligned} \tag{3.43}$$

where $\Delta\theta_1$ and $\Delta\theta_2$ are the uncertainties in the growth kinetics; $\Delta\theta_3$ and $\Delta\theta_4$ are the uncertainties in the nucleation kinetics; and $\Delta\theta_5$ is the uncertainty in the solubility curve of paracetamol in acetone-water system. Therefore, the nominal model corresponds to the case when $\Delta\theta_i = 0$ ($i = 1 \sim 5$). In this study, five different cases were considered by introducing perturbations in the kinetic model parameters as shown in Table 3.2. Furthermore, the batch time for the five cases is 120 minutes and the antisolvent addition rate is constrained between 0 to 6 ml/min. Lastly, constraint on minimum product yield of 40% is considered throughout this thesis.

To see the drawback of the existing C-control strategy, the best achievable performance of C-control strategy obtained assuming the availability of precisely known first-principles models is obtained for all the cases. The corresponding optimal relative supersaturation setpoint for each case is determined by maximizing the volume weighted mean size of the product crystals along with constraints on minimum product yield. For the ease of reference, it is referred to optimal C-control in the

Table 3.2 Different dynamics of the process.

Dynamics	Perturbations					Remarks
	$\Delta\theta_1$	$\Delta\theta_2$	$\Delta\theta_3$	$\Delta\theta_4$	$\Delta\theta_5$	
Nominal	0	0	0	0	0	–
Case 1	0.1	-0.1	-0.1	0.1	0	High nucleation and low growth
Case 2	0	0	0	0	0.05	Positive shift in solubility data
Case 3	0	0	0	0	-0.05	Negative shift in solubility data
Case 4	0.1	-0.1	-0.1	0.1	0.05	High nucleation and low growth along with shift in solubility data

subsequent discussion. Table 3.3 presents the resulting product quality values obtained by these two C-control approaches in terms of both volume weighted mean size of the product crystals and product yield for all the cases.

Table 3.3 Comparison between direct design and optimal C-control strategies.

Case	Direct design C-control		Λ^{set}	Optimal C-control		% relative improvement over direct design
	P_{size} (μm)	P_{yield} (%)		P_{size} (μm)	P_{yield} (%)	
Nominal	581.78	57.08	0.1010	581.78	57.08	00.00
1	266.37	46.68	0.0970	274.10	40.00	02.90
2	357.46	20.89	0.1583	563.92	55.42	57.76
3	455.92	60.68	0.0601	571.62	60.33	25.38
4	262.47	14.06	0.1531	289.77	40.00	10.40

It is inferred from Table 3.3 that the product quality obtained through the existing direct design C-control can be improved for Cases 2 to 4 by adapting the constant relative supersaturation setpoint depending upon the specific dynamics of the process. In Case 4, though the margin for improvement in terms of mean size of the product crystals is only around 10.4%, the direct design C-control strategy does not meet the minimum product yield requirement of 40%. Therefore, motivated by the necessity of adapting the setpoints in presence of process variations, the proposed data-based modeling framework is developed in this chapter so that it can be integrated into the C-control strategy to achieve better performance.

The database for training the data-based models is constructed using the process

data collected from thirty different batches for each of the five specific dynamics of the process considered during this study. To this end, thirty equidistant values within the range of [0.02, 0.18] are selected for the constant relative supersaturation setpoint. The database is then constructed based on the closed loop process data collected from the implementation of these thirty setpoint values for each of the specific dynamics. Note that the lower bound for the aforementioned range for the relative supersaturation setpoint is determined by satisfying the batch end constraint on the solute concentration, .i.e., $C_{t_f} \leq 0.1123$ (gm/gm).

Before the LSSVM is applied, the testing data for classification purpose is unfolded as shown in Eq. (3.44). Next, the unfolded data is auto-scaled and its dimensionality is reduced using multiway principal component analysis (MPCA). The first np principal components are selected based on the cross validation and the corresponding scores are retained in order to train the LSSVM for pattern classification. The query data is autoscaled using the mean and standard deviation of the training data and is projected onto the corresponding principal components. Using the training data with reduced dimensionality, LSSVM is trained for multi-class classification. In order to improve the performance of the standard LSSVM, an improved k -nearest neighborhood LSSVM is used, as explained earlier in Section 3.3.1. The thirty nearest neighbors of the test data among the training data are selected and sorted based on their distance measure. This subset of relevant batch data is used as the training data for multi-class classification using k -NN LSSVM. This procedure is repeated to determine the specific class of dynamics that the test batch data will follow. Thus, once the dynamics or the specific class of the test data is determined, all the batch data in the training data set that fall into this class are selected as *relevant* data set for subsequent modeling. This forms the first-stage of the framework, where a subset of training samples are selected for the prediction of solute concen-

tration and product quality.

$$X = \begin{bmatrix} \overbrace{C \quad m_w}^{i=1,k=1} & \overbrace{C \quad m_w}^{i=1,k=2} & \cdots & \overbrace{C \quad m_w}^{i=1,k=K} \\ \overbrace{C \quad m_w}^{i=2,k=1} & \overbrace{C \quad m_w}^{i=2,k=2} & \cdots & \overbrace{C \quad m_w}^{i=2,k=K} \\ \vdots & \vdots & \ddots & \vdots \\ \overbrace{C \quad m_w}^{i=I,k=1} & \overbrace{C \quad m_w}^{i=I,k=2} & \cdots & \overbrace{C \quad m_w}^{i=I,k=K} \end{bmatrix} \quad (3.44)$$

For the JITL modeling method, the local model is chosen to be a first-order ARX model given as follows:

$$\hat{C}(k) = \alpha C(k-1) + \beta m_w(k-1), \quad (3.45)$$

where $\hat{C}(k)$ is the predicted solute concentration for the k th sampling time, while α and β are the parameters of the ARX models that are obtained using JITL method.

Figure 3.3 shows samples of five batches of nominal process data that are used to construct the reference data set for the JITL method. To validate the predictive performance of the first-order ARX model employed in the JITL framework, additional ten batches data for the nominal process is generated as shown in Figure 3.4. This validation data differs from the thirty batches data of the nominal process used for constructing the database of the JITL method. With the JITL parameters k_{min} , k_{max} and κ chosen to be 8, 60 and 1, respectively, Figure 3.5 shows the validation results. It is clear that the JITL method can predict the solute concentration with good accuracy.

Using the same batch data mentioned previously, the LSSVR inner relationship based MPLS model is validated by predicting the product quality values as

$$\hat{P}(t_f) = \Psi(X_p), \quad (3.46)$$

where X_p represents the input vector to the LSSVR-based MPLS model, which contains the solute concentration and antisolvent mass percent values at each sampling instant until the end of the batch, Ψ represents the LSSVR-based MPLS model, and $\hat{P}(t_f)$ denotes the predicted product quality vector consisting of the yield and volume weighted mean size of the product crystals. Figure 3.6 shows the good prediction of the product qualities in terms of volume weighted mean size of the product crystals and product yield, which is evidenced by the reduction in their respective RMSE values by 51.8% and 44.9%, when compared to the predictions of linear MPLS model. In this study, the first three principal components are selected that capture almost greater than 99% variance in the data.

Table 3.4 Comparative study between proposed design and optimal C-control.

Case	Proposed design		Optimal C-control		% relative deviation in quality
	Λ^{set}	P_{size} (μm)	Λ^{set}	P_{size} (μm)	
Nominal	0.0961	578.946	0.1010	581.780	0.49
1	0.0977	272.564	0.0970	274.101	1.08
2	0.1560	563.835	0.1583	563.915	0.56
3	0.0639	561.132	0.0601	571.621	0.01
4	0.1553	286.631	0.1531	289.766	1.84

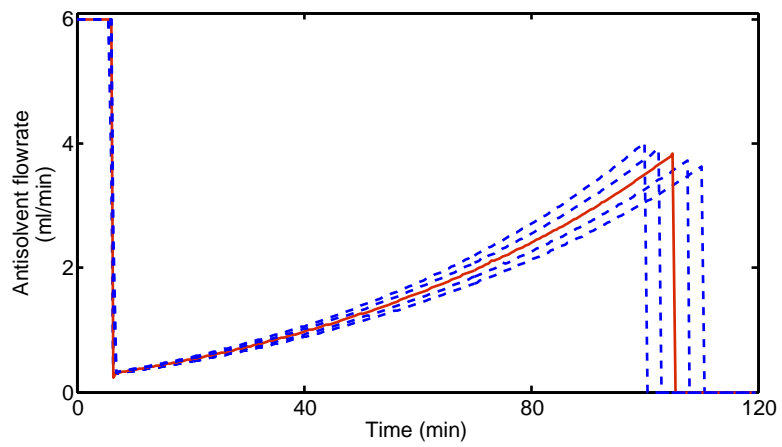
Now, the proposed modeling framework is incorporated into the existing C-control strategy to determine the optimal relative supersaturation setpoint (Λ^{set}) that results in the maximum possible product quality, which is formulated by the following optimization problem and solved using a global optimization algorithm.

$$\begin{aligned}
& \min_{\Lambda^{set}} J = -\hat{P}_{size}(t_f), \\
& \text{s.t. } \hat{C}(k) = \alpha C(k-1) + \beta m_w(k-1), \quad \forall k = 1, 2, \dots, K, \\
& \hat{P}(t_f) = \Psi(X_p), \quad \text{where } \hat{P}(t_f) = [\hat{P}_{yield}(t_f), \hat{P}_{size}(t_f)], \\
& \hat{P}_{yield}(t_f) \geq 40
\end{aligned} \tag{3.47}$$

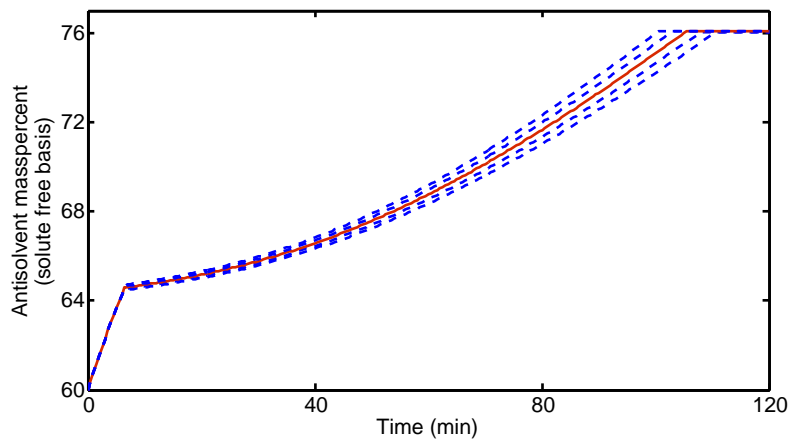
where Λ^{set} is the decision variable for the constrained minimization problem J and

the last constraint is imposed by the minimum product yield at the batch end.

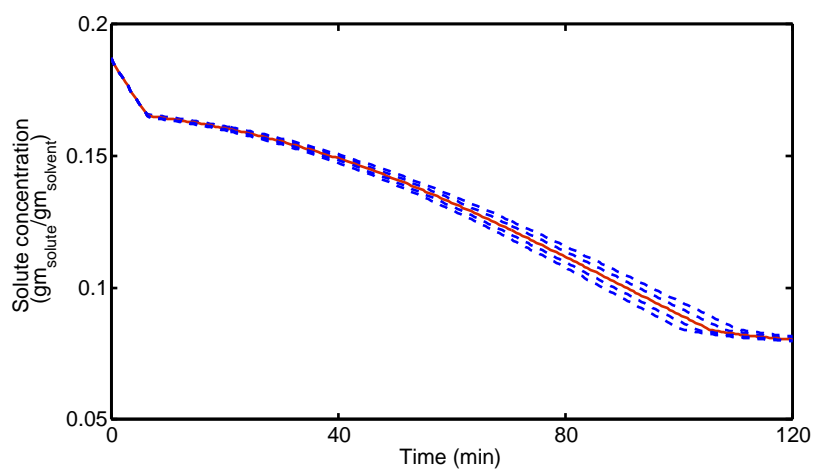
As a benchmark, the optimal product quality and the corresponding optimal setpoint values for C-control obtained assuming precisely known first-principles models for all the five case studies are compared with those obtained by the proposed design as shown in Table 3.4. From the above table, it is noted that the proposed framework is effective in determining the setpoint values that are close to the true optimal values. The solute concentration and antisolvent addition rate profiles for all the five case studies resulting from the implementation of the three C-control approaches are shown in Figures 3.7 to 3.11, respectively. Owing to the lesser deviations between the profiles resulting from the proposed approach and the optimal C-control, the proposed design is capable of determining the setpoints for concentration control to assure robust control, leading to optimal operation of the semi-batch antisolvent crystallization process.



(a) Antisolvent flowrate profiles



(b) Antisolvent mass percent profiles



(c) Solute concentration profiles

Figure 3.3 Illustration of five batches of nominal process data used to construct reference database for the JITL method.

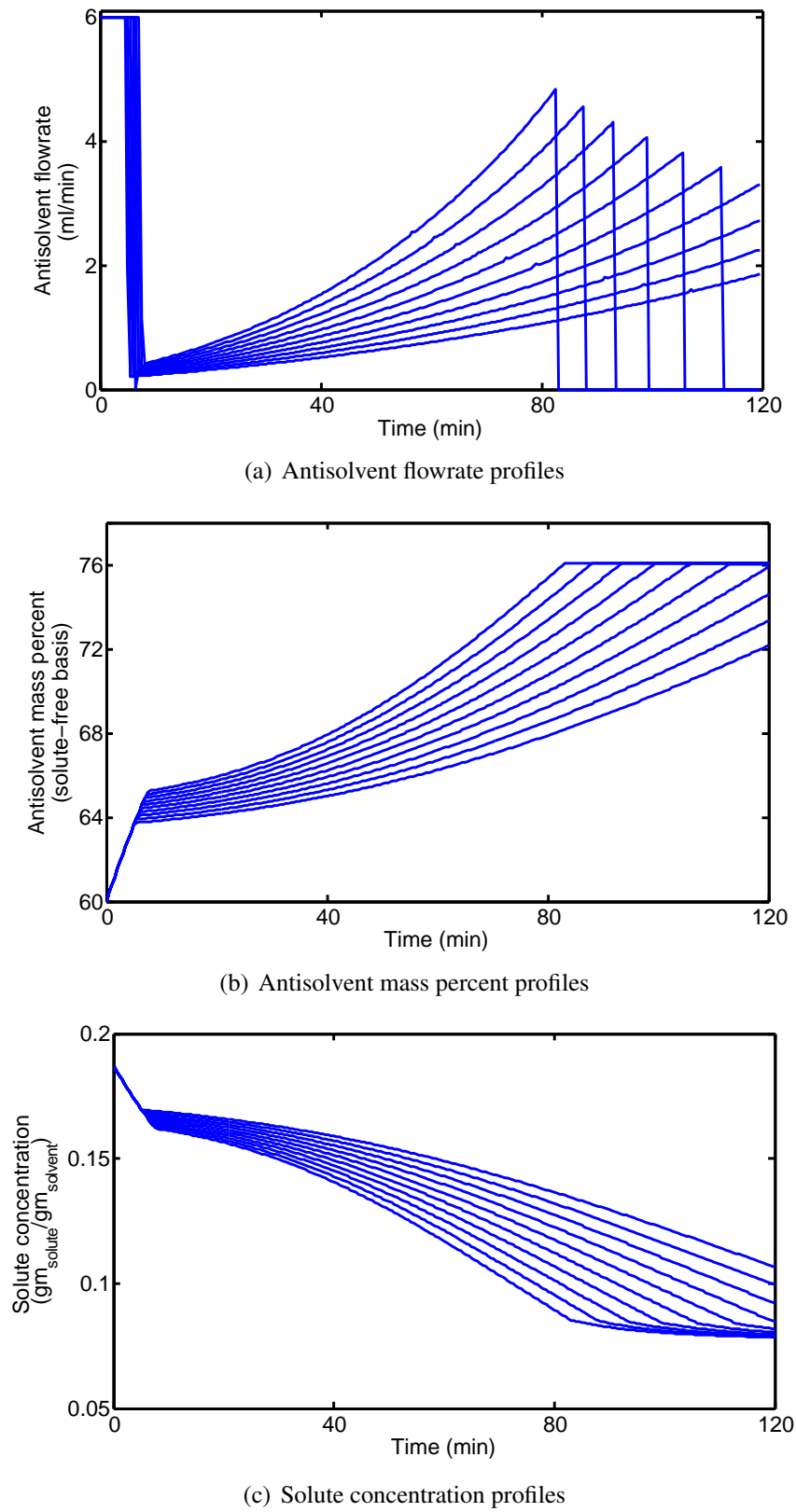


Figure 3.4 Illustration of ten batches of nominal process data used for validation of the JITL method.

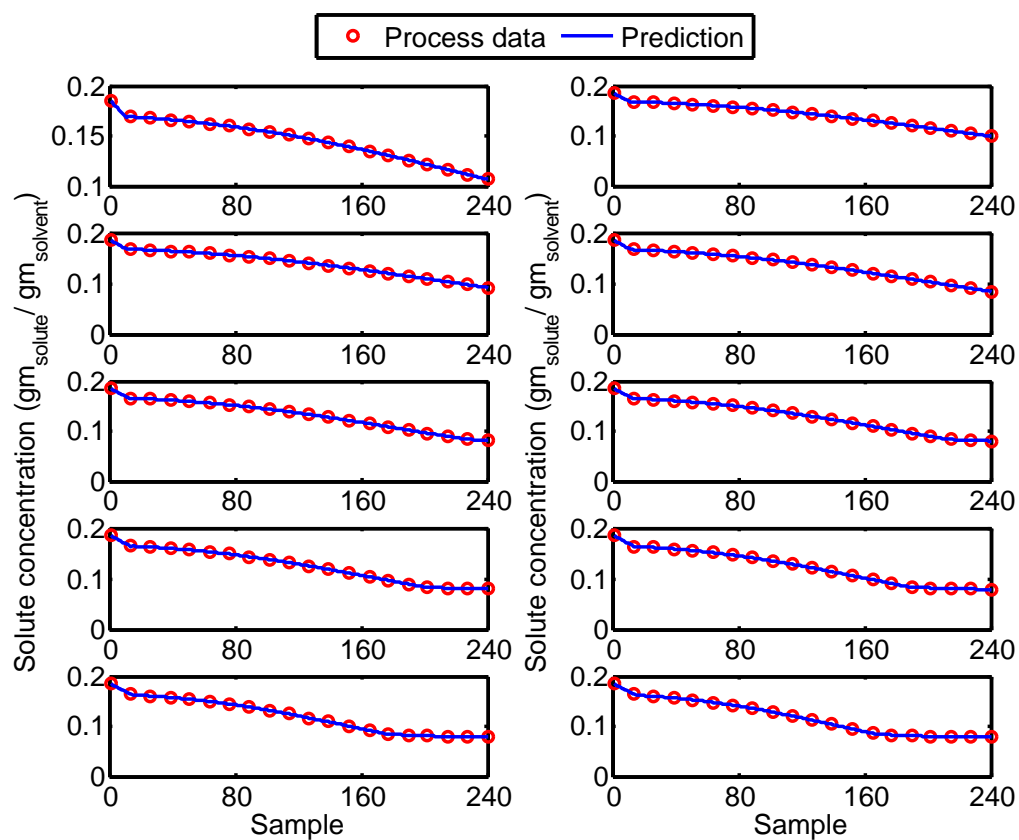


Figure 3.5 Validation results for the JITL modeling method for nominal condition.

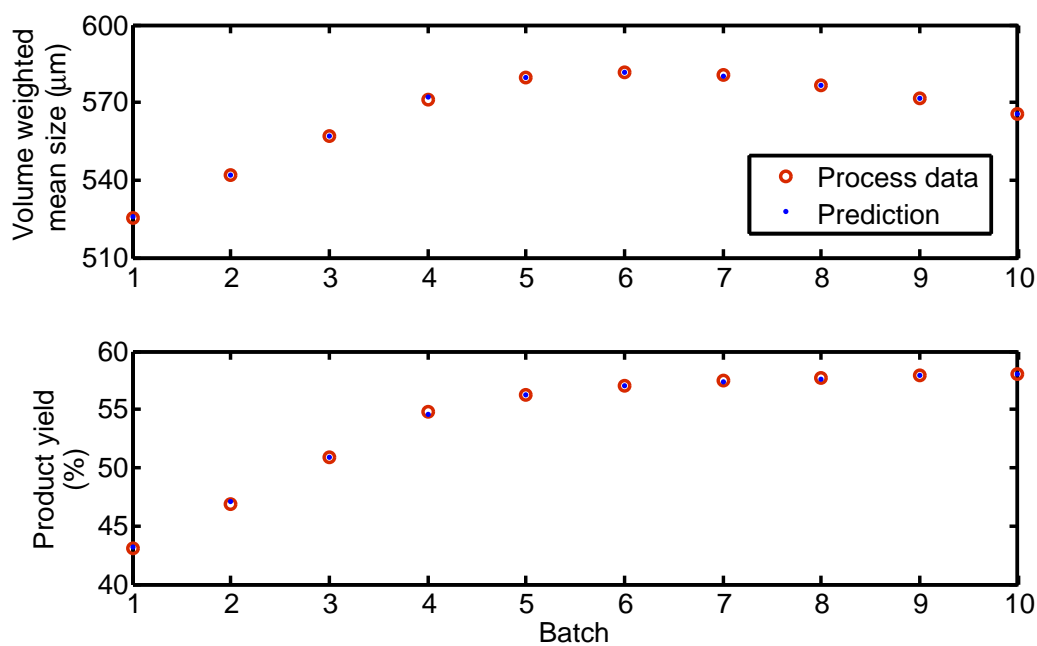
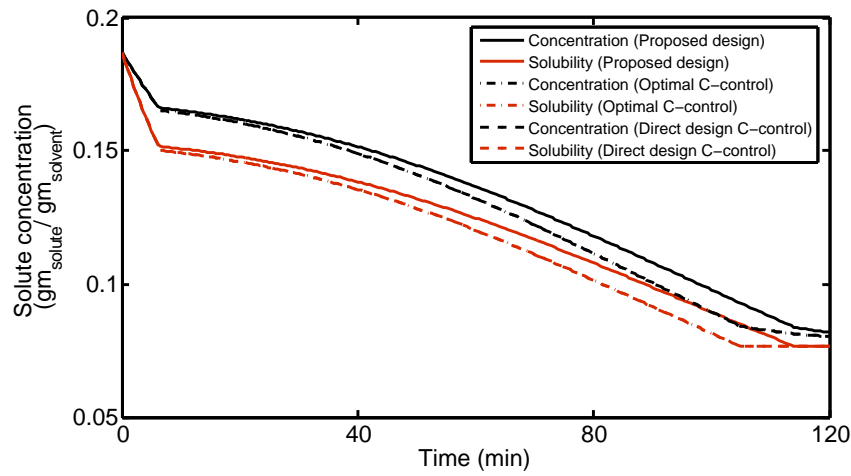
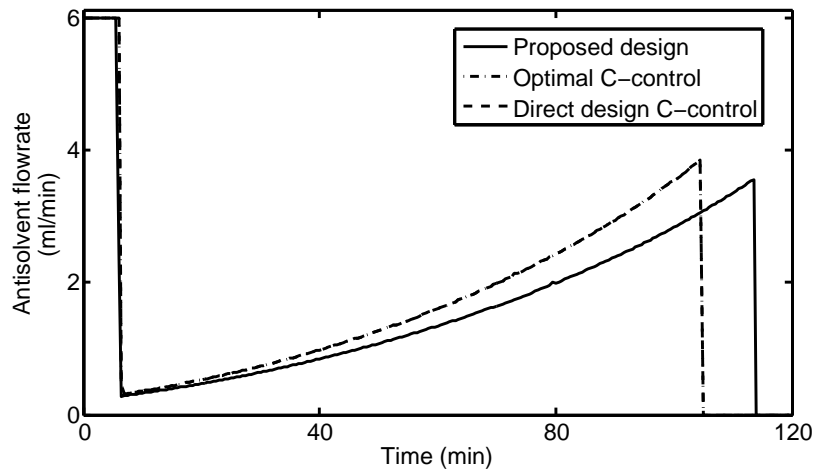


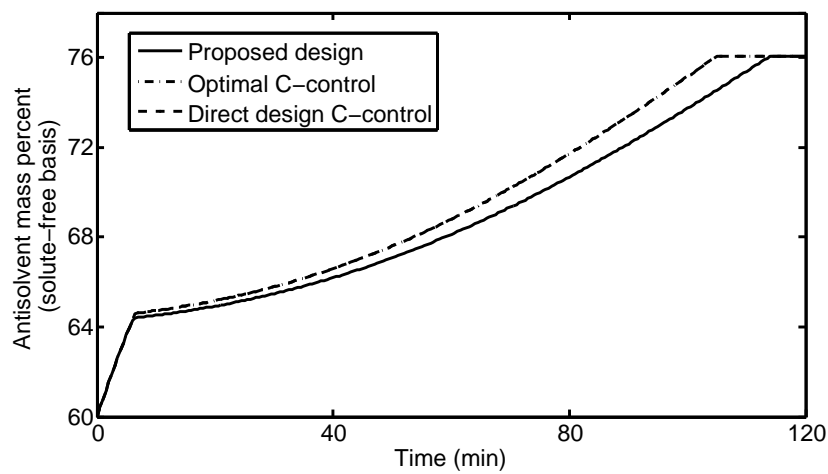
Figure 3.6 Validation results for the LSSVR inner relationship based MPLS model for nominal condition.



(a) Solute concentration profiles

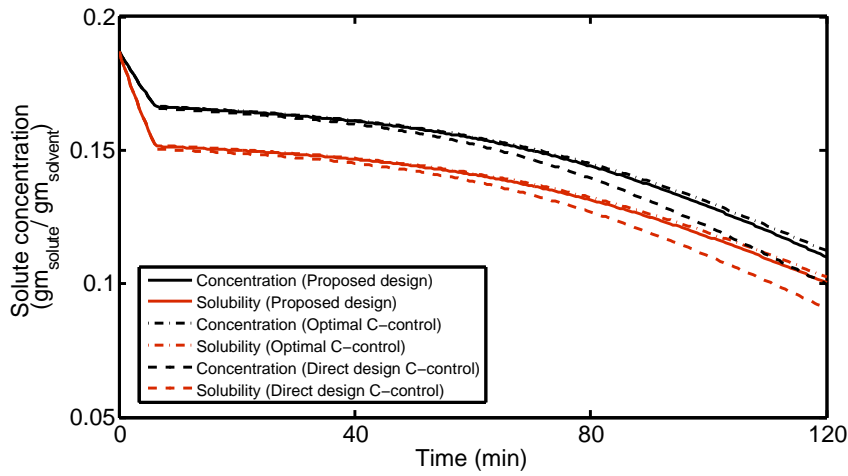


(b) Antisolvent flowrate profiles

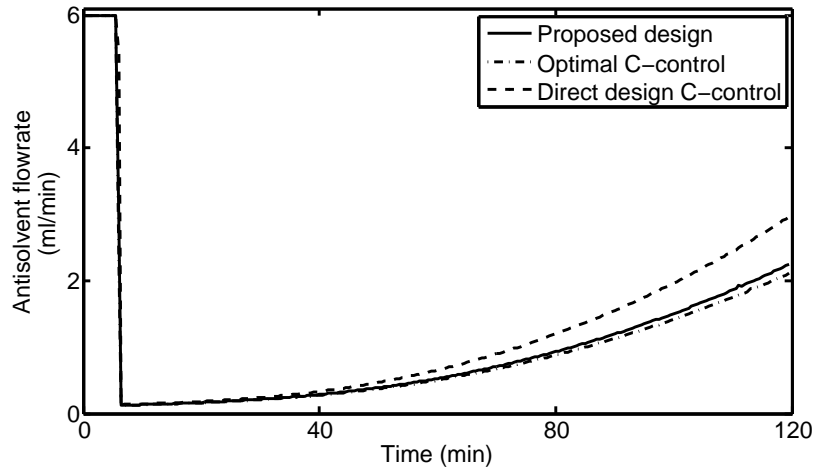


(c) Antisolvent mass percent profiles

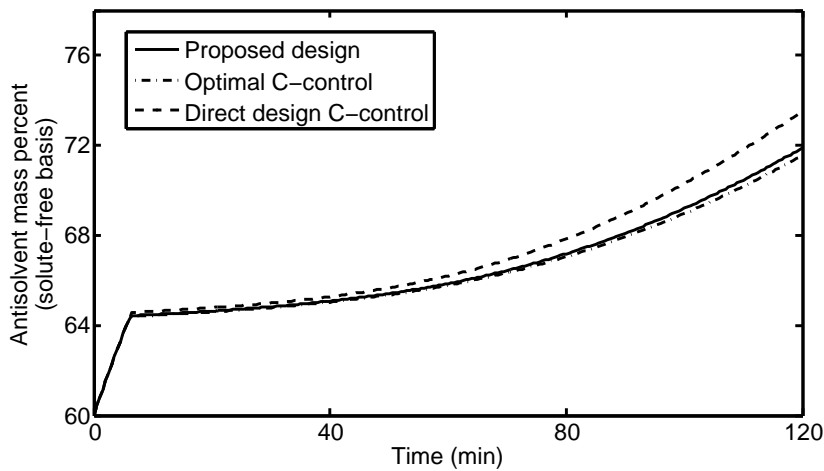
Figure 3.7 Performance of the proposed design, optimal, and direct design C-control for nominal conditions.



(a) Solute concentration profiles

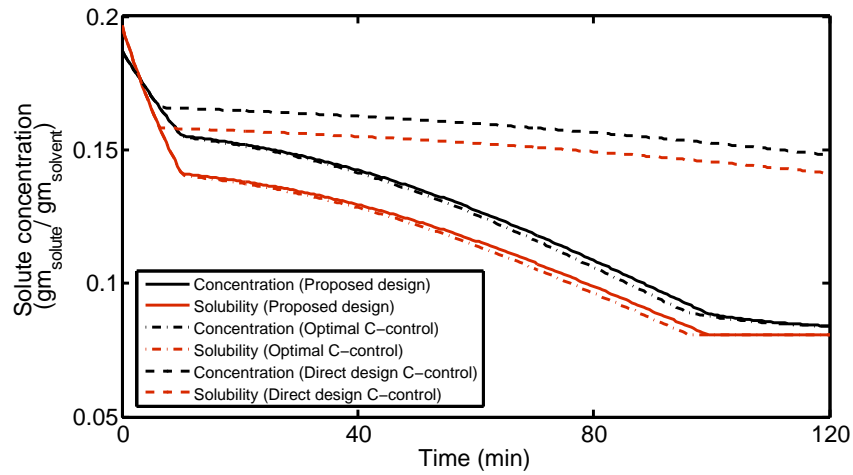


(b) Antisolvent flowrate profiles

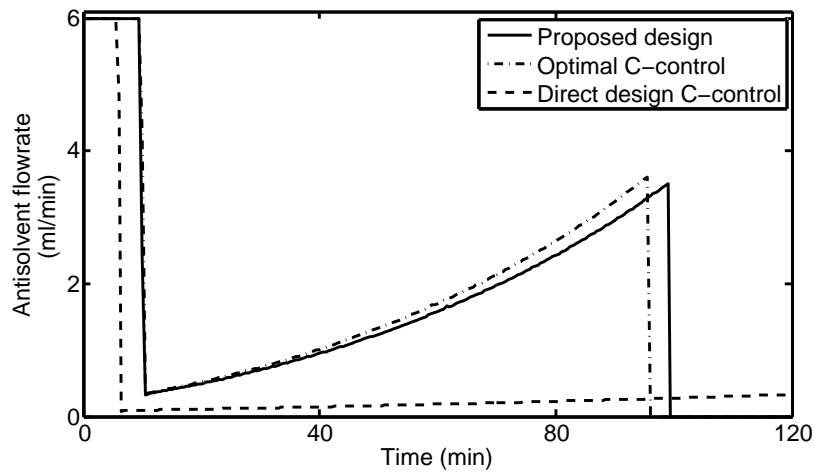


(c) Antisolvent mass percent profiles

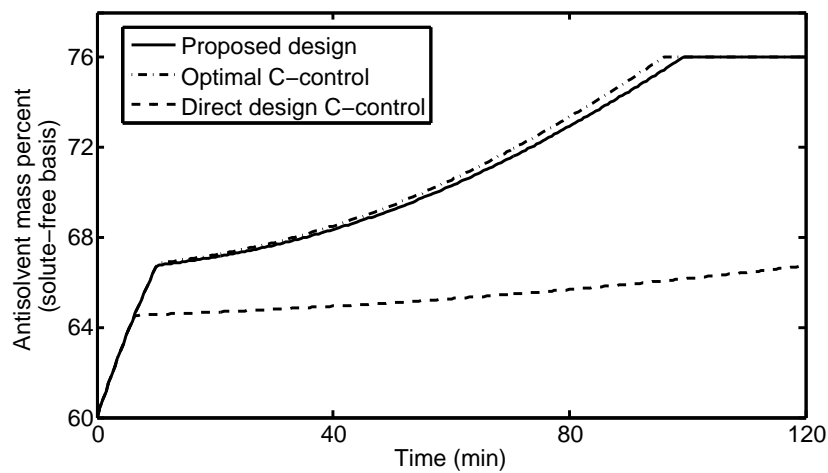
Figure 3.8 Performance of the proposed design, optimal, and direct design C-control for Case 1.



(a) Solute concentration profiles

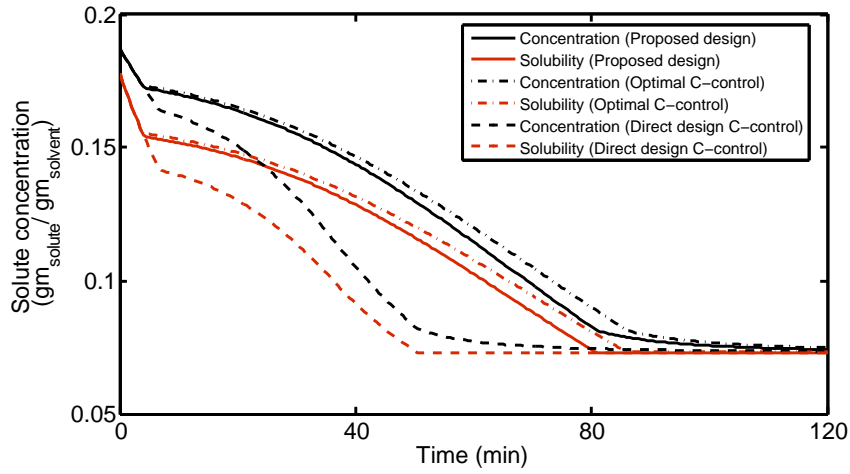


(b) Antisolvent flowrate profiles

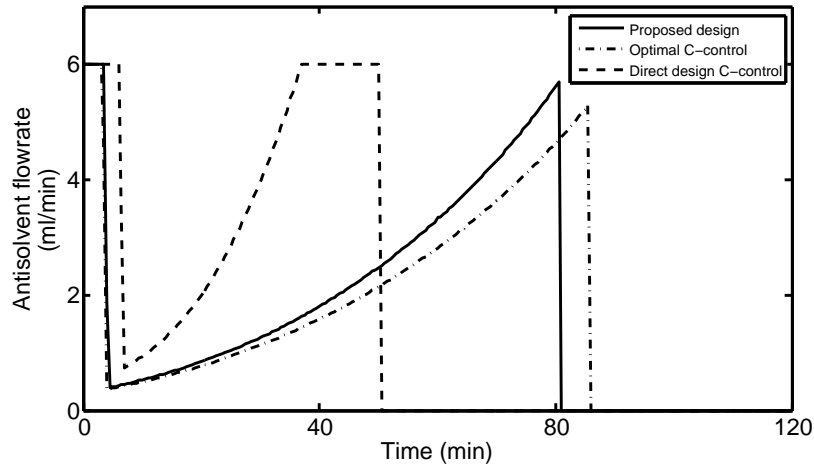


(c) Antisolvent mass percent profiles

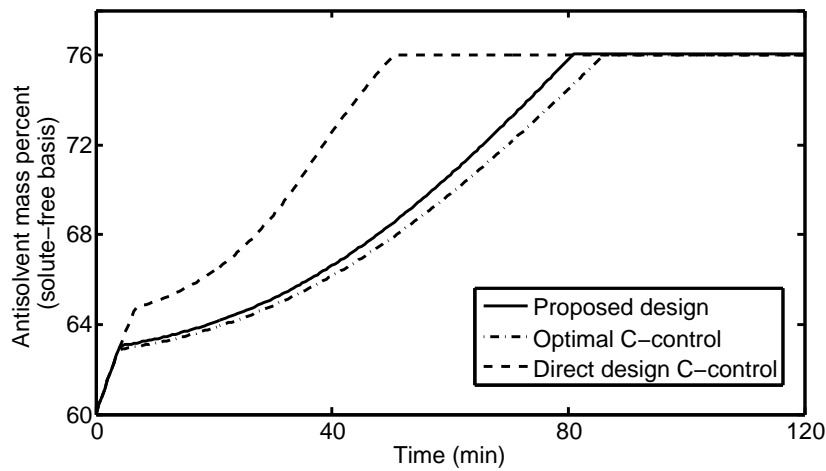
Figure 3.9 Performance of the proposed design, optimal, and direct design C-control for Case 2.



(a) Solute concentration profiles

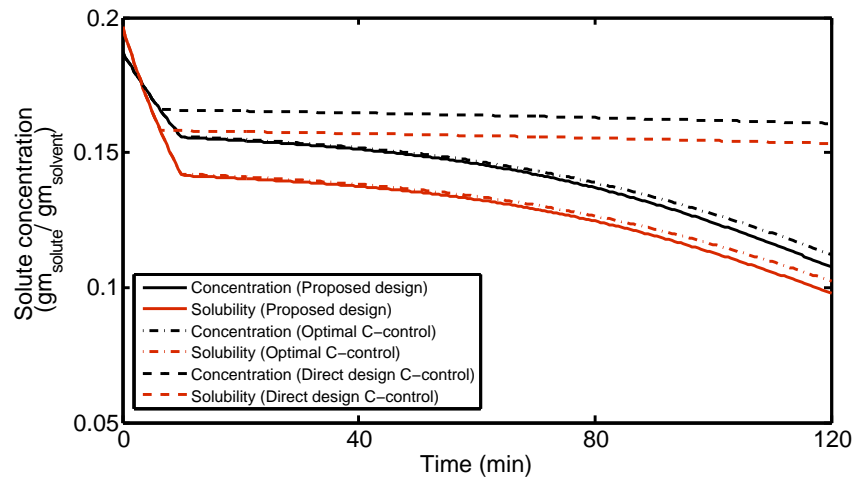


(b) Antisolvent flowrate profiles

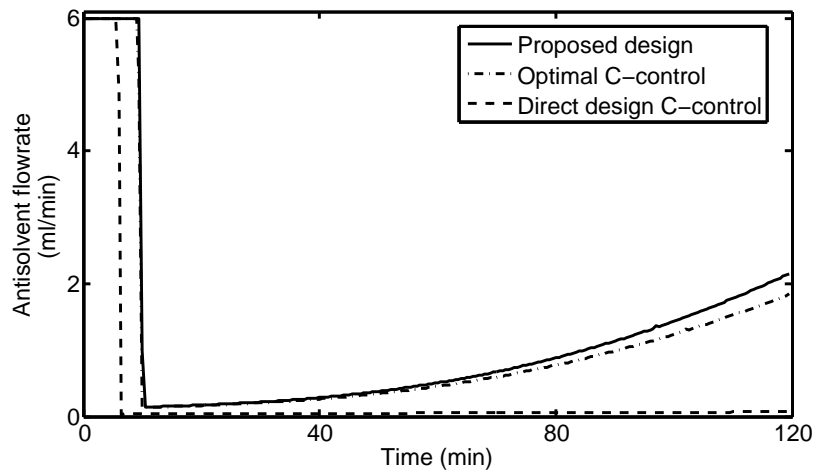


(c) Antisolvent mass percent profiles

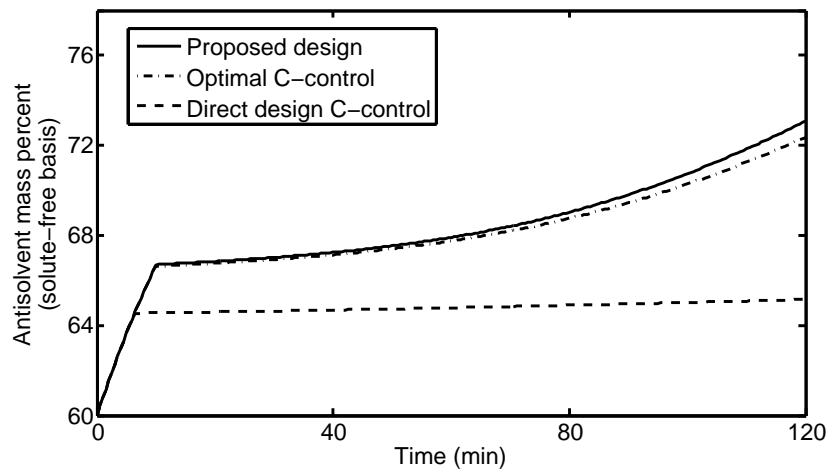
Figure 3.10 Performance of the proposed design, optimal, and direct design C-control for Case 3.



(a) Solute concentration profiles



(b) Antisolvent flowrate profiles



(c) Antisolvent mass percent profiles

Figure 3.11 Performance of the proposed design, optimal, and direct design C-control for Case 4.

3.5 Conclusions

Recognizing the grave necessity of robust control and operation of pharmaceutical (semi-)batch crystallization processes in presence of process variations, a two-staged framework which incorporates pattern classification and nonlinear modeling for product quality is presented. In the first stage, LSSVM based pattern classifier is used. In order to improve its performance, a k nearest neighborhood criterion based LSSVM is used in this study. Furthermore, the JITL modeling method is used for the dynamic modeling of solute concentration, while LSSVM-based MPLS model is used for the product quality predictions. By integrating these methods with the direct design C-control, setpoint value corresponding to the optimal product quality is determined by solving the pre-specified optimization problem. Simulation results show that setpoint determined using the proposed design helps in optimal operation of the semi-batch antisolvent crystallization processes by adapting to process variations, which manifest in the form of high nucleation and growth rates, and also shifts in solubility data.

Chapter 4

Adaptive Concentration Control for Antisolvent Crystallization Processes

In this chapter, the adaptive concentration control strategy is explored, where optimal relative supersaturation setpoint profile at each sampling time during the batch is determined through real-time optimization based on the the proposed integrated modeling framework for the semi-batch antisolvent crystallization process.

4.1 Introduction

As discussed in Chapter 3, the C-control strategy helps in mitigating the occurrence of the spontaneous nucleation events by choosing an appropriate supersaturation setpoint value based on the trial experiments. However, when the *real* process exhibits variations in kinetics and/or shift in solubility data, this strategy may only assure good product yield but not better product quality in terms of mean size or any desired specifications in terms of the product CSD, as it is ignorant of the CSD evolution of the real process (Zhou et al., 2006). Moreover, as the true objective of controlling the process is to obtain uniform crystals with narrow CSD, control strategies based on crystal size measurements along with concentration measure-

ments should be employed to achieve desired product specifications (Nagy et al., 2011a).

One of the techniques for obtaining online CSD measurements is by focused beam reflectance measurement (FBRM) probe (Ruf et al., 2000). FBRM probe provides *in situ* chord length distribution (CLD) measurements of the crystals in the dispersion and requires a model in order to transform the CLD measurements into CSD. Thus, motivated by using the online CSD information, nucleation control strategies based on *indirect* measurements of CSD information using FBRM have also gained importance. In doing so, the CSD, which is the true performance measure of the crystallization processes is controlled directly by suppressing the occurrence of nucleation events during the process (Patience and Rawlings, 2001, Abu Bakar et al., 2009b, Hermanto et al., 2010).

A recent study using a cascaded control strategy with the master controller giving supersaturation setpoints to slave controller based on the number of particle counts per second measurements obtained by FBRM probe. The slave controller subsequently determines the antisolvent mass percent setpoints given to the flow controller based on the supersaturation measurements made by ATR-FTIR. Although this adaptive strategy is robust even towards shifts in the solubility data and high nucleation rates, longer batch time from 2 hours to almost 7 hours is required for some of the scenarios (Woo et al., 2009). This leads to high variability in the batch operation time. Moreover, the implementation procedure of this adaptive strategy lacks a systematic approach to determine the setpoint values as the current practice is based on trial-and-error procedure. Thus, in order to circumvent the shortcoming of this cascaded control strategy, the master controller is replaced with a real-time controller that functions based on the philosophy of model predictive control (Eaton and Rawlings, 1992, Rawlings, 2000, Allgower et al., 2004). Towards this end, the current study provides a systematic approach for adaptive C-control strategy that enables choosing optimal relative supersaturation setpoint

values at each sampling instant through online optimization using the integrated modeling framework as developed in Chapter 3 and the measurements of concentration and number of particle counts per second as illustrated in Figure 4.1. Therefore, modifications must be made to the framework proposed in Chapter 3, in order to be suitable for online application.

Furthermore, realizing that the type of control vector parametrization (CVP) employed for the relative supersaturation setpoint profile over the remaining batch time during the online optimization has significant effect on the resulting product quality, geometric progression spacing is employed for this study, which will be highlighted through the case studies discussed in the subsequent sections.

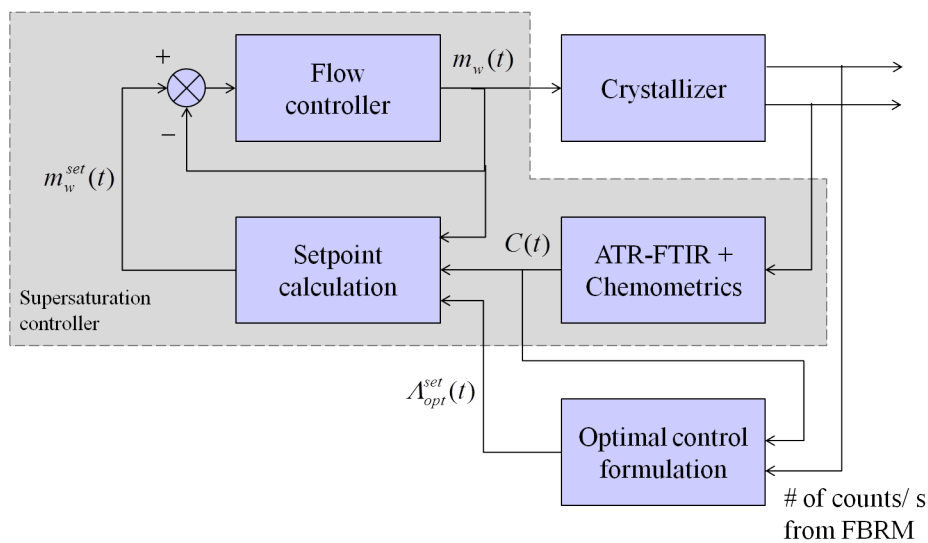


Figure 4.1 Adaptive concentration control strategy.

The rest of the chapter is organized as follows: Section 4.2 introduces the different techniques used in the proposed modeling framework for its online application, along with the necessary background information. Based on the results obtained through the implementation of the proposed methodology for various case studies considered, Section 4.3 presents the relevant discussions, which is followed by the concluding remarks given in Section 6.4.

4.2 Methodologies

This section provides the necessary background information for the techniques used in order for the proposed modeling framework to suit the online application. In short, the process data and the methodology of the LSSVM based classification presented in Section 3.3.1 must be modified in order to be used for pattern recognition based on online measurements.

4.2.1 On-line pattern classification

As most of the batch process data exhibit complexities in terms of high nonlinearity, presence of high autocorrelation and cross-correlation among different process variable at any given time during the batch, makes the application of standard PCA impossible. Therefore, MPCA is used as a standard multivariate statistical method to transform a set of unfolded observations, both the variables and their corresponding time histories, into a set of linearly uncorrelated variables. The first step of the framework requires the application of MPCA for reducing the dimensionality of the process data.

For example, consider the historical process data is represented as a three-dimensional array \mathbf{X} ($I \times J \times K$), where I is the number of batches, J is the number of process variables, and K is the number of sampling intervals during the batch. The batch-wise unfolding into a two-dimensional matrix is carried out as shown in Eq. (3.31) (Nomikos and MacGregor, 1994). Now, these JK variables in each row of X are treated as independent variables and are auto-scaled using the corresponding values of mean and standard deviation. Thus, in order evaluate the behavior of any new batch data using MPCA, the entire trajectory of the corresponding process variables x_{new} ($1 \times KJ$) must be made available. However, during its online application, only part of the trajectory of the measured variables is

available. For instance, at a given sampling instant k , the dimensionality of x_{new} is $1 \times kJ$, and the missing $1 \times (K - k)J$ future observations are unavailable.

Several methods including projection to the model plane (PMP) method, single component projection (SCP), and conditional mean replacement (CMR) method are discussed in the literature (Nomikos and MacGregor, 1995a, Nelson et al., 1996). Based on the PMP method, the new vector of observations with missing data are projected onto the plane defined by the model of principal components and thus, the resulting missing part of the data vector would be consistent with the model (Golshan et al., 2010). However, at the beginning of a new batch, this method can give t scores that are reluctant and far more different from the true values because of the limited information available (Nomikos and MacGregor, 1995b).

Due to the aforementioned limitation, an advancing window method that considers all the past observations X_k from the current time instant t_k as shown in Figure 4.2 is used as the input for the MPCA model. The first np scores and the corresponding Y_{class} data are then used for training the LSSVM based pattern classifier. Thus, for online pattern classification, the np scores corresponding to the projection of the process variables x_{new} at each sampling instant are used for determining the specific dynamics of the current batch.

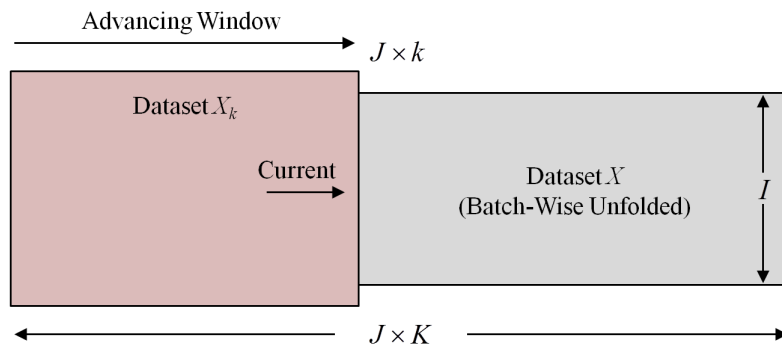


Figure 4.2 Advancing window MPCA.

Thus, the relevant data set is selected from the database using the LSSVM based pattern classifier. Subsequently, JITL based low-order ARX models of the form

shown in Eq. (4.1) are used for nonlinear dynamic modeling of solute concentration and number of crystals.

$$\hat{y}(k) = \alpha_1^k y(k-1) + \beta_1^k u(k-1), \quad (4.1)$$

where $\hat{y}(k)$ is the predicted output by the JITL model at the k th sampling time, $y(k-1)$ and $u(k-1)$ are the output and input variables at the $(k-1)$ th sampling time, respectively, and α_1^k , α_2^k and β_1^k are the model coefficients at the k th sampling time. The product quality values are predicted based on the LSSVR-based MPLS model as discussed earlier in Section 3.3.3. Thus, the two dimensional process variable matrix \mathbf{X} containing the process variables of the entire batch and the corresponding product quality data \mathbf{Y} are used to train the nonlinear MPLS model. Therefore, during the online application, the query vector to the nonlinear MPLS model is obtained as shown in Eq. (4.2)

$$x_{new} = [x_{p,new} \ x_{f,new}], \quad (4.2)$$

where x_{new} is the query vector of the new batch at the current sampling time t_k , $x_{p,new}$ is the vector of past measurements from the start of the batch to the current sampling time t_k , and $x_{f,new}$ is the vector of future process variables predicted using the aforementioned JITL based ARX models from the sampling time t_{k+1} to the end of batch t_f .

4.2.2 Proposed framework

Figure 4.3 shows the flow sheet depicting the proposed methodology for online pattern recognition and nonlinear modeling of semi-batch antisolvent crystallization process. Therefore, during the implementation of the adaptive C-control strategy, the LSSVM based pattern classifier recognizes the specific dynamics of the current

processes based on online process data. Thus, a subset of the complete database is selected as the relevant database for the prediction of solute concentration, number of crystals, (using JITL framework) and product quality values (using nonlinear MPLS model). Thus, they serve as the model necessary for the real-time controller, which finds the solution of the optimal control formulation online. The results and discussion following the implementation of the proposed adaptive C-control strategy is presented in Section 4.3.

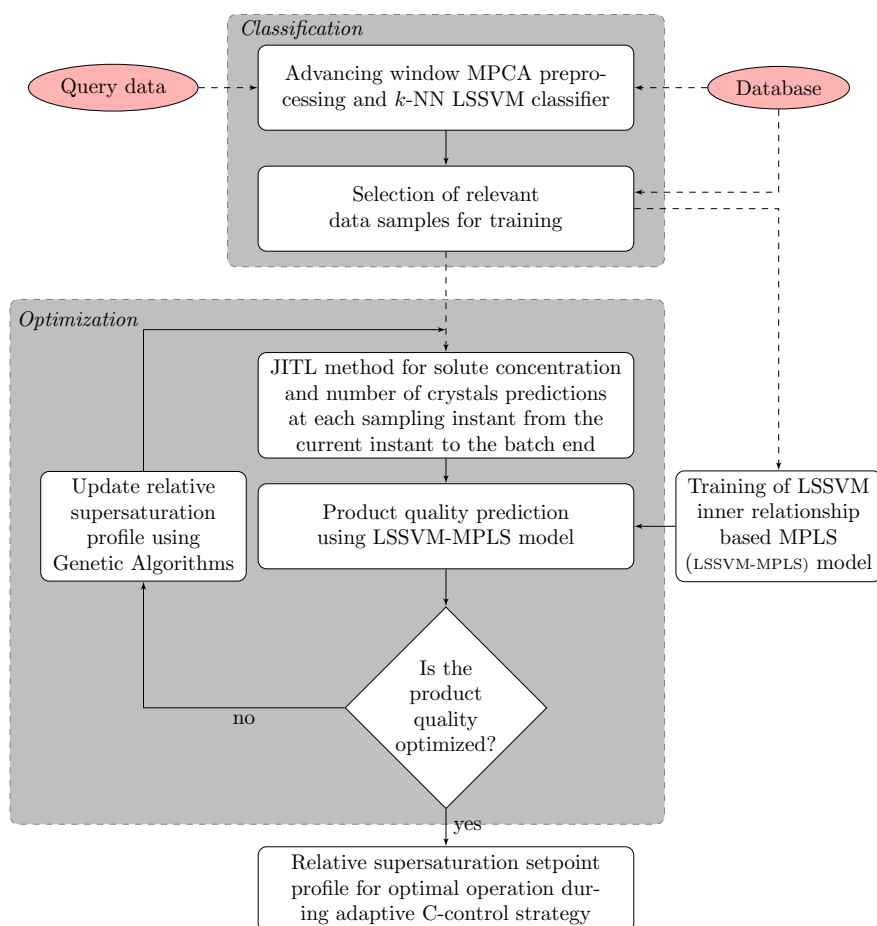


Figure 4.3 Proposed data-based modeling framework for online application.

4.3 Results and discussions

As illustrated in the Chapter 3.4, the optimality loss due to the implementation of direct design C-control in presence of process variations can be recovered by adapting the constant relative supersaturation setpoint. Thus, following the same direction, the current study focuses on online adaptation of the setpoint values based on real-time optimization and measurement feedback of the solute concentration and number of crystal counts. Therefore, the vector of relative supersaturation setpoints is parameterized over the entire batch duration, and thus providing the flexibility to change the setpoint at any given point during the batch.

Towards this end, two parameterization approaches for the control vector are considered in this study – (i) with linearly spaced equidistant intervals, and (ii) with geometric progression series corresponding to the interval spacing. The complete batch time is segmented into twelve intervals and the setpoints are piecewise constant within these intervals. Figure 4.4 shows a sample profile parameterized using both these methods. Moreover, at the start of any batch, the process is assumed to be at nominal conditions, the relative supersaturation setpoint is always kept at the nominal value of 0.101.

A comparative study using precisely known first principles models is carried out to understand the effect of these two parameterization methods. Now, for a given value of the desired number of crystals, the optimization problem as shown in Eq. (4.3) is solved at the current sampling instant t_k by considering piecewise constant values of the decision variable, $\Lambda^{set}(t)$ over the complete prediction horizon $[t_k, t_f]$. Thus, by minimizing the deviations between the desired and the predicted values of the crystal counts and simultaneously maximizing the product quality values, the relative supersaturation setpoint at each sampling instant is found through the closed-loop optimization. Furthermore, following the philosophy of MPC, the first control move $\Lambda^{set}[t_k, t_f]$ is implemented to the real process and this routine is

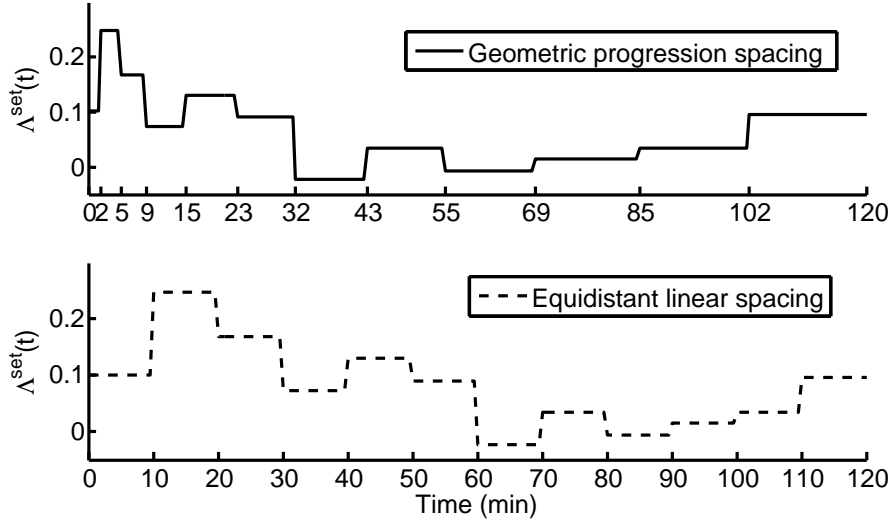


Figure 4.4 Illustration of equidistant linear and geometric progression spacing methods for CVP of relative supersaturation setpoint profile.

repeated at each sampling instant.

$$\min_{\Lambda^{set}[t_k, t_f]} J(t) = -\mathbf{W}_1 P_{size}(t_f) + \mathbf{W}_2 \sum_{i=1}^K e_i, \quad (4.3)$$

where $P_{size}(t_f)$ is the product quality in terms of mean size obtained at the batch end, e_i is the deviation term as defined in Eq. (4.4).

$$e_i = \begin{cases} n_c(i) - n_{c,max}, & \text{if } n_c(i) > n_{c,max} \\ 0, & \text{otherwise} \end{cases}, \quad \text{where } i = 1, 2, \dots, K \quad (4.4)$$

where n_c is the number of crystals, $n_{c,max}$ is the maximum number of crystals allowed, which is chosen to be 1.5×10^5 , and e_i is the absolute deviation between the number of crystals at each sampling time and the maximum number of crystals. The weights $\mathbf{W}_1 = 1$, and $\mathbf{W}_2 = 10^{-5}$ are chosen during this study. The results obtained through the implementation of the proposed adaptive C-control strategy considering the two different parameterization methods are presented in Table 4.1.

As can be inferred from the product quality values, the optimal adaptive C-control based on geometric progression spacing outperforms the rest of the ap-

proaches for all the scenarios. Moreover, the antisolvent mass percent profiles resulting from the implementation of these two approaches for all the case studies, along with the corresponding true optimal profiles are shown in Figures 4.5 to 4.8. It can be seen that the profiles resulting from the implementation of the adaptive C-control with CVP based on geometric progression spacing is always close to the true optimal profiles.

For Cases 2 and 4 as seen in Figures 4.6 and 4.8, it can be observed that the adaptive C-control strategy implemented using CVP based on equidistant spacing stays very close to the true optimal profile throughout the batch time, apart from its deviation during the initial phase and also towards the end. Besides, as the nucleation and growth kinetic rates tend to decrease with increasing antisolvent mass percent in the crystallizer, the effect of aforementioned deviations in the antisolvent mass percent profiles during the initial phase of the batch has significant impact on the final product quality (Granberg et al., 1999, 2001, Granberg and Rasmuson, 2005). Therefore, the choice of geometric progression spacing based CVP provides greater flexibility by choosing higher decision variables in the initial phase of the crystallization process. Thus, understanding its suitability to the antisolvent crystallization process, the use of geometric progression spacing based CVP of the relative supersaturation setpoint profile is considered in the subsequent studies.

Table 4.1 Comparison between optimal adaptive C-control strategy based on equidistant linear and geometric progression spacings.

Case	True optimal	Nominal profile	Direct design C-control	Optimal adaptive C-control	
				Linear	Geometric
Nominal	599.94	599.94	581.78	585.53	597.92
1	329.23	257.79	266.37	278.29	307.78
2	577.31	555.15	357.46	561.68	575.16
3	619.32	546.84	455.92	458.85	606.66
4	339.73	247.29	262.47	300.60	325.99

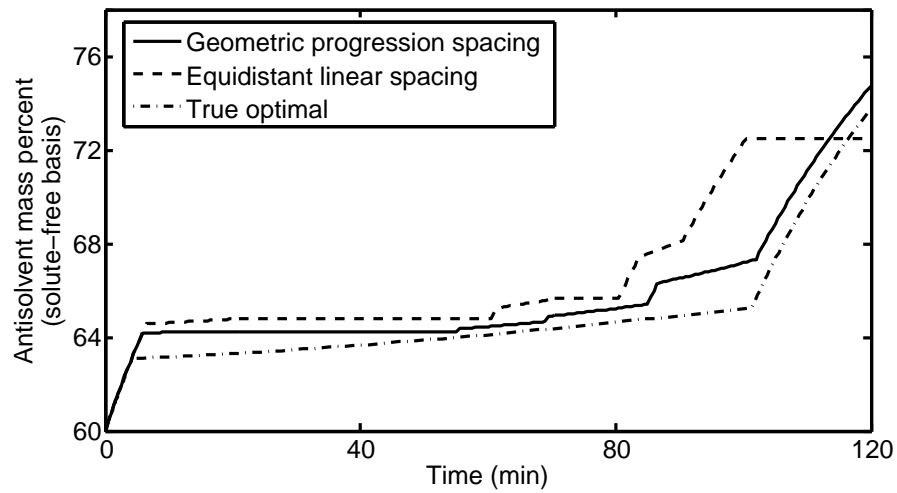


Figure 4.5 Response of geometric progression and equidistant spacing based adaptive C-control strategy for Case 1.

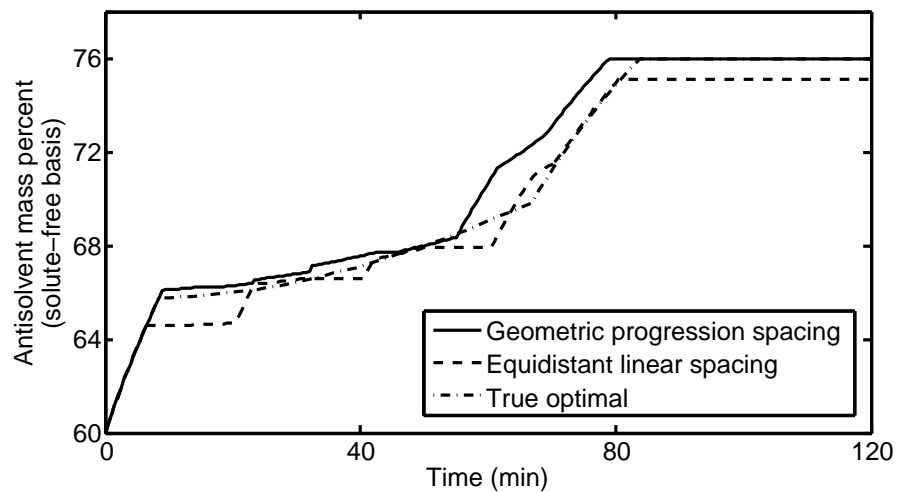


Figure 4.6 Response of geometric progression and equidistant spacing based adaptive C-control strategy for Case 2.

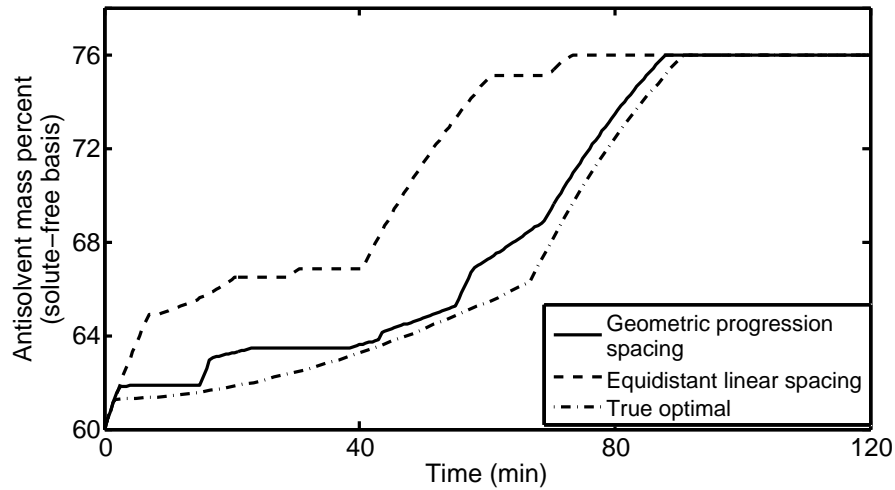


Figure 4.7 Response of geometric progression and equidistant spacing based adaptive C-control strategy for Case 3.

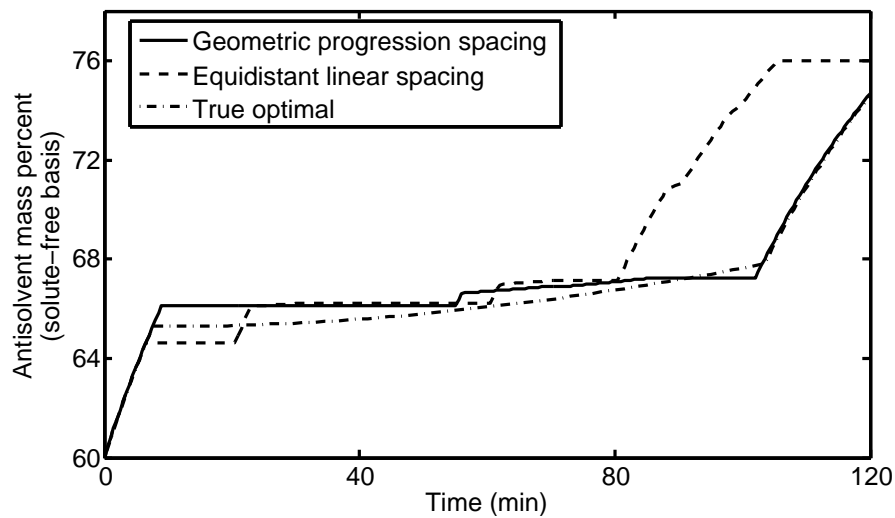


Figure 4.8 Response of geometric progression and equidistant spacing based adaptive C-control strategy for Case 4.

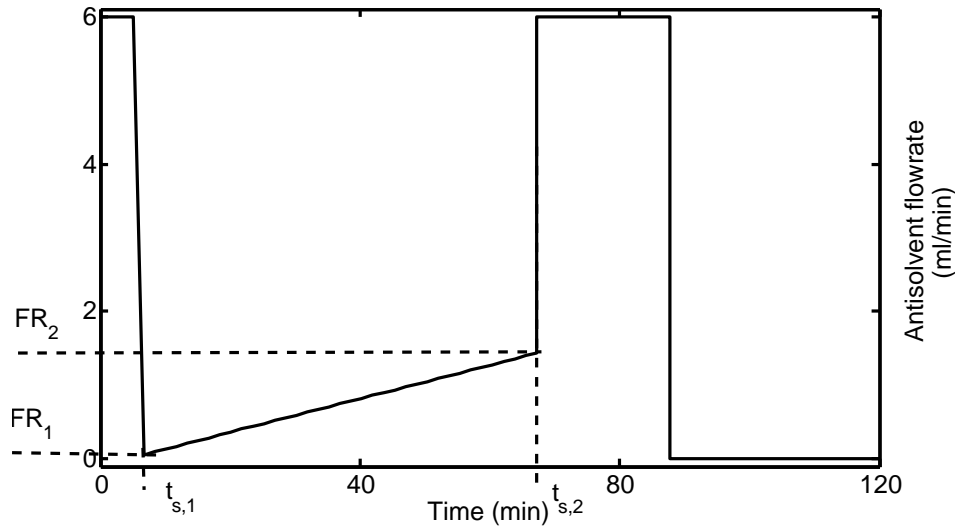


Figure 4.9 Parameters characterizing the nominal antisolvent flowrate profile.

In order to generate the required database for developing the data based models, various open loop experiments were designed by perturbing the two switching instants $t_{s,1}$ and $t_{s,2}$, and the corresponding flowrate values FR_1 and FR_2 of the nominal antisolvent flowrate profile as shown in Figure 4.9. Towards this end, a full factorial design of experiments methodology was used by selecting five values for each of these four parameters within the $\pm 100\%$ neighborhood of the corresponding nominal values.

For the purpose of training the LSSVM based pattern classifier, a similar approach as discussed earlier in Section 4.2.1 is considered. The first np principal components of the unfolded training data set X containing the antisolvent masspercent and solute concentration data until the current sampling instant k forms the input, and the corresponding output vector Y_{class} containing the information regarding the specific class of dynamics to which each of these I batches belong forms the output. Thus, once the specific class of the new test data x_{new} is determined, all the batch data in the database that belong to this class of dynamics are selected as *relevant* data for the subsequent dynamic modeling and product quality predictions.

For the prediction of solute concentration and number of crystals during the

batch, first order ARX models as shown below in Eq. (4.5) are considered.

$$\begin{aligned}\hat{C}(k+1) &= \alpha_C C(k) + \beta_C m_w(k), \\ \hat{n}_c(k+1) &= \alpha_n n_c(k) + \beta_n m_w(k),\end{aligned}\quad (4.5)$$

where $\hat{C}(k+1)$ and $\hat{n}_c(k+1)$ are the predicted solute concentration and number of crystals for the $(k+1)$ th sampling time, respectively. α_C , α_n , β_C , and β_n are the parameters of the two ARX models.

Figure 4.10 shows sample of twenty five batches of nominal process data that are used to construct the reference data set for the JITL method. For the purpose of validating the predictive ability of the ARX models based on JITL method, additional eight batches data that is different from the reference data set for the nominal process is generated as shown in Figure 4.11. During this study, the JITL parameters $k_{min} = 8$, $k_{max} = 60$, and $\kappa = 1$ were chosen. Figures 4.11 and 4.13 show the good predictive performance of JITL method for solute concentration and number of crystals during the batch.

Using the unfolded process data as shown in Eq (3.44), the nonlinear MPLS model is trained using the entire batch data corresponding to the antisolvent mass percent and solute concentration is considered as the input X_p and the corresponding product quality Y as the output. Thus, model of the form shown in Eq. (3.46) is developed using the relevant data. For the purpose of validation, process data corresponding to the validation batches are used and the corresponding results are shown in Figure 4.14.

The aforementioned data-based modeling techniques for the prediction of solute concentration and number of crystals during the batch, along with end-of-batch product qualities are used as the process model inside the adaptive C-control framework. Thus, the solution of Eq. (4.6) serves to find the optimal relative supersatura-

tion setpoint at each sampling instant t_k .

$$\begin{aligned}
& \min_{\Lambda^{set}[t_k, t_f]} J = -\mathbf{W}_1 \hat{P}_{size}(t_f) + \mathbf{W}_2 \sum_{i=1}^K e_i, \\
\text{s.t. } & \hat{C}(k) = \alpha_C C(k-1) + \beta_C m_w(k-1), \quad \forall k = k+1, k+2, \dots, K, \\
& \hat{n}_c(k) = \alpha_n n_c(k-1) + \beta_n m_w(k-1), \quad \forall k = k+1, k+2, \dots, K, \\
& \hat{P}(t_f) = \Psi(X_p), \quad \text{where } \hat{P}(t_f) = [\hat{P}_{yield}(t_f), \hat{P}_{size}(t_f)], \\
& \hat{P}_{yield}(t_f) \geq 40,
\end{aligned} \tag{4.6}$$

where $\Lambda^{set}[t_k, t_f]$ is the decision variable for the constrained minimization problem J , and the last constraint is imposed by the minimum product yield at the batch end, and e_i is the deviation term as defined in Eq. (4.4). The weights $\mathbf{W}_1 = 1$, and $\mathbf{W}_2 = 10^{-5}$ are chosen during this study.

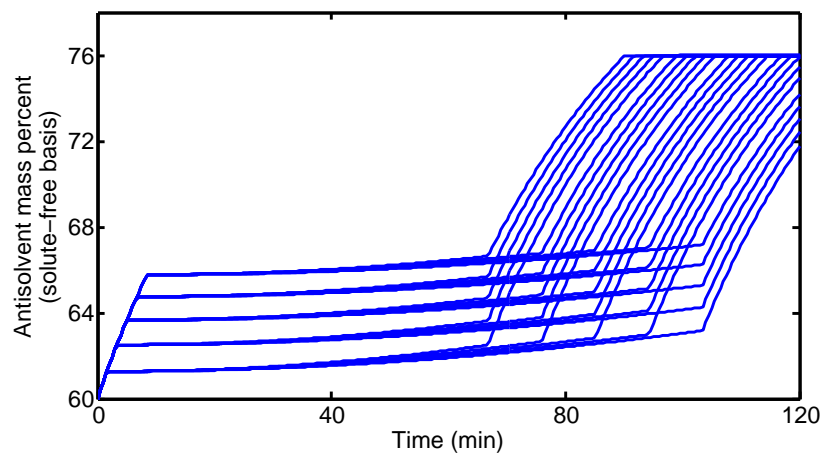
The product quality values obtained from the implementation of optimal adaptive C-control strategy that assumes precisely known first-principles models for all the five cases studies is used as a benchmark to compare the performance of the proposed design. Besides, the nominal adaptive C-control strategy the considers nominal model for all the cases is also presented, in order to illustrate the importance in adapting the relative supersaturation setpoints based on the dynamics of the real process.

From Table 4.2, it can be seen that the proposed C-control strategy is effective in steering the process towards true optimal values. Furthermore, the performance of nominal adaptive C-control is always poorer than the proposed design, which explains the importance of incorporating the pattern classifier into the modeling framework. Therefore, the selection of the relevant data set for modeling the solute concentration and number of crystals, and the product quality plays an important role in the implementation of the proposed design. Figures 4.15 to 4.18 present the corresponding solute concentration, antisolvent mass percent, and the relative

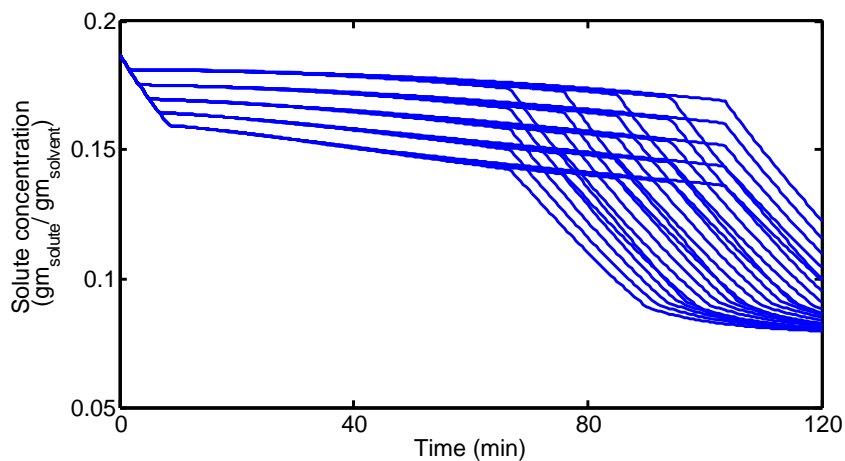
supersaturation setpoint profiles during the implementation of the aforementioned adaptive C-control strategies. It can be noticed that the proposed design and the optimal adaptive C-control strategies perform close to each other, thus being consistent with the obtained product quality values. For Cases 2 and 3, the nominal adaptive C-control drives the process away from the direction of optimality as can be seen from the antisolvent mass percent profiles depicted in Figures 4.16(b) and 4.17(b), consequently leading to poor product quality towards the batch end. Furthermore, similar to direct design C-control, the nominal adaptive C-control strategy also suffers from the limitation of not being able to adapt to shifts in solubility data. Therefore, the implementation of the proposed design not only assures robustness towards shifts in solubility data and perturbations in kinetic rates, but also ensures optimal operation of the semi-batch antisolvent crystallization processes.

Table 4.2 Comparison between proposed design, optimal and nominal adaptive C-control strategies.

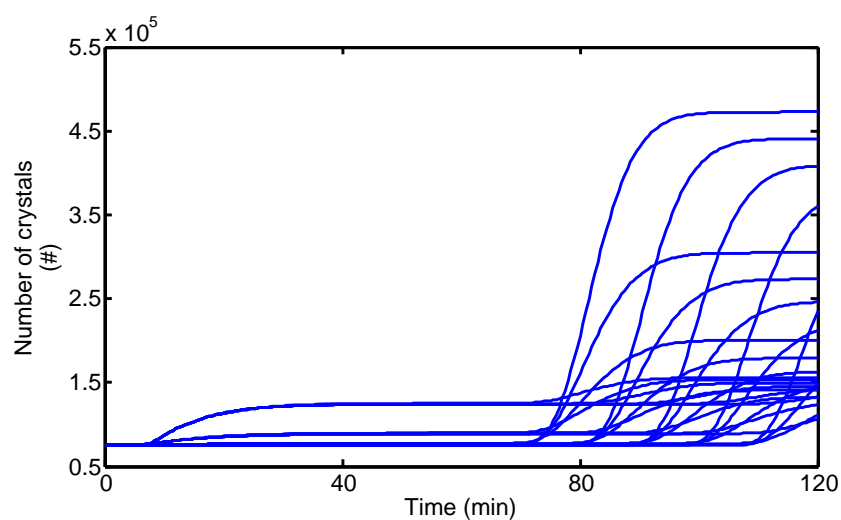
Case	Proposed design		Nominal		Optimal	
	P_{size} (μm)	P_{yield} (%)	P_{size} (μm)	P_{yield} (%)	P_{size} (μm)	P_{yield} (%)
Nominal	590.06	57.19	597.92	57.29	597.92	57.29
1	300.69	50.03	290.93	55.59	307.78	46.35
2	574.13	55.47	485.33	47.74	575.16	55.51
3	603.66	59.01	501.48	60.49	606.66	59.67
4	308.93	44.09	312.25	34.82	325.99	42.56



(a) Antisolvent mass percent profiles



(b) Solute concentration profiles



(c) Number of crystals profiles

Figure 4.10 Illustration of twenty five batches of nominal process data used to construct reference database for the JITL method.

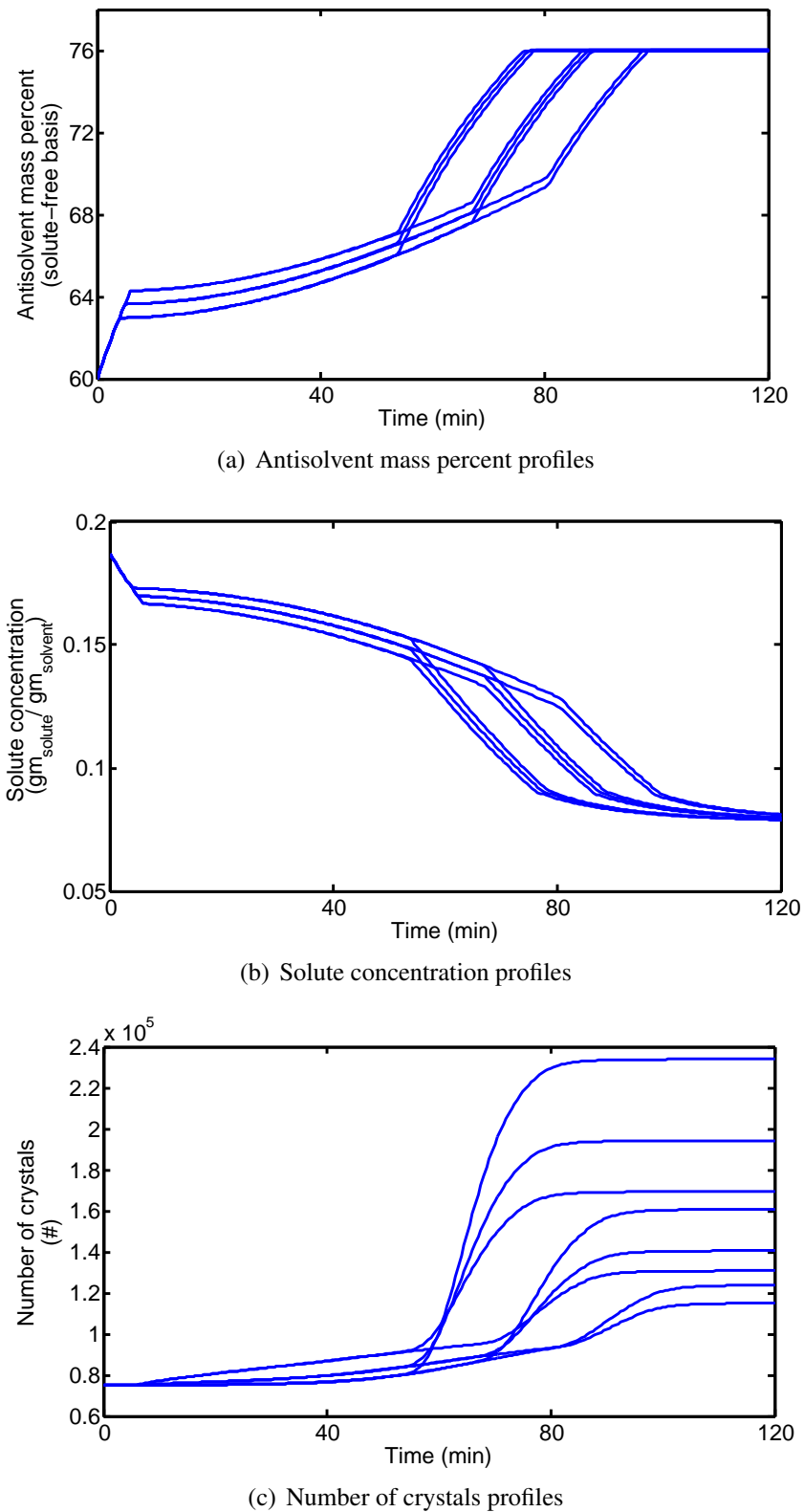


Figure 4.11 Illustration of eight batches of nominal process data used for validation of the JITL method.

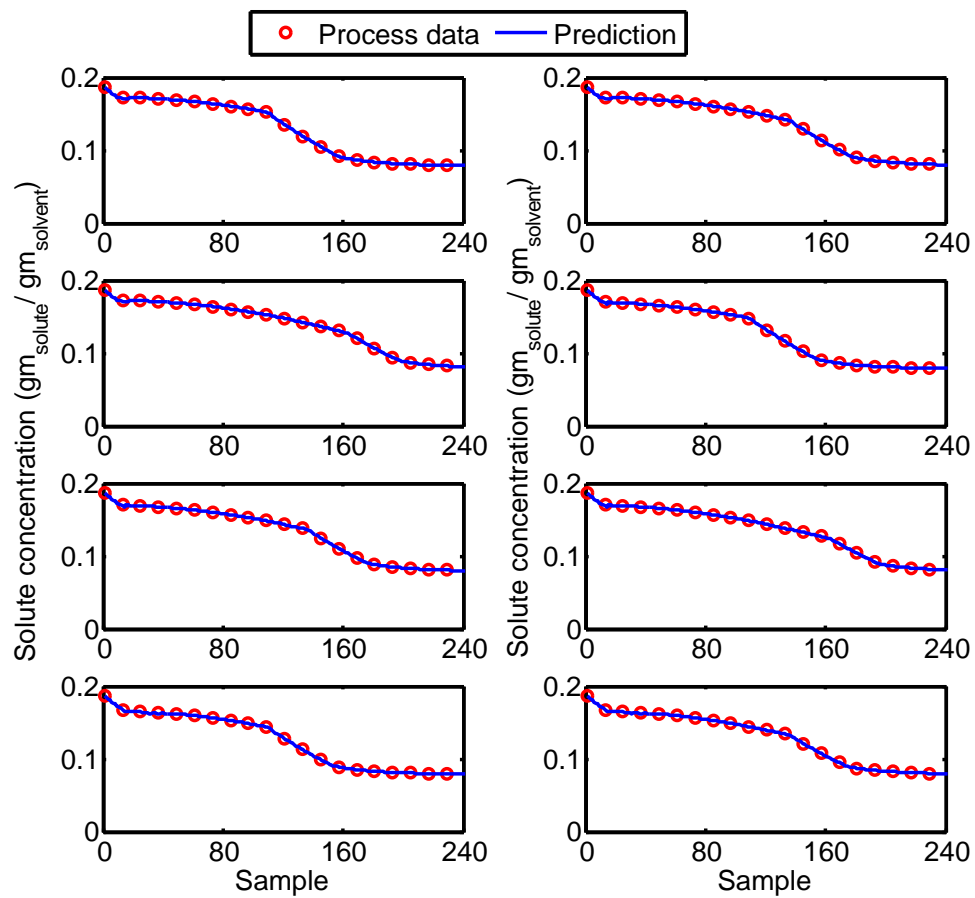


Figure 4.12 Validation results for the JITL modeling method for solute concentration predictions for nominal condition.

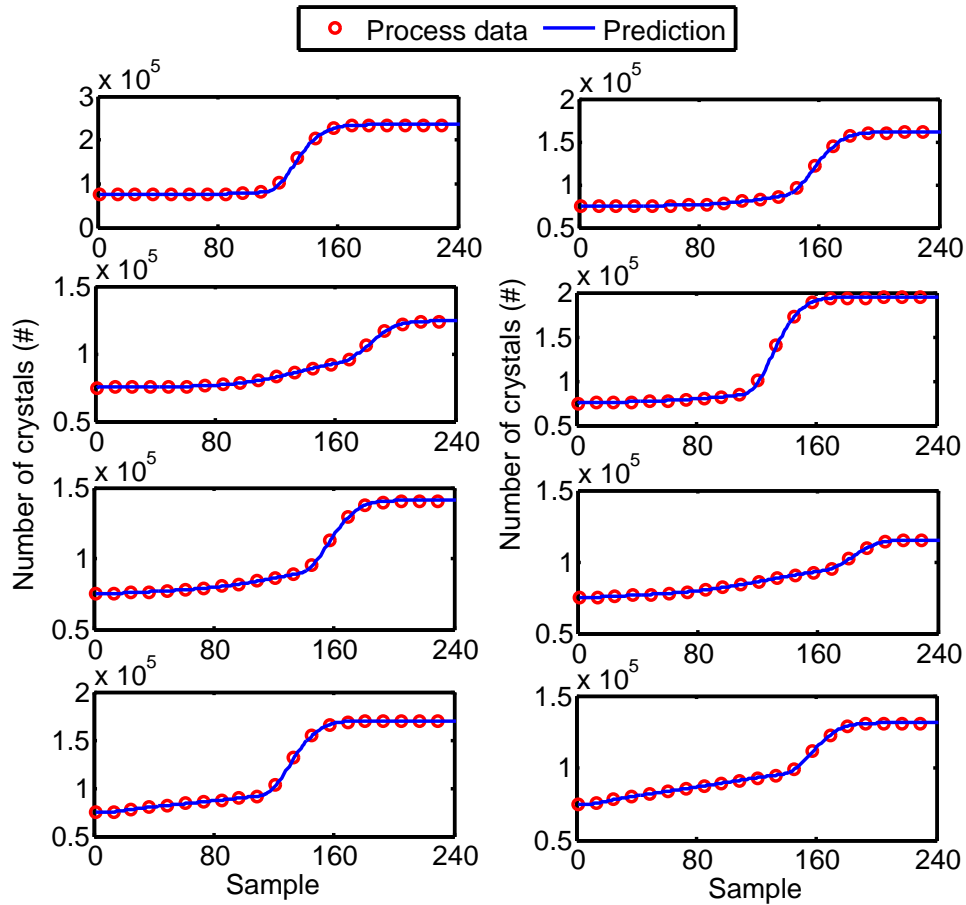


Figure 4.13 Validation results for the JITL modeling method for number of crystals predictions for nominal condition.

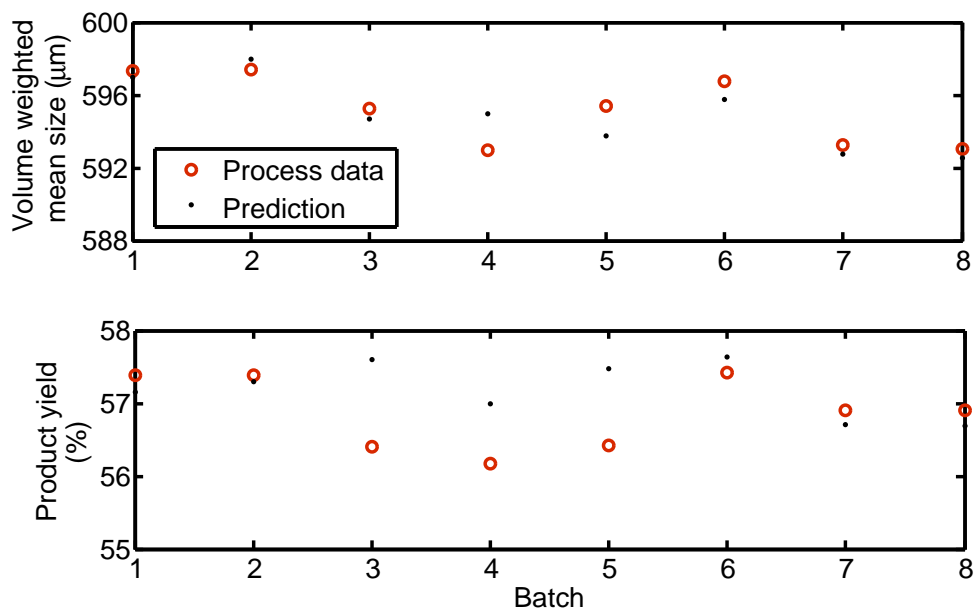
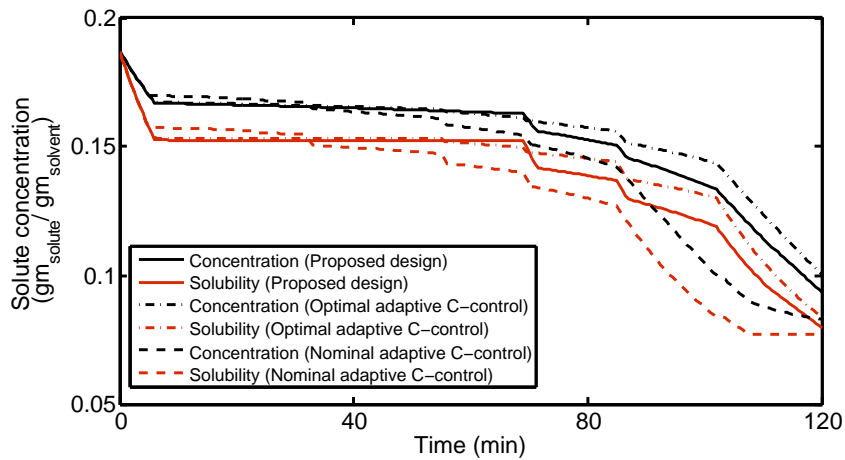
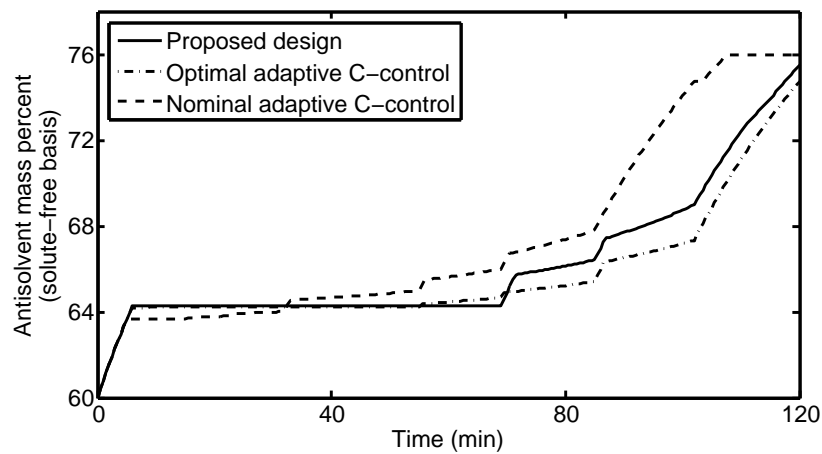


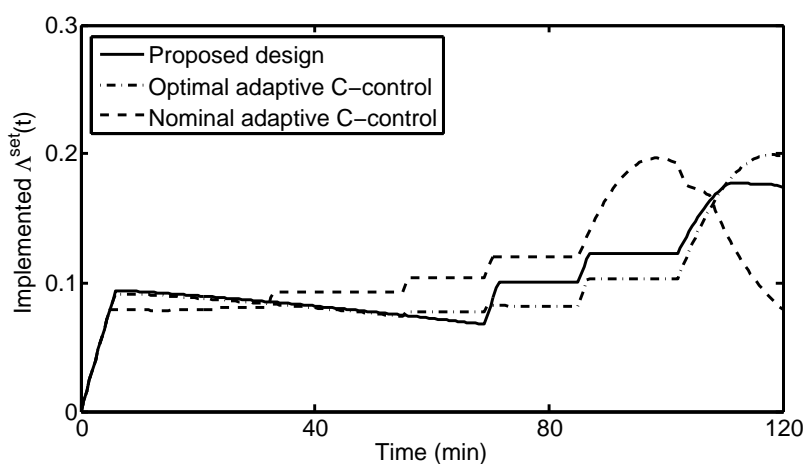
Figure 4.14 Validation results for the LSSVR inner relationship based MPLS model for nominal condition.



(a) Solute concentration profiles

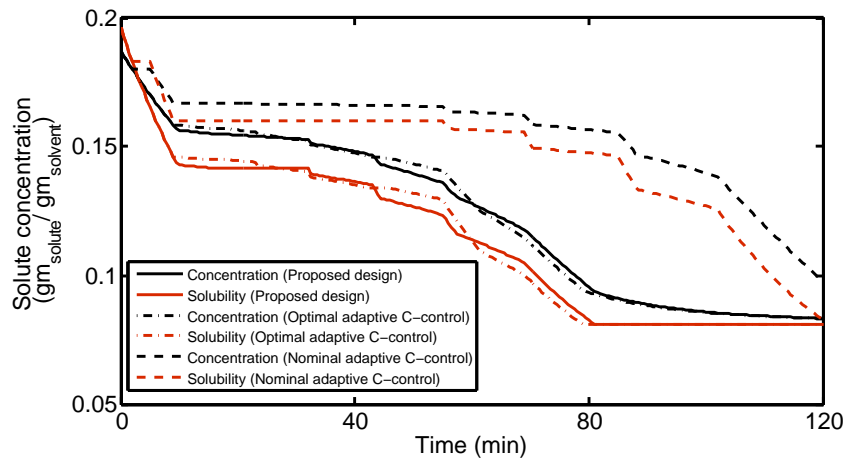


(b) Antisolvent mass percent profiles

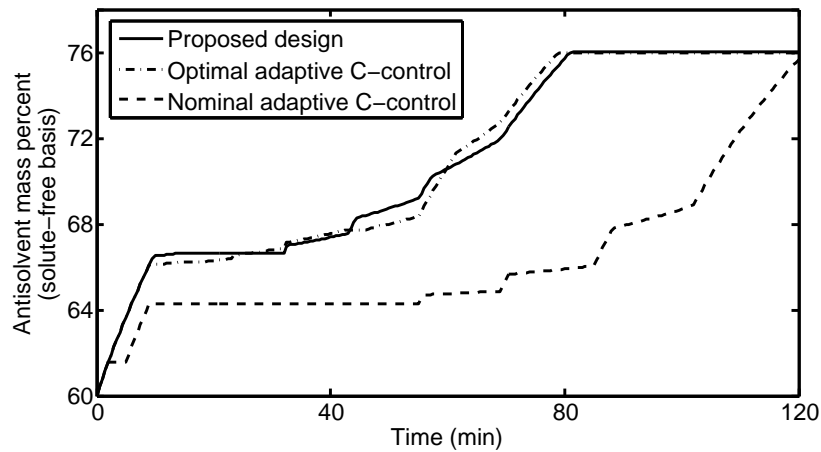


(c) Implemented relative supersaturation setpoint profiles

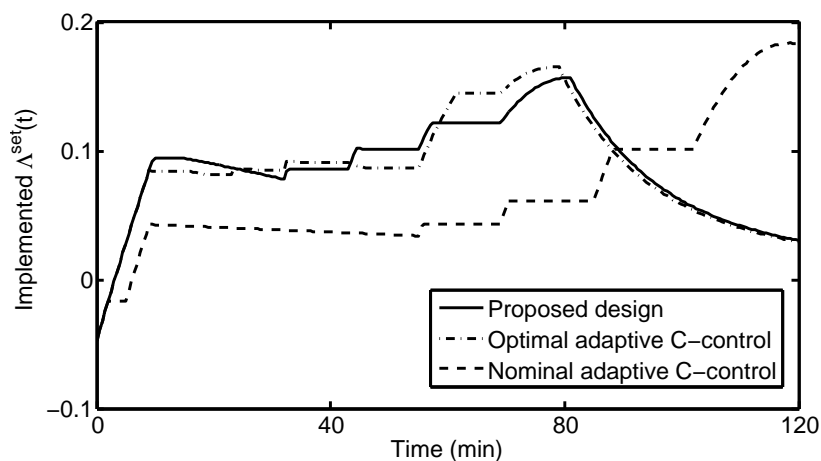
Figure 4.15 Performance of the proposed design, optimal, and nominal adaptive C-control for Case 1.



(a) Solute concentration profiles

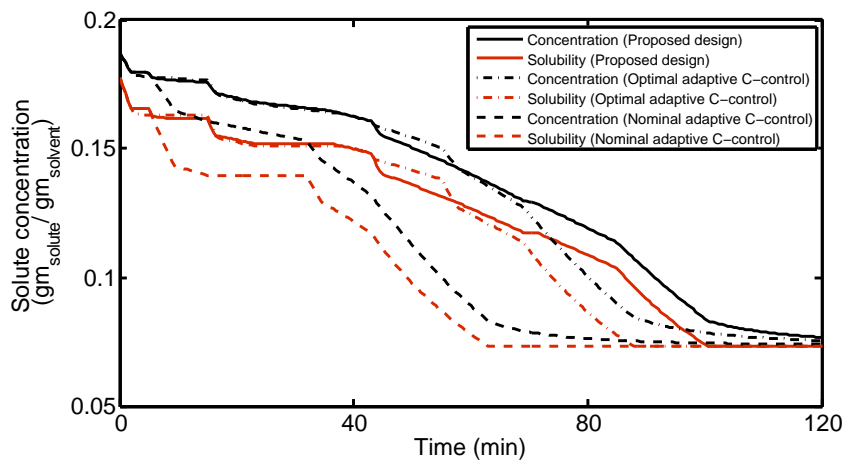


(b) Antisolvent mass percent profiles

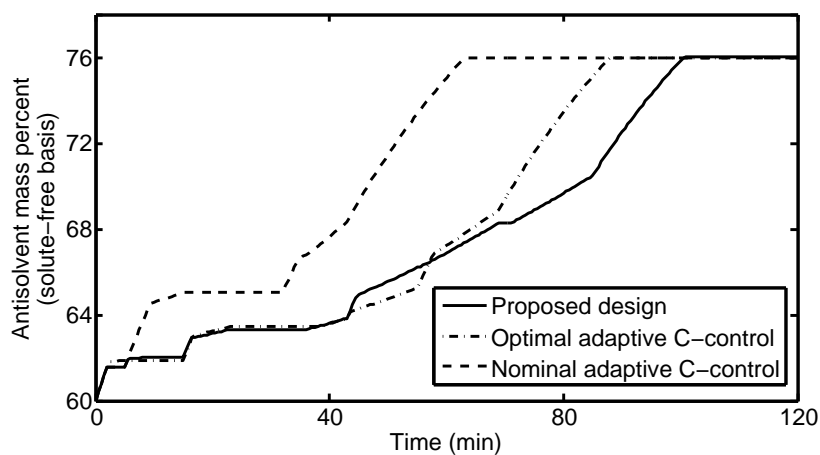


(c) Implemented relative supersaturation setpoint profiles

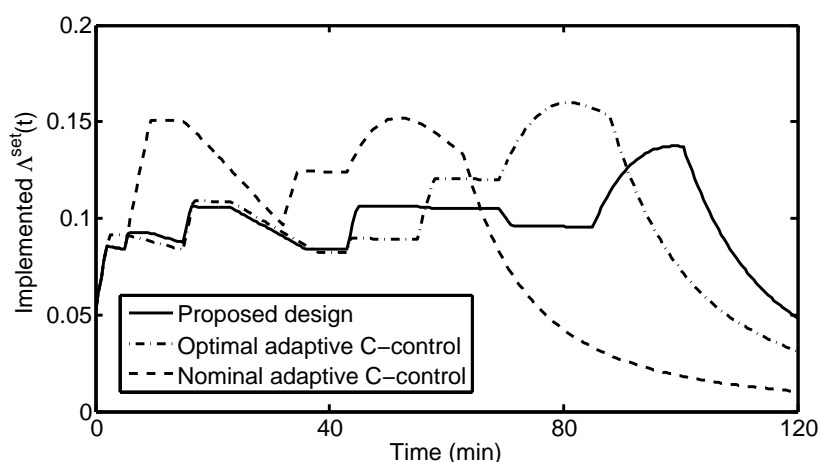
Figure 4.16 Performance of the proposed design, optimal, and nominal adaptive C-control for Case 2.



(a) Solute concentration profiles

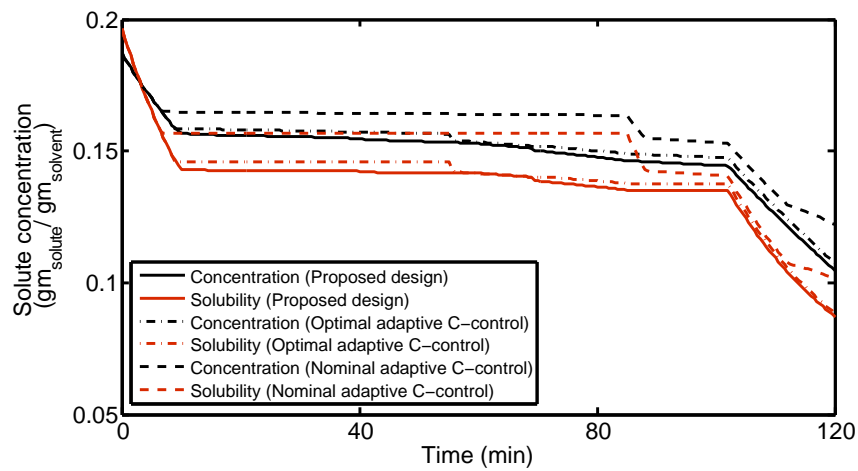


(b) Antisolvent mass percent profiles

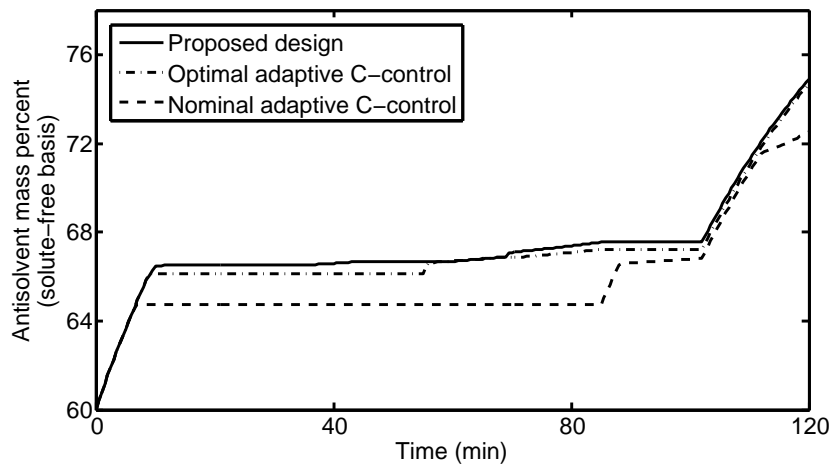


(c) Implemented relative supersaturation setpoint profiles

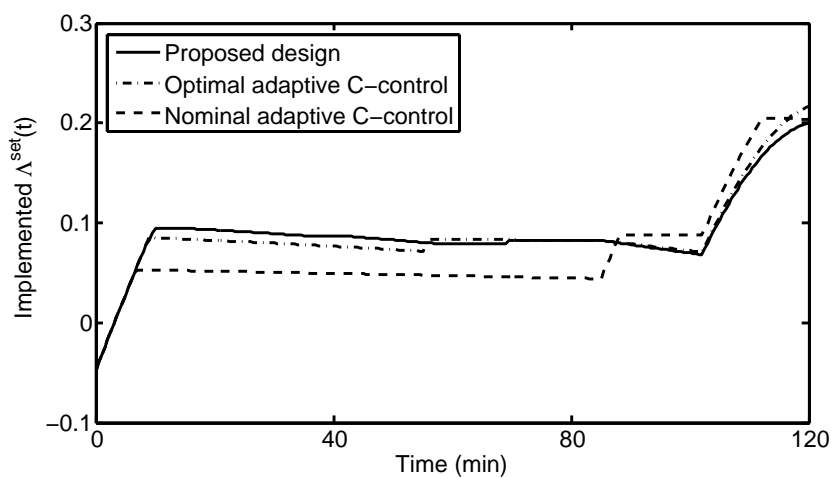
Figure 4.17 Performance of the proposed design, optimal, and nominal adaptive C-control for Case 3.



(a) Solute concentration profiles



(b) Antisolvent mass percent profiles



(c) Implemented relative supersaturation setpoint profiles

Figure 4.18 Performance of the proposed design, optimal, and nominal adaptive C-control for Case 4.

4.4 Conclusions

Understanding the necessity of adapting the relative supersaturation setpoint in presence of process variations for C-control of semi-batch antisolvent crystallization processes, a systematic approach based on online optimization schemes is proposed in this study. A two-staged data-based modeling framework is developed for online implementation of this adaptive C-control strategy. This cascaded control strategy offers additional advantages over the C-control strategy by being able to operate on-line. Simulation results show that the proposed design adapts to the variations in the process like shifts in solubility data and high nucleation rates, and simultaneously steers the process towards optimality.

Chapter 5

Measurement Based Optimal

Control of Antisolvent

Crystallization Processes

Motivated to counter the pragmatic limitations of implementing the optimal control policies in presence of plant-model mismatch, measurement-based optimization (MBO) schemes for real-time optimal operation of (semi-)batch pharmaceutical antisolvent crystallization processes is presented in this chapter. MBO schemes are based on tracking the Necessary Conditions of Optimality (NCO), usually a sequence of boundary and (or) interior arcs, using the measurement feedback. The details pertaining to the design and implementation of the NCO-tracking based control is discussed in the following sections.

5.1 Introduction

Control of crystallization processes in order to obtain desired product specifications is very critical in pharmaceutical industries, as it influences not only the efficiency of the other downstream processes but also the bioavailability of the drug (Higuchi and

Hiestand, 1963, Kim et al., 2005). Usually, for non-polymorphic systems, product crystal size distribution is the most important variable to be controlled either through the addition of antisolvent or temperature cooling or, combining both these modes in certain situations (Rawlings et al., 1992, 1993, Rohani et al., 2005a, Nagy et al., 2008b, Nowee et al., 2008a). Conventional operation of these processes involve the implementation of an optimal trajectory obtained from an offline model. However, this open loop approach has shown significant loss in optimality because the resulting product quality deviates from the desired product quality considerably in presence of process variations and disturbances (Hermanto et al., 2007, Nagy et al., 2008a). Hence, direct design approaches like supersaturation or concentration control (C-control) have been developed and it was well documented that these new design methods are less sensitive to process variations. Towards this end, owing to the advancements in sensor technology for *in situ* process measurements and application of Process Analytical Technology (PAT) tools, closed loop control strategies for batch crystallization processes that are robust to process disturbances have gained much attention (Patience and Rawlings, 2001, Zhou et al., 2006, Abu Bakar et al., 2009b, Nagy and Braatz, 2012). However, due to the limitations concerning the necessity of extended batch times and the lack of systematic approaches for selecting the setpoints during the implementation of these approaches in presence of process variations, alternative methods like MBO schemes are explored through this study for the control of semi-batch antisolvent crystallization processes.

One of the most celebrated techniques for real-time control of the batch processes is the use of model predictive control (MPC) that relies on repetitive optimization of the optimal control formulation. The state feedback is used in order to find the future optimal input moves based on a nominal model (Eaton and Rawlings, 1990, Nagy and Braatz, 2012). Besides, real-time optimal control of semi-batch antisolvent crystallization process has been recently demonstrated through experimental implementation (Sheikhzadeh et al., 2008b). Even though MPC is a proven

technology in process industries, the huge computation cost involved in repetitively solving the optimal control formulation online makes it unattractive for the control of semi-batch processes. Thus, instead of either tracking an optimal trajectory or using repetitive optimization based on an offline model, measurement based schemes that track the NCO have been developed (Srinivasan et al., 2003b, Bonvin et al., 2006). According to optimal control theory, in presence of any slight variations in the process, the optimal control policy obtained through the nominal process model has to be modified completely in order to satisfy the necessary conditions of optimality for the perturbed optimal control problem. Therefore, by designing suitable control strategies based on these principles can potentially address some of the pertinent issues concerning the real-time control of semi-batch crystallization processes.

In this current study, NCO tracking based control strategy is employed for optimal operation of semi-batch antisolvent crystallization processes in presence of plant-model mismatch. These approaches require the characterization of the nominal solution using boundary (constraint seeking) and interior (sensitivity seeking) arcs (Visser et al., 2000, Kadam et al., 2007, Welz et al., 2008). The boundary arcs can be directly tracked, but in order to track the interior arcs, a neighboring extremal (NE) controller must be designed. To evaluate the performance of proposed design, a comparative study is presented to illustrate the advantages of using NCO tracking based control over the nominal optimal control, C-control, and model predictive control strategies.

The rest of the chapter is organized as follows: Section 5.2 gives the relevant background and overview of NCO and design of NE controller. Characterization of the nominal solution and the design of NE controller are discussed in Section 5.3, and a comparative study using several case studies is discussed in Section 5.4. Finally, conclusions based on the performance and robustness of the NCO tracking based control strategy are presented in Section 5.5.

5.2 Background

This section introduces the necessary background information on the optimal control formulation for the implementation of model predictive control and the design of NCO-tracking based control for real-time control of batch processes.

5.2.1 Model predictive control formulation for batch processes

Design of model predictive control for batch processes typically involves repetitive optimization based on an offline model and the necessary states information obtained from the measurements (Chin et al., 2000). Considering the state feedback at time t_k to be x_k , an optimization problem to be solved at each sampling instant is formulated as follows,

$$\min_{u[t_k, t_f]} J = \Phi(x(t_f)) + \int_{t_k}^{t_f} \mathbf{L}(x(t), u(t)) dt, \quad (5.1)$$

$$\text{s.t.} \quad \dot{x}(t) = F(x(t), u(t)), \quad x(t_k) = x_k, \quad (5.2)$$

where $u[t_k, t_f]$ denotes the control profile between the current sampling instant t_k and the end of batch time t_f , x is the state vector, $\Phi(x(t_f))$ is the terminal cost function, \mathbf{L} is the integral cost function, J is the cost function to be minimized, and F describes the system dynamics. Thus, the MPC formulation requires the solution of the aforementioned optimization problem repetitively at each sampling time which is often computationally expensive. Therefore, in order to circumvent this shortcoming, MBO schemes have been developed in the literature (Welz et al., 2008, Gros et al., 2009b,a). One among such approaches is the NCO-based tracking control, which can be understood as a first order linear approximation of the MPC formulation, is considered during this study.

5.2.2 Necessary conditions of optimality tracking based control

Consider the formulation of the optimal control problem for batch processes as follows:

$$\min_{u(t)} J = \Phi(x(t_f)) + \int_0^{t_f} \mathbf{L}(x(t), u(t)) dt, \quad (5.3)$$

$$\text{s.t.} \quad \dot{x}(t) = F(x(t), u(t)), \quad x(0) = x_0, \quad (5.4)$$

$$u^L \leq u(t) \leq u^U, \quad (5.5)$$

where x_0 is the initial value of state vector x , and u^L and u^U are the lower and upper bounds of u , respectively. Assuming that all the functions in Eqs. (5.3) to (5.5) are continuously differentiable with respect to their arguments, then there exists optimal control $u^*(t) \in [u^L, u^U] \forall t, 0 \leq t \leq t_f$ for the nominal parameter values. Note that this solution profile consists of both boundary and interior arcs, which will become clear in the ensuing development.

Based on Pontryagin's Minimum Principle, the problem of optimizing the scalar cost functional J in Eqs. (5.3) to (5.5) can be reformulated by defining the Hamiltonian function $H(t)$ as (Bryson and Ho, 1969):

$$H(x, u, \theta, \lambda, \mu^L, \mu^U) = \mathbf{L}(x, u, \theta) + F(x, u, \theta)^T \lambda \quad (5.6)$$

$$+ \mu^L(u^L - u) + \mu^U(u - u^U), \quad (5.7)$$

and the necessary conditions of optimality become

$$H_u = \mathbf{L}_u + F_u^T \lambda - u^L + u^U = 0; \quad H_{uu} > 0, \quad (5.8)$$

where λ is the adjoint vector and given by

$$\dot{\lambda} = -H_x = -\mathbf{L}_x - F_x^T \lambda; \quad \lambda(t_f) = \Phi_x(x(t_f)), \quad (5.9)$$

and μ^L, μ^U denote the Lagrange multiplier satisfying

$$\mu^L(u^L - u) = 0; \quad \mu^L \geq 0, \quad (5.10)$$

$$\mu^U(u - u^U) = 0; \quad \mu^U \geq 0. \quad (5.11)$$

Notice that $\mu^L(t) = \mu^U(t) = 0$ only along the interior arcs, while $\mu^L(t) \neq 0$ and $\mu^U(t) \neq 0$ along the boundary arcs. During real-time control of the process, boundary arcs can be easily tracked. However, in order to push the path sensitivities to zero, approximate methods such as neighboring extremal control can be employed (Gros et al., 2009b), which will be discussed in the next subsection.

5.2.3 Neighboring extremal controller for non-singular problems

As the optimal control profile $u^*(t)$ for $0 \leq t \leq t_f$ is designed based on the initial condition x_0 and nominal operating conditions with parameters values $\bar{\theta}$, any slight variation δx_0 in the initial states requires the modification of the entire control profile. For the case of unconstrained problems or when the constraints remain inactive, the first-order approximation of the optimal trajectory for the perturbed control is considered as

$$u(t; \eta) = u^*(t) + \eta \delta u(t) + o(\eta), \quad (5.12)$$

and the correction during the implementation of the neighboring extremal controller $\delta u(t) = u(t) - u^*(t)$ is computed as the solution of the so-called accessory minimum problem, i.e., the minimization of the second-order variation of the cost functional subject to the linearized dynamics (Breakwell et al., 1963),

$$\min_{\delta u(t)} \delta^2 J = \frac{1}{2} \delta x(t_f)^T \Phi_{xx}^* \delta x(t_f) + \frac{1}{2} \int_0^{t_f} \begin{pmatrix} \delta x \\ \delta u \end{pmatrix}^T \begin{pmatrix} H_{xx}^* & H_{xu}^* \\ H_{ux}^* & H_{uu}^* \end{pmatrix} \begin{pmatrix} \delta x \\ \delta u \end{pmatrix} dt, \quad (5.13)$$

such that

$$\delta\dot{x}(t) = F_x^* \delta x + F_u^* \delta u, \quad \delta x(0) = \delta x_0, \quad (5.14)$$

$$u^L - u^*(t) \leq \delta u(t) \leq u^U - u^*(t), \quad (5.15)$$

where $\delta x(t) = x(t) - x^*(t)$, $x^*(t)$ is the state vector corresponding to $u^*(t)$ defined previously, and F_x^* and F_u^* are the partial derivatives of the state dynamics F with respect to the state vector and the inputs, respectively, that are evaluated at the nominal solution, (x^*, u^*) .

Thus, when the problem of Eqs. (5.13) to (5.15) has a solution, it can be shown that there exists an optimal control trajectory $u(t; \eta)$ in the neighborhood of $\eta = 0$. Therefore, the correction $\delta u(t)$ satisfying the strengthened Legendre-Clebsch condition $H_{uu}^*(t) > 0$ along the nominal solution $u^*(t)$, $x^*(t)$, $\lambda^*(t)$ is then given by

$$\delta u(t) = -(H_{uu}^*)^{-1} [H_{ux}^* \delta x(t) + F_u^{*\top} \delta \lambda]. \quad (5.16)$$

Furthermore, a NE state feedback law that enforces the necessary conditions of optimality can be designed via backward sweep method that assumes linear relation between the states and adjoint variables as $\delta \lambda(t) = S_x(t) \delta x(t)$ (Bryson and Ho, 1969).

$$\delta u(t) = -K(t) \delta x(t), \quad (5.17)$$

$$K(t) = (H_{uu}^*)^{-1} (H_{ux}^* + F_u^{*\top} S_x(t)), \quad (5.18)$$

$$\begin{aligned} \dot{S}_x(t) = & -H_{xx}^* - S_x(t) F_x^* - F_x^{*\top} S_x(t) \\ & + (H_{xu}^* + S_x(t) F_u^*) K(t); \text{ with } S_x(t_f) = \Phi_{xx}^*, \end{aligned} \quad (5.19)$$

where $K(t)$ is the gain of the NE controller. Thus, the traditional design of the NE controller is carried out by solving the above Riccati equation within the uncon-

strained arcs.

5.3 NCO-tracking based control of antisolvent crystallization processes

As mentioned in Chapter 3, the control objective of the chosen antisolvent process in this study is to adjust the antisolvent flowrate or antisolvent mass percent for that matter to maximize the volume-weighted mean size of the product crystals. Therefore, the cost function is given by

$$\min_{u(t)} J = \phi(x(t_f)) = - \left(\frac{\mu_4}{\mu_3} \right) \Big|_{t_f}, \quad (5.20)$$

$$\text{subject to, } V(t) - V_{max} \leq 0, \quad (5.21)$$

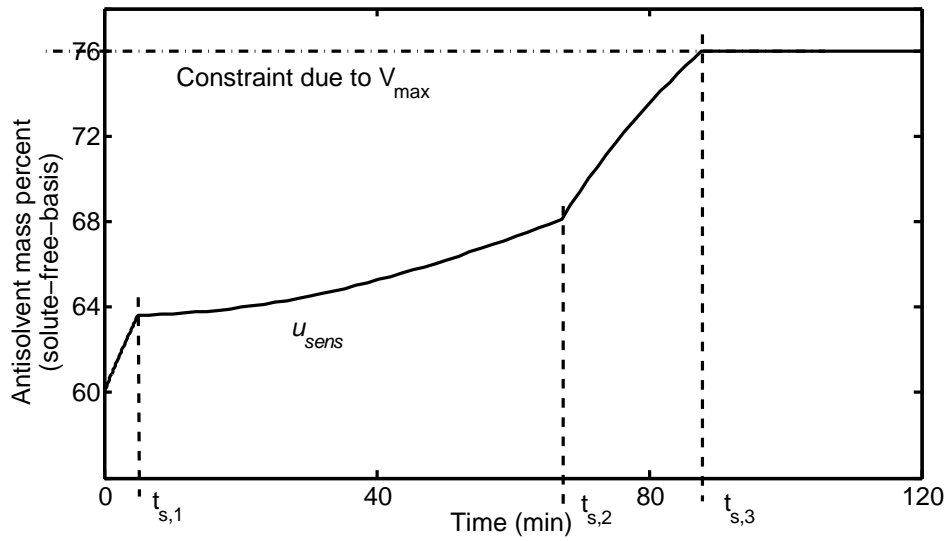
where μ_3 and μ_4 are the third and fourth moments of the product crystal size distribution, respectively, at the batch end, t_f . $V(t)$ is the volume of the solution at any given time t , and V_{max} is the maximum allowable volume of the solution in the crystallizer.

To determine the solution of the optimization problem described in Eq. (5.20) subject to the equality and inequality constraints given in Eq. (3.7), the entire antisolvent flowrate profile of the batch is parameterized using three switching times and hence, the entire flowrate trajectory is dissected into four intervals. The resulting optimal antisolvent mass percent and flowrate trajectories shown in Figure 5.1. In order to design the NCO-tracking based controller, the nominal solution is dissected into multiple intervals. During the first interval between $t = 0$ and the first switching instant ($t_{s,1}$), the flowrate is kept constant at maximum flowrate value FR_{max} . The maximum volume constraint on the amount of antisolvent that can be added into the system dictates the third switching instant ($t_{s,3}$) and consequently the

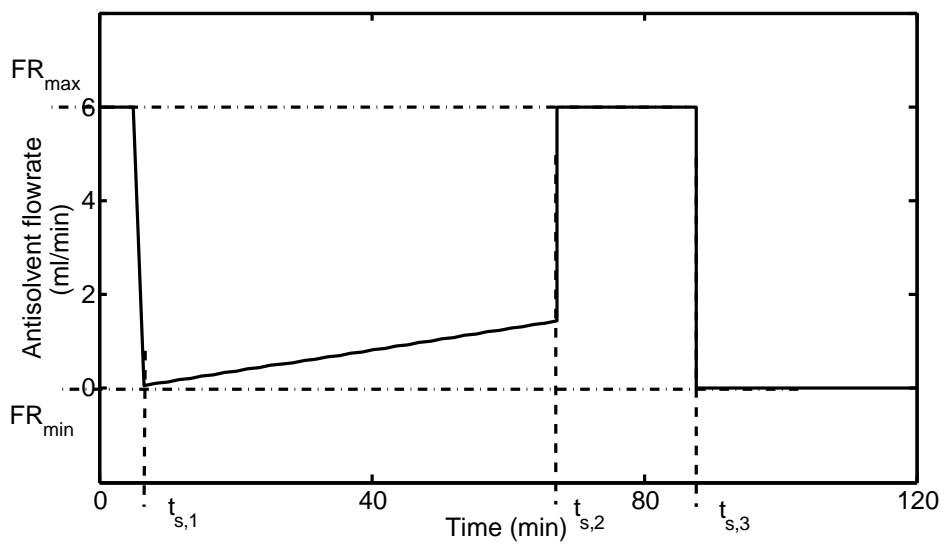
flowrate between $t_{s,3}$ and t_f is set equal to its minimum flowrate value FR_{min} . Furthermore, the flowrate is kept constant at FR_{max} during the third interval between $t_{s,2}$ and $t_{s,3}$. The flowrate profile between the two switching times $t_{s,1}$ and $t_{s,2}$ is described using a first order spline. Thus, the two time instants, $t_{s,1}$ and $t_{s,2}$, and the values of the antisolvent flowrate at these two instants are determined through optimization based on nominal operating conditions. This arc is considered as the interior arc or the sensitivity arc u_{sens} , as none of the constraints are active within this interval.

It is noted that antisolvent mass percent m_w is considered as the manipulated variable u for the design of the NE controller because when the antisolvent flowrate is considered as the input, the formulation results in a input-affine system, which usually exhibits singularity and thus poses difficulty while obtaining the solution of the interior arc.

For designing the NE controller, all the states $x = [\mu_0, \mu_1, \mu_2, \mu_3, \mu_4, C]^T$ are assumed to be measurable and hence a full state feedback law is integrated backward in time from t_f to 0 along the nominal solution $u^*(t), x^*(t), \lambda^*(t), 0 \leq t \leq t_f$. Thus, the obtained NE controller gain vector, $K(t) = [K_{\mu_0}(t), K_{\mu_1}(t), K_{\mu_2}(t), K_{\mu_3}(t), K_{\mu_4}(t), K_C(t)]$ constitutes of all the corresponding gain vectors of each of the states as shown in Figure 5.2. Therefore, as can be inferred from the plots, the NE controller gain vector is kept active only between the switching times $t_{s,1}$ and $t_{s,2}$ in order to track the interior arcs of the perturbed process. While, the boundary arcs are implemented directly without any corrections to the antisolvent flowrate trajectory.



(a)



(b)

Figure 5.1 Optimal antisolvent mass percent and flowrate profiles for nominal case.

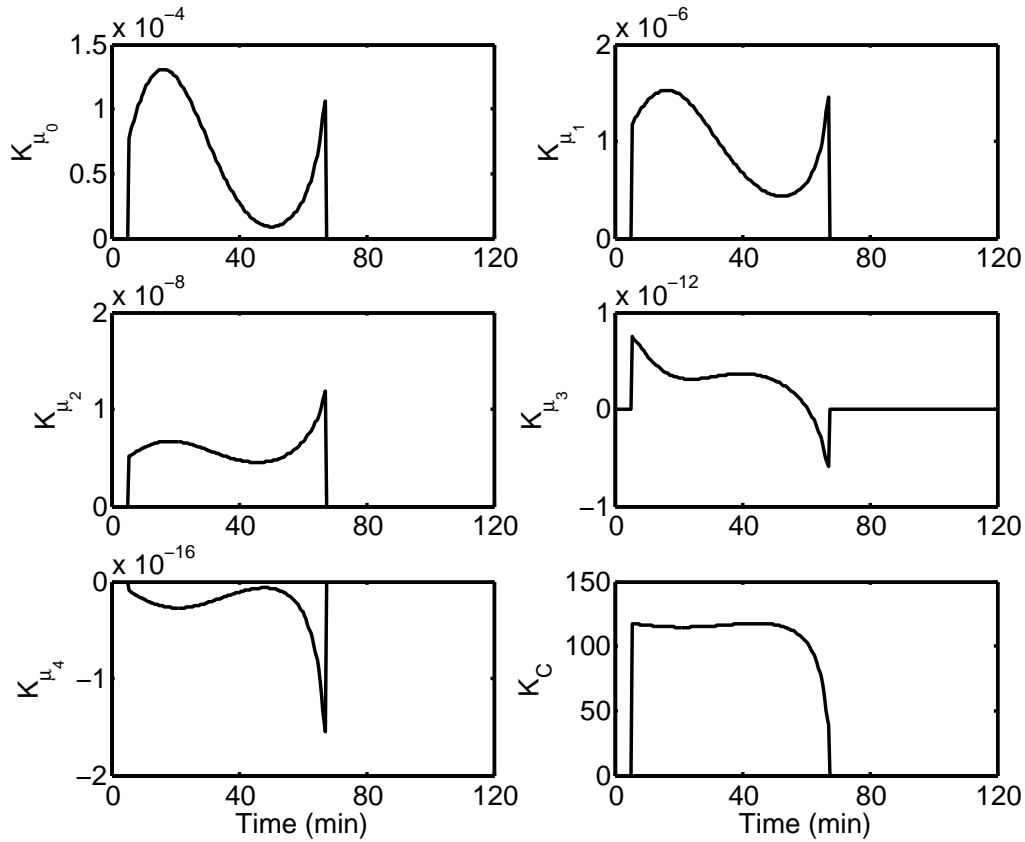


Figure 5.2 Neighboring extremal controller gain, $K(t)$.

5.4 Results and discussions

In order to compare the performance of the NE controller, various scenarios of plant-model mismatch are considered by introducing uncertainties in the kinetic parameters of growth and nucleation rates as considered in the earlier chapters. Besides, considering the advantages of NCO-tracking control to effectively handle the state disturbances, deviation in the initial conditions is considered as

$$x'_0 = x_0(1 + \Delta\theta_6), \quad (5.22)$$

where $\Delta\theta_6$ is the disturbance in the initial condition of the states x_0 . Thus, $\Delta\theta_6 = 0$, represents the nominal operating condition. Table 5.1 provides the details of the perturbations introduced into the process corresponding to seven case studies used

Table 5.1 Case studies considered in Chapter 5.

Case	Perturbations in model parameters					Deviations in initial conditions
	$\Delta\theta_1$	$\Delta\theta_2$	$\Delta\theta_3$	$\Delta\theta_4$	$\Delta\theta_5$	$\Delta\theta_6$
Nominal	0	0	0	0	0	0
1	0.1	-0.1	-0.1	0.1	0	0
2	0	0	0	0	0.05	0
3	0	0	0	0	-0.05	0
4	0.1	-0.1	-0.1	0.1	0.05	0
5	0	0	0	0	0	-0.1
6	0	0	0	0	-0.05	-0.1
7	0.1	-0.1	-0.1	0.1	0.05	-0.1

in a comparative study between the NCO tracking based control and its conventional counterparts including the optimal control profile obtained based on the nominal process model, C-control designed based on the nominal process model, and the true optimal control obtained for each case study.

Table 5.2 Product quality (in μm) obtained by various controller design methods.

Case	True optimal	Open-loop profile	NCO tracking controller	MPC formulation	C-control
Nominal	599.94	599.94	599.94	599.94	581.78
1	329.23	257.79	264.51	267.63	269.11
2	577.31	555.15	540.43	540.06	484.99
3	619.32	546.84	548.25	548.16	456.19
4	339.73	247.29	231.95	235.03	272.17
5	539.40	477.11	532.27	533.86	522.85
6	569.85	540.86	556.24	542.74	521.10
7	327.74	231.39	284.67	292.42	270.16

In this study, in order to make a fair comparison among all these approaches, the flexibility offered by the C-control strategy to operate the process with variable batch time is avoided by imposing the volume constraint that when at any instant during the batch satisfies the inequality, $V(t) \leq V_{max} - FR_{max}(t_f - t)$, the antisolvent flowrate is set as FR_{max} so that the volume constraint at the end of the batch is always satisfied. For the implementation of the C-control strategy, a value of 0.101 is chosen as the constant relative supersaturation setpoint, which is tuned based on optimizing the product quality using the nominal model.

Furthermore, a MPC is designed based on the nominal process model for making a comparative study with the NE controller. The optimization problem given in Eqs. (5.1) and (5.2) is solved at each sampling time within the two switching times $t_{s,1}$ and $t_{s,2}$, with antisolvent flowrate parameterized using four equidistant first order splines, while those in the interval $[0, t_{s,1}]$ and $[t_{s,2}, t_f]$ are considered as constant antisolvent flowrate to be fair with the NE controller design. During the real-time implementation of the MPC formulation, the parameters of these spline representations are repetitively optimized using a nominal model and the state feedback from the *real* process.

Table 5.2 provides the product quality values for all the case studies obtained by the four control strategies that are discussed previously. Figures 5.3 to 5.9 provide the corresponding antisolvent mass percent profiles obtained through the implementation of the above mentioned control strategies.

From the values of the product qualities, it can be inferred that the NCO tracking control provides better robustness over the C-control strategy for most of the cases. It can be seen that the optimality loss due to the implementation of the NCO tracking control is either less or sometimes similar to the loss obtained by the nominal optimal control profile and also the C-control strategy. Besides, one of the important observations made through this study is that the performance of the NE controller is always very close to that of the MPC formulation. Therefore, NCO tracking based

control with a NE controller that tracks the interior arc provides better robustness to process variations for the antisolvent crystallization process investigated in this thesis.

However, it fails to adapt in scenarios where simultaneous perturbations in all the kinetic parameters take place. As noticed in Cases 1 and 4, the product quality values deviate to a larger extent from the true optimal values. In order to understand the reason behind this, the corresponding input profiles for these two cases, as shown in Figures 5.3 and 5.6 are considered. It can be seen that the true optimal antisolvent mass percent profiles for these two cases do not converge towards the constraint imposed by the maximum allowable volume during the crystallization process. Thus, the corresponding active constraint set towards the end of the batch for both these cases are different from the rest of the cases. Meaning, the active constraint set towards the end of the batch are changed in order to either meet the minimum yield constraint or has none of the constraints active. Hence, the NCO tracking control designed based on the boundary and interior arcs obtained through the dissection of the nominal optimal profile does not remain valid in these scenarios. Therefore, this leads to one of the shortcomings of the traditional NCO tracking control of being unable to handle changes in active constraint set in presence of plant-model mismatch. Thus, the change in active constraints towards the end of the batch explains the high loss in optimality for Cases 1 and 4 during the implementation of the NCO tracking based control.

For Cases 2, 3, and 6, the NCO tracking control clearly performs better than the C-control strategy, thus adding more robustness to the shifts in the solubility data. However, the loss in optimality is still high because the linear approximations of the model may not remain valid when the NE controller is kept active *.i.e.*, between the switching times $t_{s,1}$ and $t_{s,2}$. This can be understood from the plots shown in Figures 5.4 and 5.5. The NE controller tries to make corrective actions $\delta u(t)$ to the nominal input profiles at each sampling time t in a direction away from the true

optimal profiles. Thus, it results in a deteriorated performance towards the end of the batch. Therefore, the inability to capture the *true* directional information of the input corrections to be made in presence of certain plant-model mismatch forms yet another shortcoming of NCO tracking based control.

The true potential of the NCO tracking control is realized in presence of disturbances in the initial conditions. Evidently, it outperforms all the other control strategies for Cases 5, 6, and 7. Also, from Figures 5.7 to 5.9, it can be seen that the input corrections to the nominal optimal profile made by the NE controller for all these cases are towards the right directions. However, in Case 5 and 7, the magnitude of the input change is slightly conservative, while it overcompensates in Case 6.

Therefore, the NCO tracking control provides better robustness over the other competing control strategies discussed in this thesis. However, recognizing the pertinent issues concerning the inability to withstand certain scenarios of plant-model mismatch, alternative design methods that alleviate the shortcomings of the traditional NCO controller design will be investigated in the further chapter.

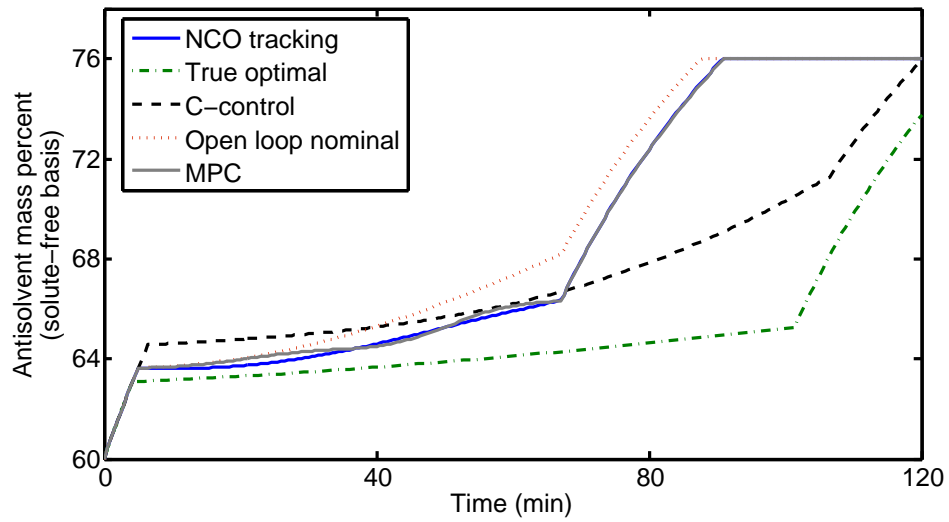


Figure 5.3 Response of various control strategies for Case 1.

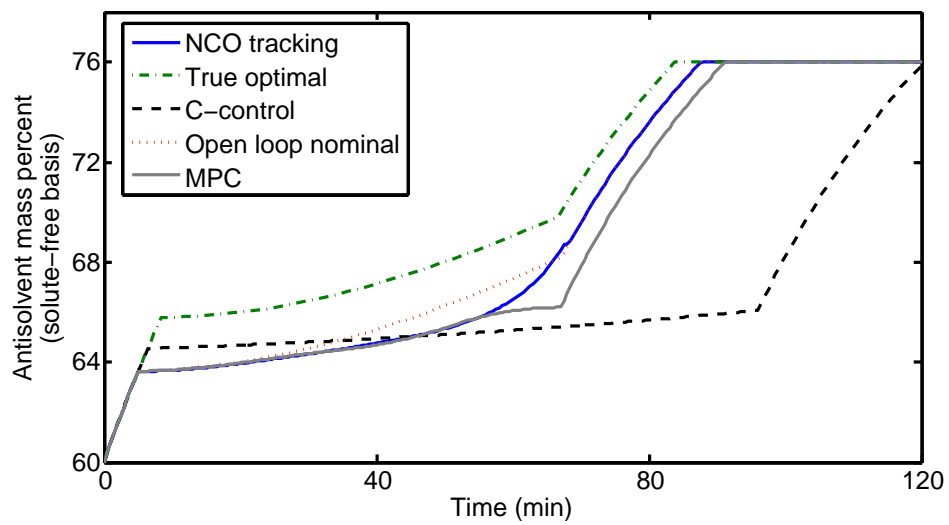


Figure 5.4 Response of various control strategies for Case 2.

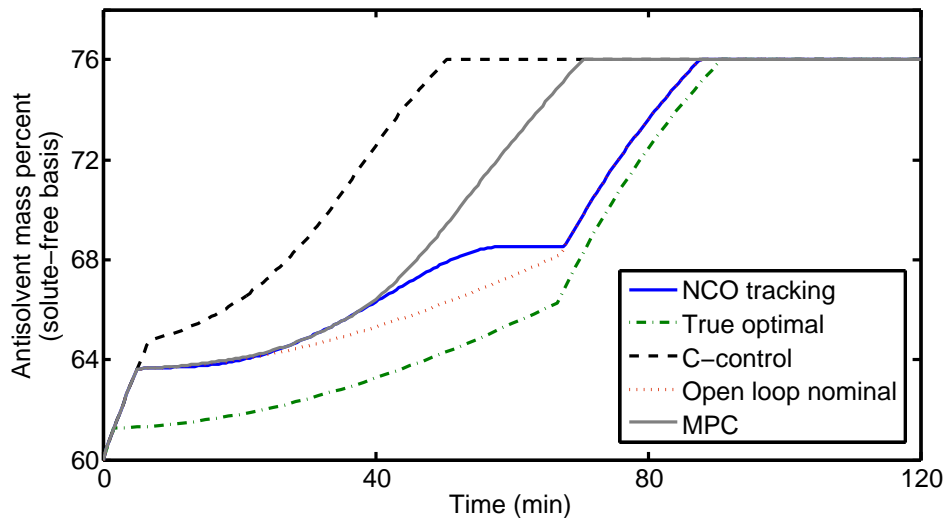


Figure 5.5 Response of various control strategies for Case 3.

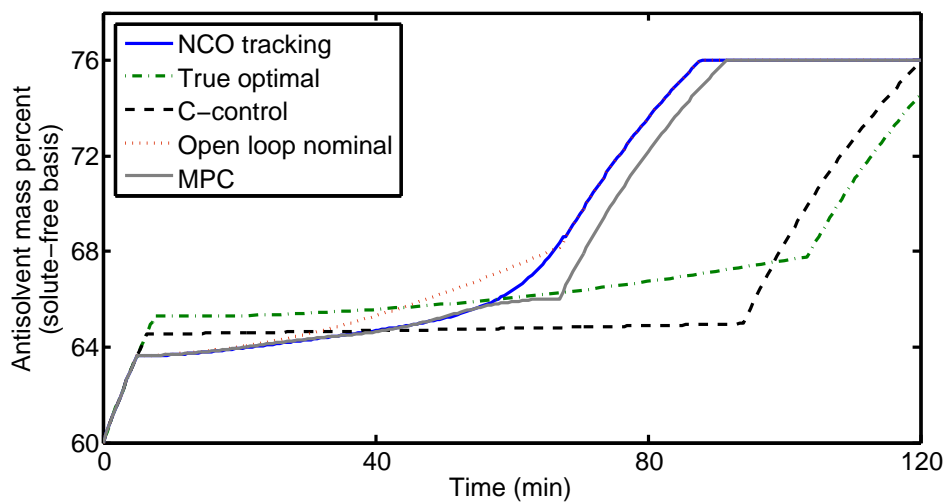


Figure 5.6 Response of various control strategies for Case 4.

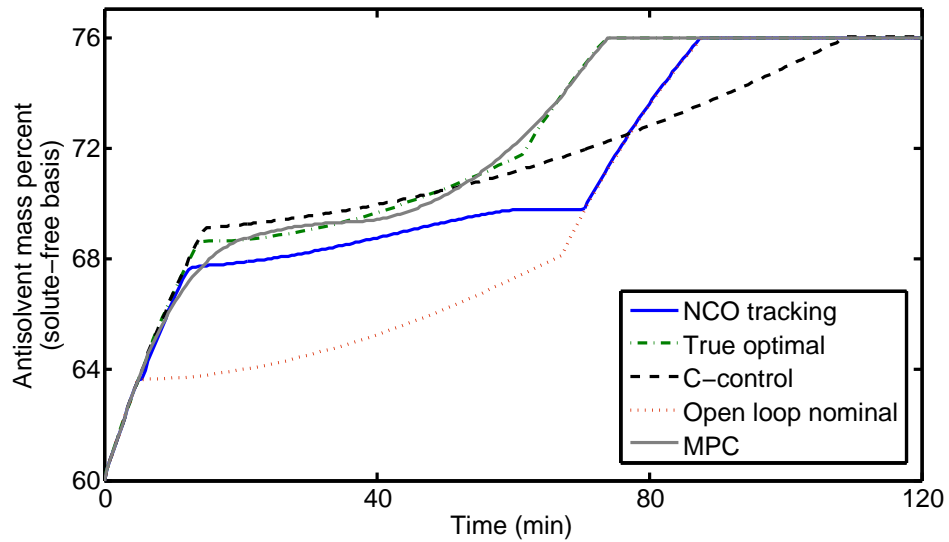


Figure 5.7 Response of various control strategies for Case 5.

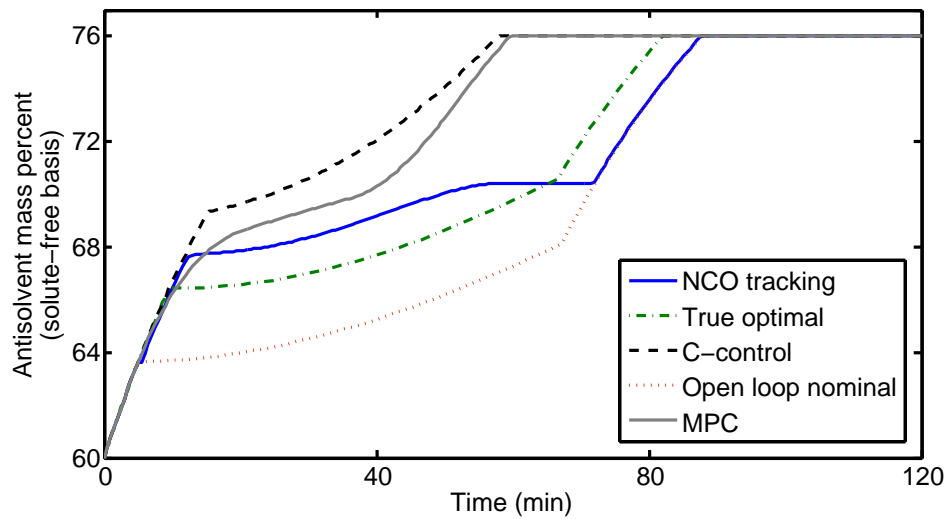


Figure 5.8 Response of various control strategies for Case 6.

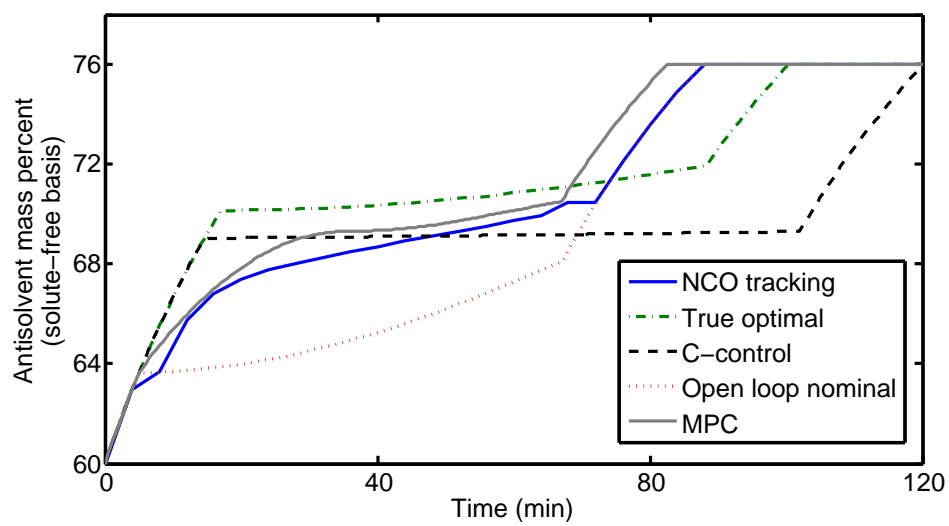


Figure 5.9 Response of various control strategies for Case 7.

5.5 Conclusions

Real-time optimal control for semi-batch antisolvent crystallization processes based on tracking the necessary conditions of optimality is presented in this chapter. Based on the given nominal solution, the input profile is dissected into boundary and interior arcs. In order to track the interior arcs in presence of uncertainties and process disturbances, the neighboring extremal controller is designed. Besides, based on the product quality values, the performance of the NE controller is compared with the MPC design. Simulation results show that the NE controller performs very close to the MPC technique. Furthermore, it has been observed that the traditional NE controller adapts to shifts in solubility curves better than the C-control strategy. However, the NCO tracking based control still suffers from the issues concerning the changes in active constraint set, which arise due to large or simultaneous deviations in the model parameters.

Chapter 6

Reformulated Neighboring

Extremals for Control of Antisolvent

Crystallization Processes

With an intention to improve the robustness of the NCO tracking based control, a reformulated feedback for the neighboring extremal control in order to track the interior arcs of the optimal control profile is discussed in this chapter. Simulation studies were carried out to demonstrate the efficacy of this approach and the importance of incorporating the knowledge of parameter variations in real-time optimal control.

6.1 Introduction

Real-time optimal control of batch crystallization processes in presence of model uncertainty has been posing as an invincible challenge to the crystallization control community. Traditionally, open loop optimal trajectory using a nominal offline model is employed for operation of batch crystallization processes due to the lack of accurate measurements for online control. Hence, alternative approaches based

on optimal control theory have been developed in order to meet the desired product specifications even in presence of plant-model mismatch. Robust optimal trajectory that minimizes either the worst case deviation of the batch end performance index or the variance of the objective around the nominal value (caused due to the uncertainty in the parameters) is employed for obtaining the desired product specifications (Nagy and Braatz, 2004). Also, run-to-run adaption strategies with repetitive identification of the uncertain parameters at the end of each batch have been developed in the literature (Lee et al., 2002b, Lee and Lee, 2003, 2007).

By the late 1990s, the advancements in sensor technology enabled the development of new PAT tools like ATR-FTIR, FBRM probe, laser diffraction particle sizing measurements, and PVM (Nagy and Braatz, 2012). Thus, with the availability of reliable *in situ* measurements for the crystallization process, several direct design approaches have found their application for CSD control (Liotta and Sabesan, 2004, Yu et al., 2006a,b, Zhou et al., 2006, Abu Bakar et al., 2009b, Woo et al., 2009, Hermanto et al., 2010). Besides, model based control techniques were simultaneously developed for tighter control and improved robustness (Nagy and Braatz, 2003, 2004, Fujiwara et al., 2005, Nagy, 2009, Aamir et al., 2010).

With the advent of the model predictive control (MPC) real-time optimal control by repetitive optimization of the dynamic formulation is made possible. The MPC formulation uses a nominal model along with state feedback in order to find the future optimal input moves at each sampling instant (Eaton and Rawlings, 1990). Besides, when all the states are not measureable, suitable state estimation techniques are also required. Furthermore, model parameters might also be updated, if necessary. Hence, the computation cost involved in finding the solution of the optimization problem and adaptation of model parameters makes it formidably unattractive for online control of batch crystallization processes, even when significant progress is made in addressing these issues in the recent past (Biegler et al., 2002, Lee et al., 2002b, Nagy and Braatz, 2003, Nagy et al., 2007a,b). Thus, measurement based op-

timization schemes that track the NCO have been developed, which characterize the nominal solution using boundary (constraint seeking) and interior (sensitivity seeking) arcs are developed in the literature (Srinivasan et al., 2003b, Srinivasan and Bonvin, 2007, Kadam et al., 2007, Welz et al., 2008). The current study, explores the NCO tracking based controller for the sensitivity seeking arcs by designing a neighboring extremal (NE) controller. NE controller is a first-order approximation of the MPC where the deviation of the input is obtained from the deviation of the states (Bryson and Ho, 1969, Gros et al., 2009b). It is a computationally efficient solution for small variations and for processes that are not heavily nonlinear.

Traditionally, the nominal model is used as a basis for both MPC and NE. Parameters of the model are typically not adapted due to the absence of persistency of excitation (Eaton and Rawlings, 1990). The corrections are based only on the state deviations. Such an approach is valid in presence of additive uncertainty, i.e., state and process noise. However when state deviations are caused by model uncertainties, the correction should depend not only on the state uncertainties (the effect), but also on the model uncertainties (the cause). So, the objective of this work is to emphasize the importance of incorporating the model uncertainty information in the correction. Incorporating model uncertainty information in the MPC based control strategy needs prudence since adapted parameter values with poor confidence would cause the input to chatter. So a safer bet would be to use the NE feedback law that incorporates corrections based on both state and parameter variations.

The rest of the chapter is organized as follows: Section 6.2 introduces the MPC formulation and the reformulated NE controller design in presence of model uncertainties. Section 6.3 presents the simulation results and the discussions, followed by the conclusions in Section 6.4.

6.2 Model predictive control vs NCO-tracking based control

6.2.1 MPC formulation

Design of model predictive control for batch processes typically involves repetitive optimization based on an offline model and the necessary states information obtained from the measurements (Chin et al., 2000). Considering the state feedback at time, t_k to be x_k , an optimization problem is formulated as follows,

$$\min_{u[t_k, t_f]} J = \Phi(x(t_f)) + \int_{t_k}^{t_f} \mathbf{L}(x(t), u(t), \theta) dt, \quad (6.1)$$

$$\text{s.t. } \dot{x}(t) = F(x(t), u(t), \theta), \quad x(t_k) = x_k, \quad (6.2)$$

where t_f is the batch time, $\Phi(x(t_f))$ is the terminal cost function, \mathbf{L} is the integral cost function, θ is the perturbed model parameter, while J is the cost function to be minimized. x is the state vector to be integrated from time t_k to t_f with the initial conditions as $x(t_k) = x_k$, while F describes the system dynamics. However, instead of this scheme that requires the explicit solution of the above formulation at each sampling time, measurement based optimization (MBO) schemes have been developed in the literature (Welz et al., 2008, Gros et al., 2009b,a). One among such approaches is the NCO-based tracking control, which requires the characterization of the nominal solution using boundary (constraint seeking) and interior (sensitivity seeking) arcs.

As discussed in the earlier chapter, boundary arcs can be easily tracked. However, in order to push the path sensitivities to zero, approximate methods such as neighboring extremal (NE) control can be employed (Gros et al., 2009b). In this study, the necessity of the reformulating the NE controller by incorporating the

sensitivities of the nominal input profile with respect to the model parameters is emphasized.

6.2.2 Neighboring extremal feedback in presence of model uncertainties

In presence of model uncertainties, the unconstrained optimal control problem as described using Eqs. (5.3) and (5.4) is reformulated as follows:

$$\min_{u(t)} J = \Phi(x(t_f)) + \int_0^{t_f} \mathbf{L}(x(t), u(t), \theta) dt, \quad (6.3)$$

$$\text{s.t} \quad \dot{x}(t) = F(x(t), u(t), \theta), \quad x(0) = x_0, \quad (6.4)$$

The Hamiltonian function $H(t)$ for the above formulation can thus be derived as,

$$H(x, u, \theta, \lambda) = \mathbf{L}(x, u, \theta) + F(x, u, \theta)^T \lambda, \quad (6.5)$$

while the *accessory minimum problem* will be,

$$\begin{aligned} \min_{\delta u(t)} \delta^2 J &= \frac{1}{2} \delta x(t_f)^T \Phi_{xx}^* (\delta x(t_f)) \\ &+ \frac{1}{2} \int_0^{t_f} \begin{pmatrix} \delta x \\ \delta u \\ \delta \theta \end{pmatrix}^T \begin{pmatrix} H_{xx}^* & H_{xu}^* & H_{x\theta}^* \\ H_{ux}^* & H_{uu}^* & H_{u\theta}^* \\ H_{\theta x}^* & H_{\theta u}^* & H_{\theta\theta}^* \end{pmatrix} \begin{pmatrix} \delta x \\ \delta u \\ \delta \theta \end{pmatrix} dt, \end{aligned} \quad (6.6)$$

$$\text{s.t} \quad \delta \dot{x}(t) = F_x^* \delta x + F_u^* \delta u + F_\theta^* \delta \theta, \quad \delta x(0) = \delta x_0. \quad (6.7)$$

Thus, when the problem of (6.6) and (6.7) has a solution, it can be shown that there exists an optimal control trajectory $u(t; \eta)$, in the neighborhood of $\eta = 0$. Therefore, the correction δu satisfying the strengthened Legendre-Clebsch condition $H_{uu}^*(t) >$

0 condition along the nominal solution $u^*(t), x^*(t), \lambda^*(t)$, is then given by

$$\delta u(t) = -(H_{uu}^*)^{-1}[H_{ux}^* \delta x(t) + F_u^{*\top} \delta \lambda + H_{u\theta}^* \delta \theta]. \quad (6.8)$$

Furthermore, a NE state feedback law that enforces the necessary conditions of optimality can be designed via backward sweep method that assumes linear relation between the states and adjoint variables and parameters as $\delta \lambda(t) = S_x(t) \delta x(t) + S_\theta(t) \delta \theta$ (Gros et al., 2009b).

$$\delta u(t) = -K_x \delta x(t) - K_\theta \delta \theta, \quad (6.9)$$

$$K_x(t) = (H_{uu}^*)^{-1}(H_{ux}^* + F_u^{*\top} S_x(t)), \quad (6.10)$$

$$K_\theta(t) = (H_{uu}^*)^{-1}(H_{u\theta}^* + F_u^{*\top} S_\theta(t)), \quad (6.11)$$

$$\begin{aligned} \dot{S}_x(t) = & -H_{xx}^* - S_x(t)F_x^* - F_x^{*\top} S_x(t) \\ & + (H_{xu}^* + S_x(t)F_u^*)K_x(t); \text{ with } S_x(t_f) = \Phi_{xx}^*, \end{aligned} \quad (6.12)$$

$$\begin{aligned} \dot{S}_\theta(t) = & -H_{x\theta}^* - S_x(t)F_\theta^* - F_x^{*\top} S_\theta(t) \\ & + (H_{xu}^* + S_x(t)F_u^*)K_\theta(t); \text{ with } S_\theta(t_f) = 0. \end{aligned} \quad (6.13)$$

Remark: The gains of the neighboring extremal controller, K_x and K_θ , are obtained by solving the Riccati equation within the unconstrained arcs. However, in cases where the analytical expression for the nominal input trajectory, $u^*(t)$, is known, the above procedure can be avoided. Instead, as the gains represent the input sensitivities to the states and model parameters, they can be derived as,

$$K_x(t) = -\frac{\partial u^*}{\partial x}, \quad (6.14)$$

$$K_\theta(t) = -\frac{\partial u^*}{\partial \theta}. \quad (6.15)$$

Although, the reformulated NE feedback incorporates the input sensitivities with respect to the model parameters, the information regarding the deviations in

the model parameters is not readily available. Hence, methods for parameter identification based on online state feedback have to be incorporated into this framework. However, the scope of this work is restricted to evaluate the optimality loss that can be recovered with the inclusion of K_θ gain of the NE controller. Also, this can provide the motivation for the development of adaptation strategies based on integrating the run-to-run control to counter the uncertainty in the parameters. Nevertheless, the relevant theory and discussion regarding online parameters identification is provided elsewhere for a simple isomerization reaction system (Kamaraju et al., 2013).

6.3 Results and discussions

During this study, the optimal antisolvent mass percent and flowrate trajectories shown in Figures 5.1(a) and 5.1(b), respectively are used to design the reformulated NE controller. Thus, as discussed earlier (in Section 5.3), antisolvent mass percent m_w is considered as the input u . For designing the NE controller, all the states $x = [\mu_0, \mu_1, \mu_2, \mu_3, \mu_4, C]^T$ are assumed to be measurable and hence a full state feedback law is integrated backward from time t_f to 0, along the nominal solution $u^*(t), x^*(t), \lambda^*(t), 0 \leq t \leq t_f$. The vector of model parameters were restricted to $\theta = [g, k_g, b, k_b, C_{sat}]^T$ in this study. Thus, the gain vectors of the NE controller, $K_x(t)$ and $K_\theta(t)$ are obtained based on Eqs. (6.10) and (6.11). Figure 6.1 shows the controller gain corresponding to the state feedback. Figure 6.2 shows the reformulated NE controller gain corresponding to the deviations in the model parameters.

By introducing perturbations in the kinetic parameters of growth and nucleation rates and disturbance in the initial conditions, various scenarios of plant-model mismatch as described in Table 5.1 (in Section 5.4) are considered during this study. Thus, the performance of the reformulated NCO tracking based control is compared to its traditional design approach for these scenarios. Besides, a model predictive

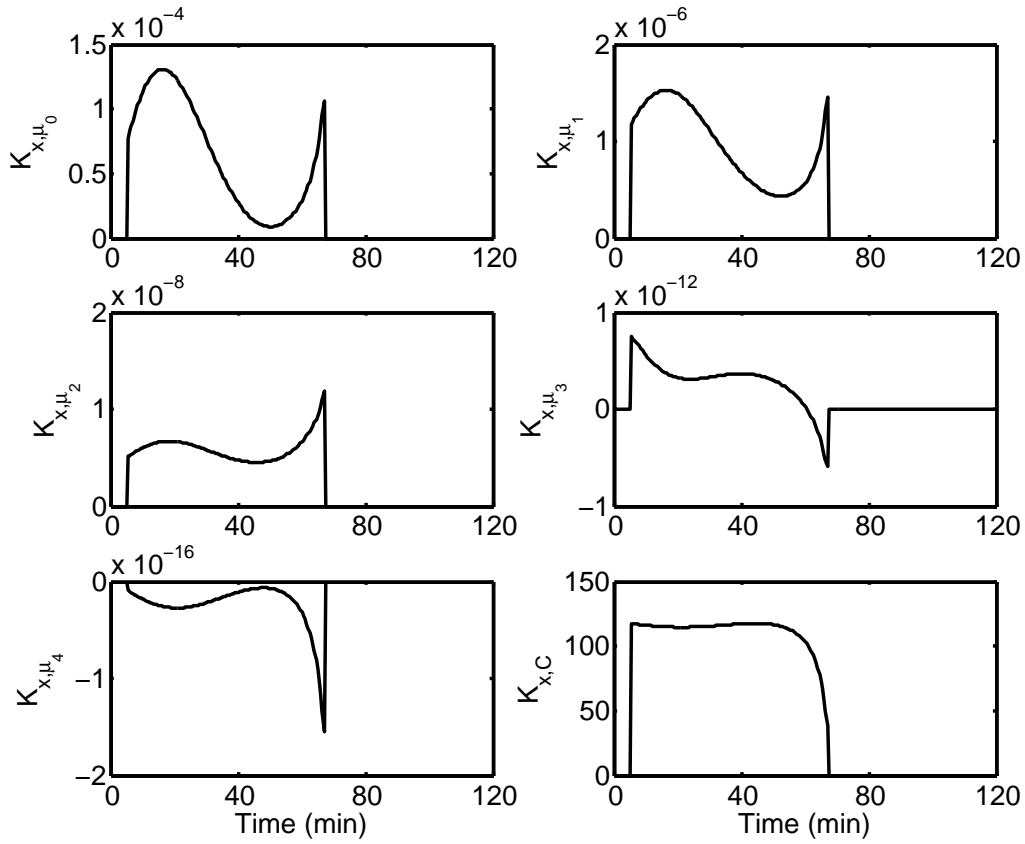


Figure 6.1 Neighboring extremal controller gain corresponding to state feedback, $K_x(t)$.

control is designed assuming the availability of nominal process. Based on repetitive optimization of the formulation described by Eqs. (6.1) and (6.2) is solved within the two switching times, by parameterizing the flowrate profile between $t_{s,1}$ and $t_{s,2}$ using four equidistant first order splines. Thus, during this study, two versions of the NE controller are considered depending on the availability of the information about the uncertainty in the parameters – (i) traditional NE controller with only K_x with δx feedback (NE- K_x) and (ii) reformulated NE controller with both K_x and K_θ with δx and *known* $\delta\theta$ feedback (NE- K_x - K_θ). When the perturbations in the parameters are precisely known, the controller gain corresponding to sensitivity of the parameters, K_θ is kept active along with K_x . Similarly, two versions of MPC formulation – (i) traditional MPC with δx feedback (MPC- δx) and (ii) reformulated MPC with both δx and *known* $\delta\theta$ feedback (MPC- δx - $\delta\theta$). Thus, towards

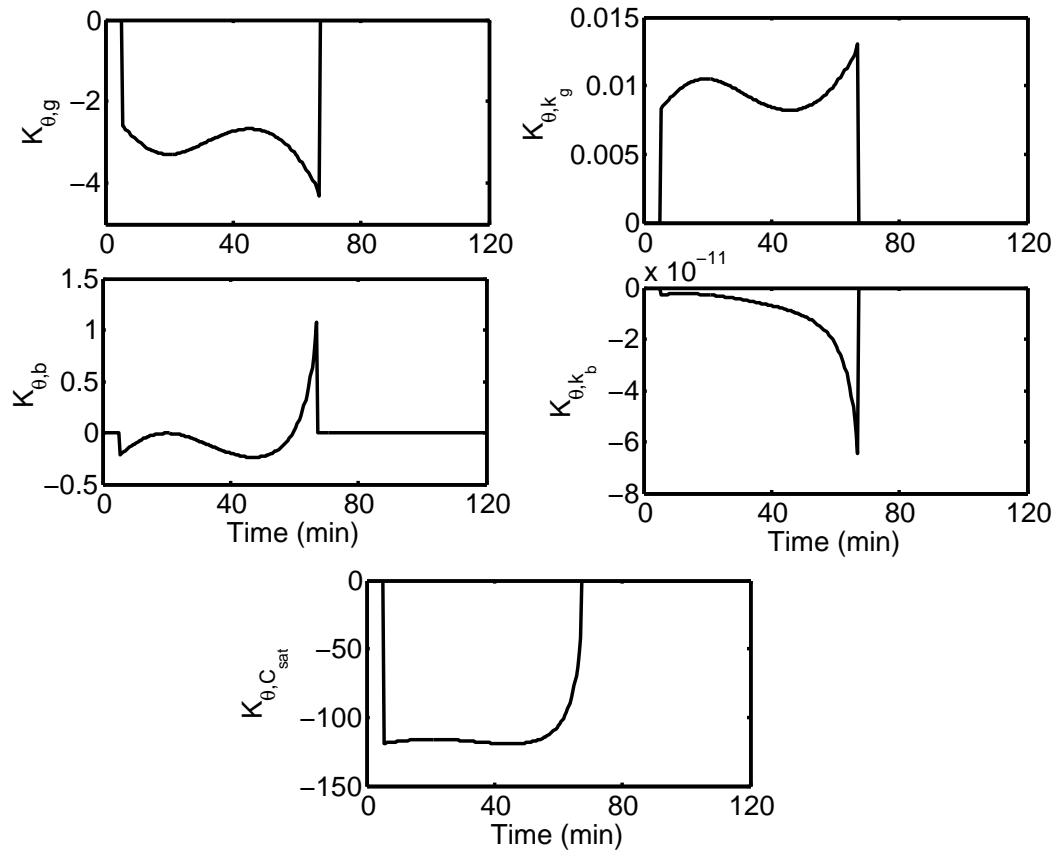


Figure 6.2 Neighboring extremal controller gain corresponding to model parameter deviations, $K_{\theta}(t)$.

this end, the study also tries to compare the performance of NE controller and MPC formulation when the nominal solution of the optimal control problem is given. Furthermore, the performance is compared to the C-control strategy implemented with a constant relative setpoint value of 0.101 that is fine-tuned for the nominal operating conditions. As discussed in the earlier chapter, in order to make a fair comparison between all these approaches, the flexibility offered by the C-control strategy to operate the process with variable batch time is avoided.

Table 6.1 provides the product quality in terms of the volume weighted mean size values and Figures 6.3 to 6.9 present the antisolvent mass percent profiles resulting from the implementation of the all the control strategies discussed above. For the sake of comparison, the nominal open loop and the true optimal values are also provided. It can be inferred from this comparative study that NE- K_x - K_{θ}

outperforms all the other control techniques for the cases of plant-model mismatch considered during this study.

Table 6.1 Product quality values (in μm).

Case	True optimal	Open-loop profile	NCO tracking controller		MPC formulation		C-control
			NE- K_x	NE- K_x - K_θ	MPC- δx	MPC- δx - $\delta\theta$	
Nominal	599.94	599.94	599.94	599.94	599.94	599.94	581.78
1	329.23	257.79	264.51	273.37	267.63	275.80	269.11
2	577.31	555.15	540.43	576.42	540.06	576.58	484.99
3	619.32	546.84	548.25	558.00	548.16	559.83	456.19
4	339.73	247.29	231.95	289.82	235.03	292.00	272.17
5	539.4	477.11	532.27	532.27	533.86	533.86	522.85
6	569.85	540.86	556.24	568.06	542.74	564.41	521.1
7	327.74	231.39	284.67	321.81	292.42	314.97	270.16

As discussed in the earlier chapter, Cases 1 and 4 correspond to the scenarios where the active constraint set towards the end of the batch are changed in order to meet either the minimum product yield constraint or sometimes none of the constraints. Therefore, as seen in Figure 6.3 and 6.6, even though the inclusion of $\delta\theta$ information into the feedback law helps in recovering only a small portion of the optimality loss, as even the input profiles resulting from NE- K_x - K_θ and MPC- δx - $\delta\theta$ deviate significantly from the true optimal profile.

Case 2 provides an interesting scenario where NE- K_x - K_θ and MPC- δx - $\delta\theta$ provide better performance compared to their traditional counterparts NE- K_x and MPC- δx , which perform even poorer than the open loop profile. Thus, the inclusion of $\delta\theta$ into the feedback law not only steers the process towards optimality, but also improves the robustness of the designed controller. It can be noticed in Figure 6.4 that the corresponding input profiles resulting from the implementation of NE- K_x - K_θ and MPC- δx - $\delta\theta$ track very close to the true optimal profile. While, NE- K_x and MPC- δx provide corrective actions to the input profiles that significantly deviate away from the true optimal profile and thus, results in poor product quality. As explained earlier, the performance of C-control in Cases 2, 3, and 6 is poor due to its inherent limitation of not being able to handle the uncertainties in solubility

data (Woo et al., 2009). Thus, as discussed in this chapter, the NCO-tracking based control scheme provides an attractive alternative over C-control strategy for robust control of semi-batch crystallization processes in presence of shifts in solubility data.

In Case 5, all the control strategies perform equally good in obtaining the product quality that is close to the true optimal value, which clearly indicates that the closed loop strategies are robust to changes in initial conditions. To further support the inference, it can be noticed that the antisolvent mass percent plots corresponding to all the different control techniques are close to the true optimal profile as seen in Figure 6.7. In Case 7, the recovery in the optimality loss is large for the controllers that have the feedback information of $\delta\theta$. This can also be inferred from the plots shown in Figure 6.9, where the antisolvent mass percent profiles corresponding to NE- K_x - K_θ and MPC- δx - $\delta\theta$ track very close to the true optimal profile.

Thus, this discussion leads us to the most important insight of incorporating the model parameter deviations along with the state feedback during real-time optimal control of semi-batch antisolvent crystallization processes. Precisely, as discussed in the literature (Eaton and Rawlings, 1990, Agarwal, 1997), robust control and real-time optimal operation are possible when online re-estimation of the model parameters or their deviations from the nominal values is enabled along with the state feedback. Hence, in presence of uncertainty, repetitive online optimization based only on the state feedback may be futile.

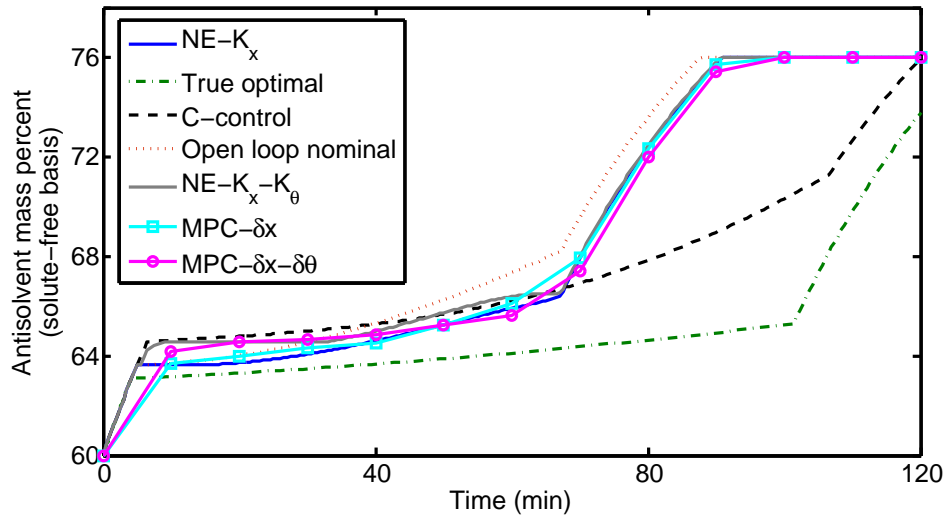


Figure 6.3 Response of various control strategies for Case 1.

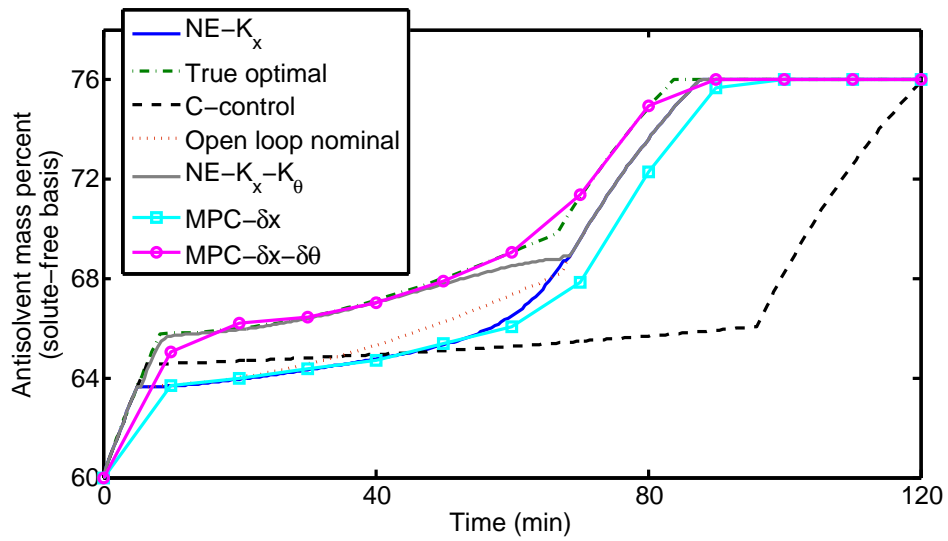


Figure 6.4 Response of various control strategies for Case 2.

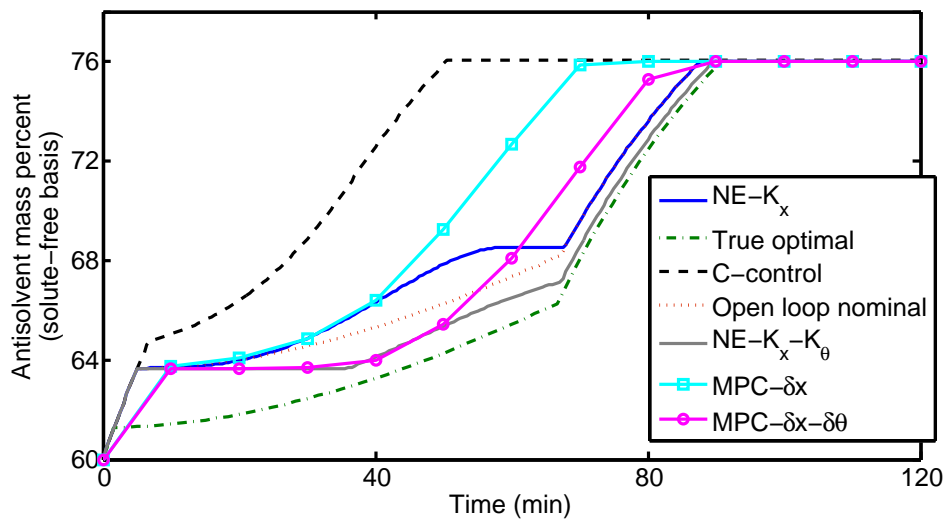


Figure 6.5 Response of various control strategies for Case 3.

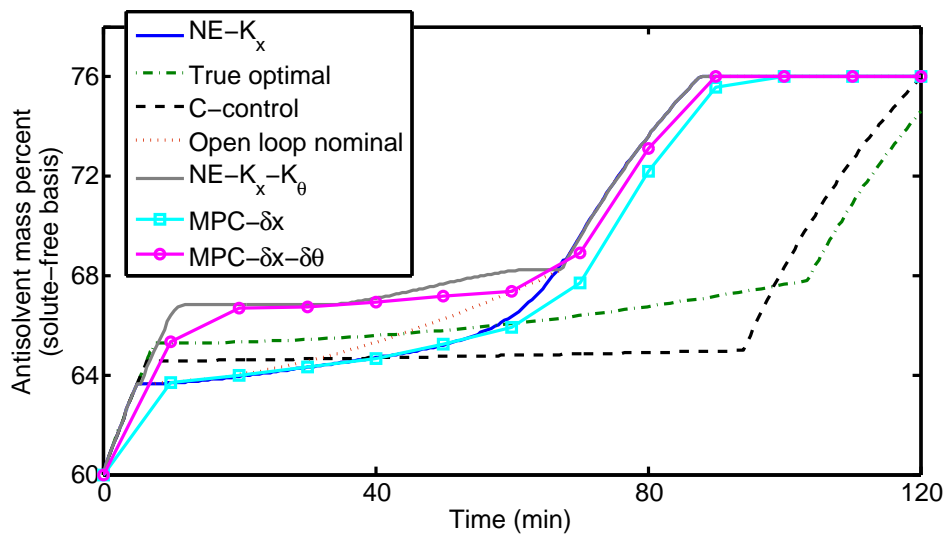


Figure 6.6 Response of various control strategies for Case 4.

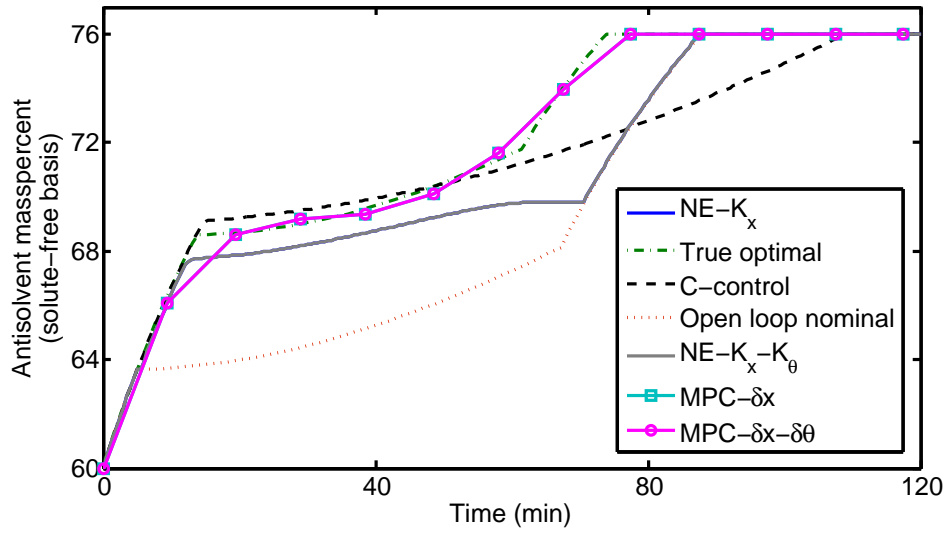


Figure 6.7 Response of various control strategies for Case 5.

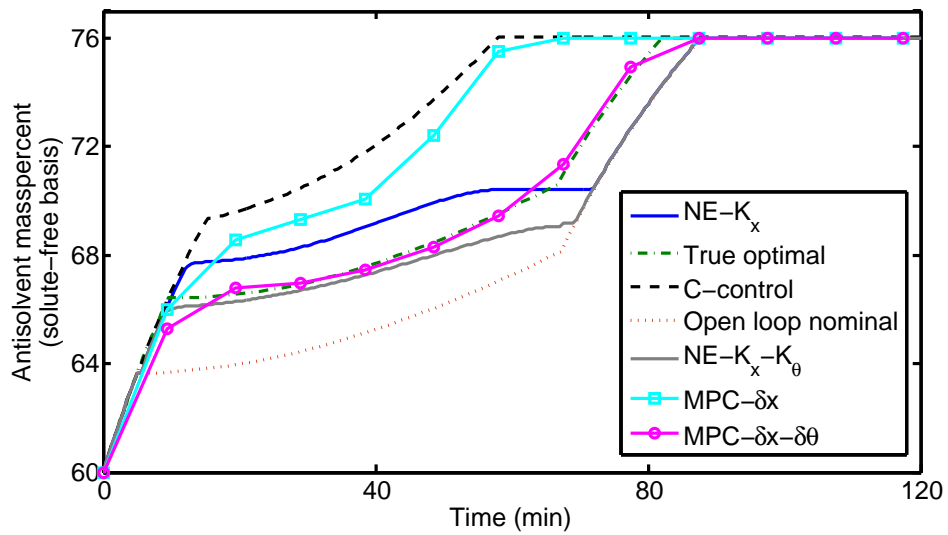


Figure 6.8 Response of various control strategies for Case 6.

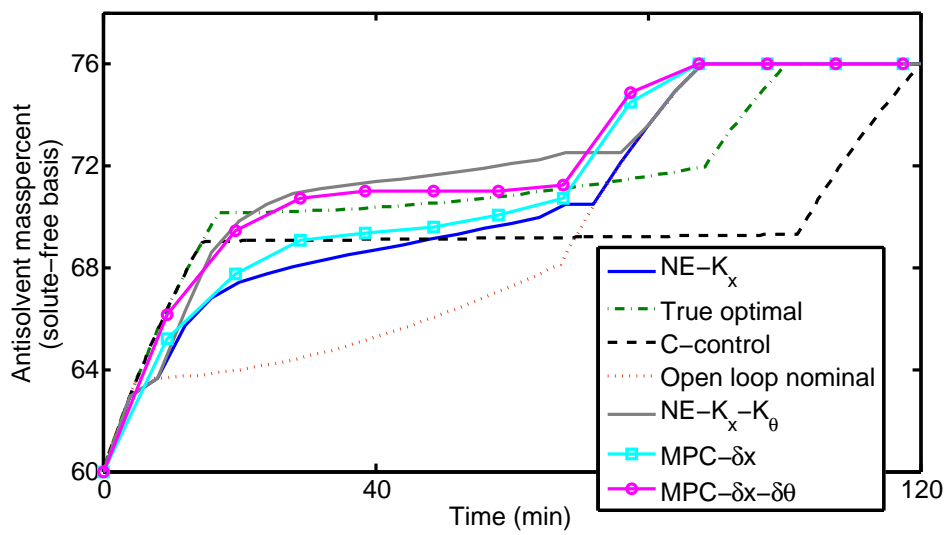


Figure 6.9 Response of various control strategies for Case 7.

6.4 Conclusions

Real-time optimal control using a reformulated neighboring extremal controller that incorporates the input sensitivities with respect to parameter deviations for tracking the interior arcs is developed in this study. To this end, the need of reformulation of NE controller design is revisited, leading to the same conclusion as the previous investigation by Agarwal (1997), that the input and state trajectories corresponding to the NE controller design incorporating the input sensitivities of both the state and parameters is capable of tracking the *true* optimal profiles closely. A comparative study with the C-control strategy shows that the reformulated NE controller minimizes the loss in optimality to a much greater extent and thus providing an attractive solution to the real time optimal control of semi-batch crystallization processes.

Chapter 7

Conclusions and Future Work

7.1 Conclusions

Crystallization forms the initial stage of the downstream operations in pharmaceutical manufacturing processes. Thus, poor product quality in terms of crystal size distribution can significantly affect the efficiency of the other downstream operations and also the efficacy of the final drug. Therefore, recognizing the grave necessity for tighter control of pharmaceutical antisolvent crystallization processes, this thesis investigates the application of various advanced control strategies for real-time control of product crystal size distribution in presence of process variations. Furthermore, paracetamol in acetone/ water mixture is chosen as the model system and the process variations were introduced as uncertainties in the model parameters of the crystallization kinetic rates and shifts in the solubility data.

In presence of the aforementioned process variations, the direct design approaches were shown to display improved robustness over the traditional flowrate control strategy due to their closed loop nature (Fujiwara et al., 2005, Zhou et al., 2006). However, these approaches suffer from being operated in sub-optimal manner because the relevant design parameters, for example relative supersaturation setpoint for C-control are determined by trial-and-error procedure from the plant tests. More-

over, in presence of certain process variations like high crystal nucleation rate and shifts in solubility data, the C-control strategy performs poorer than the traditional flowrate control strategy (Nagy et al., 2008a, Woo et al., 2009). Therefore, in order to circumvent these shortcomings, a new two-staged modeling framework is developed in Chapter 3 for determining the optimal setpoints to achieve improved control performance of the C-control strategy. In the first stage, LSSVM based pattern classifier is used, while in the second stage, JITL framework is used for the dynamic modeling of the process and LSSVM-based MPLS model is used for the product quality predictions. Thus, by integrating these algorithms, the proposed framework helps in determining the setpoint value corresponding to the optimal product quality by solving a constrained optimization problem. Simulation results show that the relative supersaturation setpoints determined using this proposed modeling framework helps in optimal operation of the semi-batch antisolvent crystallization processes by adapting to the variations in the process.

In Chapter 4, the idea of adaptive concentration control presented in Woo et al. (2009) is given a systematic approach. Inspired by the idea of model predictive control for real time optimal control of semi-batch crystallization processes, the relative supersaturation setpoint at each time instant during the batch is adjusted adaptively. Thus, the relative supersaturation setpoint profile over the entire batch time is segmented based on control vector parameterization and the corresponding optimal values are determined based on the feedback of solute concentration values and repetitive online optimization of the product quality. Simulation results show that the proposed adaptive C-control not only helps in providing improved robustness over the existing C-control strategy, but also achieves product quality values that are close to the true optimal. Through this study, it observed that that even the parameterization approach for segmenting the control vectors for the constant relative supersaturation profile also has a significant effect on the batch end product quality. This clearly shows the necessity for tighter control during the initial phase

of the batch crystallization processes, in order to achieve improved robustness and better operational efficiency.

In Chapter 5, real-time optimal control for semi-batch antisolvent crystallization processes based on tracking the necessary conditions of optimality is presented. Motivated to counter the pragmatic limitations of implementing the optimal control policies in presence of plant-model mismatch, measurement-based optimization (MBO) schemes, that bypass the necessity of repetitive online optimization for real-time control (Francois et al., 2005, Srinivasan and Bonvin, 2007) is considered. Based on the given nominal solution, the input profile is dissected into boundary and interior arcs. In order to track the interior (sensitivity seeking) arcs in presence of uncertainties and process disturbances, the neighboring extremal controller is designed. Besides, based on the product quality values, the performance of the NE controller is compared with the MPC design. Simulation results show that the NE controller performs very close to the MPC formulation. Furthermore, it has been observed that the traditional NE controller adapts to shifts in solubility curves better than the C-control strategy. However, the NCO tracking based control still suffers from the issues concerning the change in active constraint set, which arise due to large or simultaneous deviations in the model parameters.

Real-time optimal control using a reformulated neighboring extremal controller that incorporates the input sensitivities with respect to parameter deviations for tracking the interior arcs is developed in Chapter 6. A comparative study with the C-control strategy shows that the reformulated NE controller minimizes the loss in optimality to a much greater extent and thus providing an attractive solution to the real time optimal control of batch crystallization processes.

Furthermore, the importance of considering the reformulated NE controller design is revisited through this study. It has been observed that the input and state trajectories corresponding to the NE controller design that incorporates the input sensitivities of both the state and parameters will track the *true* optimal profiles

very closely. Thus, the necessity of reformulating the NE feedback to counter the deviations in the model parameters has been addressed and validated by simulation studies provided in Chapter 6.

7.2 Suggestions for future works

Listed below are the directions recommended for future research:

- The Design of Experiments (DoE) is a rational and systematic methodology that helps in determining the sufficient number of dissimilar experiments that provide maximum process information within the design space. Based on the process data collected from these finite number of experiments, the input – output relationships are developed for batch industrial processes. Recent advances in this direction have provided significant progress towards addressing pertinent issues in the design and operation of chemical processes with input multiplicity and time-varying input variables (Boukouvala et al., 2010, 2011, Georgakis, 2013). The application of these methodologies as a pre-requisite for the data-based modeling methods employed in Chapters 3 and 4 can be considered for significantly reducing the process data necessary for implementing the proposed modeling framework.
- During the pharmaceutical manufacturing, multiple process measurements such as solute concentration, particle counts, temperature, torque, power consumption, pH, pressure, and so forth are made available at regular sampling intervals. With the continuing adoption of PAT and the sluggish development in sensor technology, the necessity of soft sensors for online monitoring and control of the product quality attributes in real-time is also expanding. Therefore, the creation of soft sensors that can be used as diagnostic tools to rapidly identify multivariate process deviations and thus, can further be used

as inputs for various control schemes to ensure required process performance is receiving interest (Ge and Song, 2010, Fujiwara et al., 2009, Nagy et al., 2011b, Nagy and Braatz, 2012). Hence, understanding the potential of multivariate statistical analysis, demonstrations based on real time experiments using specialized tools that ensure robust control and operational efficiency of the crystallization processes are necessary.

- In order to circumvent some of the shortcomings of the NCO tracking control such as changing active set constraints and the optimal switching times in presence of model uncertainty (as discussed in Chapters 5 and 6), methods based on various *modified adaptation* strategies are proposed in the literature (Chachuat et al., 2008, Srinivasan et al., 2008, Marchetti et al., 2009, 2010). Thus, these strategies that consider additional constraint-gradient information in the feedback law for adapting the inputs are worthy investigating for real-time control of semi-batch crystallization processes. Besides, methods based on *model-parameter adaptation* for simultaneous control and parameter estimation as discussed elsewhere are worthy investigating further (Kamaraju et al., 2013).
- With the increasing interest towards new modes of operation of the batch crystallization processes, the combined cooling and antisolvent crystallization processes have recently received attention. This hybrid mode, which offers the advantage of higher product quality with shorter batch time has been investigated on laboratory scale experiments (Lindenberg et al., 2009, Nagy et al., 2008a). However, development of control strategies for robust control of this multiple-input-multiple-output process require further investigation.

Lastly, recent advances in continuous crystallization microreactors/ channels have provided significant benefits to innovative manufacture. The key challenge of real time robust monitoring of quantitative attributes like form, shape,

and size of solute crystals still remains a massive challenge (Chen et al., 2011, Nagy and Braatz, 2012).

References

- E. Aamir, Z. K. Nagy, and C. D. Rielly. Optimal seed recipe design for crystal size distribution control for batch cooling crystallisation processes. *Chemical Engineering Science*, 65(11):3602 – 3614, 2010.
- M. R. Abu Bakar, Z. K. Nagy, and C. D. Rielly. Seeded batch cooling crystallization with temperature cycling for the control of size uniformity and polymorphic purity of sulfathiazole crystals. *Organic Process Research & Development*, 13(6):1343 – 1356, 2009a.
- M. R. Abu Bakar, Z. K. Nagy, A. N. Saleemi, and C. D. Rielly. The impact of direct nucleation control on crystal size distribution in pharmaceutical crystallization processes. *Crystal Growth & Design*, 9(3):1378 – 1384, 2009b.
- M. R. Abu Bakar, Z. K. Nagy, and C. D. Rielly. A combined approach of differential scanning calorimetry and hot-stage microscopy with image analysis in the investigation of sulfathiazole polymorphism. *Journal of Thermal Analysis and Calorimetry*, 99(2):609 – 619, 2010.
- M. Agarwal. Feasibility of on-line reoptimization in batch processes. *Chemical Engineering Communications*, 158(1):19–29, 1997.
- D. W. Aha, D. Kibler, and M. K. Albert. Instance-based learning algorithms. *Machine Learning*, 6(1):37–66, 1991.

- E. M. Alander and A. C. Rasmuson. Mechanisms of crystal agglomeration of paracetamol in acetone-water mixtures. *Industrial & Engineering Chemistry Research*, 44(15):5788 – 5794, 2005.
- F. Allgower, R. Findeisen, and Z. K. Nagy. Nonlinear model predictive control: From theory to application. *Journal of the Chinese Institute of Chemical Engineers*, 35(3):299 – 315, 2004.
- C. G. Atkeson, A. W. Moore, and S. Z. Schaal. Locally weighted learning for control. *Artificial Intelligence Review*, 11(1-5):75–113, 1997.
- P. Barrett and B. Glennon. Characterizing the metastable zone width and solubility curve using Lasentec FBRM and PVM. *Chemical Engineering Research & Design*, 80:799 – 805, 2002.
- L. T. Biegler, A. M. Cervantes, and A. Wachter. Advances in simultaneous strategies for dynamic process optimization. *Chemical Engineering Science*, 57(4):575 – 593, 2002.
- G. Bontempi, H. Bersini, and M. Birattari. The local paradigm for modeling and control: from neuro-fuzzy to lazy learning. *Fuzzy Sets and Systems*, 121(1):59 – 72, 2001.
- D. Bonvin, B. Srinivasan, and D. Hunkeler. Control and optimization of batch processes. *IEEE Control Systems Magazine*, 26(6):34 – 45, 2006.
- F. Boukouvala, F. J. Muzzio, and M. G. Ierapetritou. Design space of pharmaceutical processes using data-driven-based methods. *Journal of Pharmaceutical Innovation*, 5(3):119 – 137, 2010.
- F. Boukouvala, F. J. Muzzio, and M. G. Ierapetritou. Dynamic data-driven modeling of pharmaceutical processes. *Industrial & Engineering Chemistry Research*, 50(11):6743 – 6754, 2011.

- J. Breakwell, J. Speyer, and A. Bryson. Optimization and control of nonlinear systems using the second variation. *Journal of the Society for Industrial and Applied Mathematics Series A Control*, 1(2):193 – 223, 1963.
- A.E. Bryson and Y.C. Ho. *Applied optimal control: optimization, estimation, and control*. Blaisdell Pub. Co., 1969.
- B. Chachuat, A. Marchetti, and D. Bonvin. Process optimization via constraints adaptation. *Journal of Process Control*, 18(3-4):244 – 257, 2008.
- J. Chen, B. Sarma, J. M. B. Evans, and A. S. Myerson. Pharmaceutical crystallization. *Crystal Growth & Design*, 11(4):887 – 895, 2011.
- C. Cheng and M. S. Chiu. A new data-based methodology for nonlinear process modeling. *Chemical Engineering Science*, 59(13):2801 – 2810, 2004.
- In S. Chin, Kwang S. Lee, and Jay H. Lee. A technique for integrated quality control, profile control, and constraint handling for batch processes. *Industrial & Engineering Chemistry Research*, 39(3):693–705, 2000.
- S. H. Chung, D. L. Ma, and R. D. Braatz. Optimal seeding in batch crystallization. *Canadian Journal of Chemical Engineering*, 77(3):590 – 596, 1999.
- R. J. Davey. The role of the solvent in crystal-growth from solution. *Journal of Crystal Growth*, 76(3):637 – 644, 1986.
- J. A. Dirksen and T. A. Ring. Fundamentals of crystallization: Kinetic effects on particle size distributions and morphology. *Chemical Engineering Science*, 46(10):2389 – 2427, 1991.
- J. W. Eaton and J. B. Rawlings. Feedback control of chemical processes using on-line optimization techniques. *Computers & Chemical Engineering*, 14(4-5):469 – 479, 1990.

- J. W. Eaton and J. B. Rawlings. Model-predictive control of chemical processes. *Chemical Engineering Science*, 47(4):705 – 720, 1992.
- FDA. Guidance for Industry: PAT - A Framework for Innovative Pharmaceutical Development, Manufacturing and Quality Assurance (www.fda.gov/cvm/guidance/published.html). 2004.
- G. Francois, B. Srinivasan, and D. Bonvin. Use of measurements for enforcing the necessary conditions of optimality in the presence of constraints and uncertainty. *Journal of Process Control*, 15(6):701 – 712, 2005.
- K. Fujiwara, M. Kano, S. Hasebe, and A. Takinami. Soft-sensor development using correlation-based just-in-time modeling. *AIChE Journal*, 55(7):1754 – 1765, 2009.
- M. Fujiwara, Z. K. Nagy, J. W. Chew, and R. D. Braatz. First-principles and direct design approaches for the control of pharmaceutical crystallization. *Journal of Process Control*, 15(5):493 – 504, 2005.
- Z. Q. Ge and Z. H. Song. A comparative study of just-in-time-learning based methods for online soft sensor modeling. *Chemometrics and Intelligent Laboratory Systems*, 104(2):306 – 317, 2010.
- C. Georgakis. Design of dynamic experiments: A data-driven methodology for the optimization of time-varying processes. *Industrial & Engineering Chemistry Research*, 52(35):12369 – 12382, 2013.
- B. Glennon, D. O’Grady, M. Barrett, and E. Casey. The effect of mixing on the metastable zone width and nucleation kinetics in the anti-solvent crystallization of benzoic acid. *Chemical Engineering Research & Design*, 85(A7):945 – 952, 2007.

- M. Golshan, J. F. MacGregor, M.-J. Bruwer, and P. Mhaskar. Latent variable model predictive control (LV-MPC) for trajectory tracking in batch processes. *Journal of Process Control*, 20(4):538 – 550, 2010.
- R. A. Granberg and A. C. Rasmuson. Solubility of paracetamol in binary and ternary mixtures of water plus acetone plus toluene. *Journal of Chemical and Engineering Data*, 45(3):478 – 483, 2000.
- R. A. Granberg and A. C. Rasmuson. Crystal growth rates of paracetamol in mixtures of water plus acetone plus toluene. *AIChE Journal*, 51(9):2441 – 2456, 2005.
- R. A. Granberg, D. G. Bloch, and A. C. Rasmuson. Crystallization of paracetamol in acetone-water mixtures. *Journal of Crystal Growth*, 199:1287 – 1293, 1999.
- R. A. Granberg, C. Ducreux, S. Gracin, and A. C. Rasmuson. Primary nucleation of paracetamol in acetone-water mixtures. *Chemical Engineering Science*, 56(7):2305 – 2313, 2001.
- S. Gros, B. Srinivasan, and D. Bonvin. Optimizing control based on output feedback. *Computers & Chemical Engineering*, 33(1):191 – 198, 2009a.
- S. Gros, B. Srinivasan, B. Chachuat, and D. Bonvin. Neighbouring-extremal control for singular dynamic optimisation problems. Part I: Single-input systems. *International Journal of Control*, 82(6):1099 – 1112, 2009b.
- M. W. Hermanto, M. S. Chiu, X. Y. Woo, and R. D. Braatz. Robust optimal control of polymorphic transformation in batch crystallization. *AIChE Journal*, 53(10):2643 – 2650, 2007.
- M. W. Hermanto, M. S. Chiu, and R. D. Braatz. Nonlinear model predictive control for the polymorphic transformation of L-glutamic acid crystals. *AIChE Journal*, 55(10):2631 – 2645, 2009.

- M. W. Hermanto, P. S. Chow, and R. B. H. Tan. Implementation of focused beam reflectance measurement (FBRM) in antisolvent crystallization to achieve consistent product quality. *Crystal Growth & Design*, 10(8):3668 – 3674, 2010.
- M. W. Hermanto, R. D. Braatz, and M. S. Chiu. Integrated batch-to-batch and non-linear model predictive control for polymorphic transformation in pharmaceutical crystallization. *AIChE Journal*, 57(4):1008 – 1019, 2011.
- M. W. Hermanto, A. Phua, P. S. Chow, and R. B. H. Tan. Improved C-control of crystallization with reduced calibration effort via conductometry. *Chemical Engineering Science*, 97:126 – 138, 2013.
- W. I. Higuchi and E. N. Hiestand. Dissolution rates of finely divided drug powders .1. Effect of a distribution of particle sizes in a diffusion-controlled process. *Journal of Pharmaceutical Sciences*, 52(1):67 – 71, 1963.
- H. Hojjati, M. Sheikhzadeh, and S. Rohani. Control of supersaturation in a semi-batch antisolvent crystallization process using a fuzzy logic controller. *Industrial & Engineering Chemistry Research*, 46(4):1232 – 1240, 2007.
- K. S. Howard, Z. K. Nagy, B. Saha, A. L. Robertson, G. Steele, and D. Martin. A process analytical technology based investigation of the polymorphic transformations during the antisolvent crystallization of sodium benzoate from IPA/Water mixture. *Crystal Growth & Design*, 9(9):3964 – 3975, 2009.
- Q. Hu, S. Rohani, and A. Jutan. Modelling and optimization of seeded batch crystallizers. *Computers & Chemical Engineering*, 29(4):911 – 918, 2005.
- H. M. Hulburt and S. Katz. Some problems in particle technology - A statistical mechanical formulation. *Chemical Engineering Science*, 19(8):555 – 574, 1964.
- A. K. Jain, R. P. W. Duin, and J. C. Mao. Statistical pattern recognition: A re-

- view. *IEEE Transactions on Pattern Analysis and Machine Intelligence*, 22:4 – 37, 2000.
- J.-S.R. Jang and C.-T. Sun. Neuro-fuzzy modeling and control. *Proceedings of the IEEE*, 83(3):378–406, 1995.
- A. G. Jones. Optimal operation of a batch cooling crystallizer. *Chemical Engineering Science*, 29(5):1075 – 1087, 1974.
- J. V. Kadam, M. Schlegel, B. Srinivasan, D. Bonvin, and W. Marquardt. Dynamic optimization in the presence of uncertainty: From off-line nominal solution to measurement-based implementation. *Journal of Process Control*, 17:389 – 398, 2007.
- V. K. Kamaraju, M. S. Chiu, and B. Srinivasan. Reformulating real-time optimal feedback based on model uncertainty. In *Dynamics and Control of Process Systems*, pages 756 – 761, 2013.
- P. H. Karpinski and J. Nyvlt. Metastable zone width in salting-out crystallization. *Crystal Research and Technology*, 18(7):959 – 965, 1983.
- S. Kim, B. Lotz, M. Lindrud, K. Girard, T. Moore, K. Nagarajan, M. Alvarez, T. Lee, F. Nikfar, M. Davidovich, S. Srivastava, and S. Kiang. Control of the particle properties of a drug substance by crystallization engineering and the effect on drug product formulation. *Organic Process Research & Development*, 9(6): 894 – 901, 2005.
- J. H. Lee and K. S. Lee. Iterative learning control applied to batch processes: An overview. *Control Engineering Practice*, 15(10):1306 – 1318, 2007.
- K. Lee, J. H. Lee, M. Fujiwara, D. L. Ma, and R. D. Braatz. Run-to-run control of multidimensional crystal size distribution in a batch crystallizer. *Proceedings of the 2002 American Control Conference, Vols 1-6*, pages 1013 – 1018, 2002a.

- K. Lee, J. H. Lee, D. R. Yang, and A. W. Mahoney. Integrated run-to-run and on-line model-based control of particle size distribution for a semi-batch precipitation reactor. *Computers & Chemical Engineering*, 26(7-8):1117 – 1131, 2002b.
- K. S. Lee and J. H. Lee. Iterative learning control-based batch process control technique for integrated control of end product properties and transient profiles of process variables. *Journal of Process Control*, 13(7):607 – 621, 2003.
- Y. F. Li, Z. F. Wang, and J. Q. Yuan. On-line fault detection using SVM-based dynamic MPLS for batch processes. *Chinese Journal of Chemical Engineering*, 14(6):754 – 758, 2006.
- C. Lindenberg, M. Krattli, J. Cornel, M. Mazzotti, and J. Brozio. Design and optimization of a combined cooling/antisolvent crystallization process. *Crystal Growth & Design*, 9(2):1124 – 1136, 2009.
- V. Liotta and V. Sabesan. Monitoring and feedback control of supersaturation using atr-ftir to produce an active pharmaceutical ingredient of a desired crystal size. *Organic Process Research & Development*, 8(3):488 – 494, 2004.
- D. L. Ma, S. H. Chung, and R. D. Braatz. Worst-case performance analysis of optimal batch control trajectories. *AIChE Journal*, 45(7):1469 – 1476, 1999.
- A. J. Mahajan and D. J. Kirwan. Nucleation and growth-kinetics of biochemicals measured at high supersaturations. *Journal of Crystal Growth*, 144(3-4):281 – 290, 1994.
- A. Marchetti, B. Chachuat, and D. Bonvin. Modifier-adaptation methodology for real-time optimization. *Industrial & Engineering Chemistry Research*, 48(13):6022 – 6033, 2009.
- A. Marchetti, B. Chachuat, and D. Bonvin. A dual modifier-adaptation approach for real-time optimization. *Journal of Process Control*, 20(9):1027 – 1037, 2010.

- A. Mesbah, A. E. M. Huesman, H. J. M. Kramer, Z. K. Nagy, and P. M. J. Van den Hof. Real-time control of a semi-industrial fed-batch evaporative crystallizer using different direct optimization strategies. *AIChE Journal*, 57(6):1557 – 1569, 2011.
- R. Mohan and A. S. Myerson. Growth kinetics: A thermodynamic approach. *Chemical Engineering Science*, 57(20):4277 – 4285, 2002.
- K. R. Muller, S. Mika, G. Ratsch, K. Tsuda, and B. Scholkopf. An introduction to kernel-based learning algorithms. *IEEE Transactions on Neural Networks*, 12(2):181 – 201, 2001.
- J. W. Mullin and J. Nyvlt. Programmed cooling of batch crystallizers. *Chemical Engineering Science*, 26(3):369 – 377, 1971.
- J.W. Mullin. *Crystallization*. Butterworth-Heinemann, Oxford, 4th edition, 2001.
- A. Myerson. *Handbook of industrial crystallization*. Butterworth-Heinemann, 2002.
- Z. K. Nagy. Model based robust control approach for batch crystallization product design. *Computers & Chemical Engineering*, 33(10):1685 – 1691, 2009.
- Z. K. Nagy and R. D. Braatz. Robust nonlinear model predictive control of batch processes. *AIChE Journal*, 49(7):1776 – 1786, 2003.
- Z. K. Nagy and R. D. Braatz. Open-loop and closed-loop robust optimal control of batch processes using distributional and worst-case analysis. *Journal of Process Control*, 14(4):411 – 422, 2004.
- Z. K. Nagy and R. D. Braatz. Advances and new directions in crystallization control. *Annual Review of Chemical and Biomolecular Engineering*, 3(1):55 – 75, 2012.

- Z. K. Nagy, B. Mahn, R. Franke, and F. Allgower. Evaluation study of an efficient output feedback nonlinear model predictive control for temperature tracking in an industrial batch reactor. *Control Engineering Practice*, 15(7):839 – 850, 2007a.
- Z. K. Nagy, B. Mahn, R. Franke, and F. Allgower. Real-time implementation of nonlinear model predictive control of batch processes in an industrial framework. *Assessment and Future Directions of Nonlinear Model Predictive Control*, 358: 465 – 472, 2007b.
- Z. K. Nagy, J. W. Chew, M. Fujiwara, and R. D. Braatz. Comparative performance of concentration and temperature controlled batch crystallizations. *Journal of Process Control*, 18(3 - 4):399 – 407, 2008a.
- Z. K. Nagy, M. Fujiwara, and R. D. Braatz. Modelling and control of combined cooling and antisolvent crystallization processes. *Journal of Process Control*, 18(9):856 – 864, 2008b.
- Z. K. Nagy, E. Aamir, and C. D. Rielly. Internal fines removal using population balance model based control of crystal size distribution under dissolution, growth and nucleation mechanisms. *Crystal Growth & Design*, 11(6):2205 – 2219, 2011a.
- Z. K. Nagy, M. Baker, N. Pedge, and G. Steele. Supersaturation and direct nucleation control of an industrial pharmaceutical crystallization process using a crystallization process informatics system (CryPRINS). In *Proc. Int. Workshop Ind. Cryst., 18th, Delft, The Netherlands*, pages 7–9. Delft Univ. Tech. Delft, The Netherlands, 2011b.
- P. R. C. Nelson, P. A. Taylor, and J. F. MacGregor. Missing data methods in PCA and PLS: Score calculations with incomplete observations. *Chemometrics and Intelligent Laboratory Systems*, 35(1):45 – 65, 1996.

- P. Nomikos and J. F. MacGregor. Monitoring batch processes using multiway principal component analysis. *AIChE Journal*, 40(8):1361 – 1375, 1994.
- P. Nomikos and J. F. MacGregor. Multi-way partial least squares in monitoring batch processes. *Chemometrics and Intelligent Laboratory Systems*, 30(1):97 – 108, 1995a.
- P. Nomikos and J. F. MacGregor. Multivariate SPC charts for monitoring batch processes. *Technometrics*, 37(1):41 – 59, 1995b.
- S. M. Nowee, A. Abbas, and J. A. Romagnoli. Antisolvent crystallization: Model identification, experimental validation and dynamic simulation. *Chemical Engineering Science*, 63(22):5457 – 5467, 2008a.
- S. M. Nowee, A. Abbas, and J. A. Romagnoli. Model-based optimal strategies for controlling particle size in antisolvent crystallization operations. *Crystal Growth & Design*, 8(8):2698 – 2706, 2008b.
- J. Nyvlt. Kinetics of nucleation in solutions. *Journal of Crystal Growth*, 3:377 – 383, 1968.
- J. Nyvlt. *The kinetics of industrial crystallization*. Elsevier Science Pub. Co., Inc., Amsterdam; New York, 1985. ISBN 0444996109.
- J. Nyvlt. Batch salting-out crystallization. *Chemical Engineering and Processing*, 31(1):39 – 42, 1992.
- D. B. Patience and J. B. Rawlings. Particle-shape monitoring and control in crystallization processes. *AIChE Journal*, 47(9):2125 – 2130, 2001.
- K. Pelckmans, J. A. K. Suykens, T. van Gestel, J de Brabanter, L. Lukas, B. Hamers, B de Moor, and J. Vandewalle. LS-SVMlab : A MATLAB / C toolbox for least squares support vector machines. *Tutorial. KULeuven-ESAT. Leuven, Belgium*, 2002.

- K. Pollanen, A. Hakkinen, S. P. Reinikainen, J. Rantanen, and P. Minkkinen. Dynamic PCA-based MSPC charts for nucleation prediction in batch cooling crystallization processes. *Chemometrics and Intelligent Laboratory Systems*, 84(1-2): 126 – 133, 2006.
- S. Qamar, M. P. Elsner, I. A. Angelov, G. Warnecke, and A. Seidel-Morgenstern. A comparative study of high resolution schemes for solving population balances in crystallization. *Computers & Chemical Engineering*, 30(6 - 7):1119 – 1131, 2006.
- S. J. Qin and T. J. McAvoy. Nonlinear PLS modeling using neural networks. *Computers & Chemical Engineering*, 16(4):379 – 391, 1992.
- A. D. Randolph and M. A. Larson. *Theory of particulate processes, analysis and techniques of continuous crystallization*. Academic Press, New York, 1971.
- A. D. Randolph, L. Chen, and A. Tavana. Feedback-control of CSD in a KCl crystallizer with a fines dissolver. *AIChE Journal*, 33(4):583 – 591, 1987.
- J. B. Rawlings. Tutorial overview of model predictive control. *IEEE Control Systems Magazine*, 20(3):38 – 52, 2000.
- J. B. Rawlings, W. R. Witkowski, and J. W. Eaton. Modeling and control of crystallizers. *Powder Technology*, 69(1):3 – 9, 1992.
- J. B. Rawlings, S. M. Miller, and W. R. Witkowski. Model identification and control of solution crystallization processes - A review. *Industrial & Engineering Chemistry Research*, 32(7):1275 – 1296, 1993.
- C. Rhodes, M. Morari, L. S. Tsimring, and N. F. Rulkov. Data-based control trajectory planning for nonlinear systems. *Physical Review E*, 56:2398–2406, 1997.
- S. Rohani, S. Horne, and K. Murthy. Control of product quality in batch crystallization of pharmaceuticals and fine chemicals. Part 1: Design of the crystallization

- process and the effect of solvent. *Organic Process Research & Development*, 9(6):858 – 872, 2005a.
- S. Rohani, S. Horne, and K. Murthy. Control of product quality in batch crystallization of pharmaceuticals and fine chemicals. Part 2: External control. *Organic Process Research & Development*, 9(6):873 – 883, 2005b.
- A. Ruf, J. Worlitschek, and M. Mazzotti. Modeling and experimental analysis of PSD measurements through FBRM. *Particle & Particle Systems Characterization*, 17(4):167 – 179, 2000.
- S. A. Russell, P. Kesavan, J. H. Lee, and B. A. Ogunnaike. Recursive data-based prediction and control of batch product quality. *AIChE Journal*, 44(11):2442 – 2458, 1998.
- M. Sheikhzadeh, M. Trifkovic, and S. Rohani. Fuzzy logic and rigid control of a seeded semi-batch, anti-solvent, isothermal crystallizer. *Chemical Engineering Science*, 63(4):991 – 1002, 2008a.
- M. Sheikhzadeh, M. Trifkovic, and S. Rohani. Real-time optimal control of an anti-solvent isothermal semi-batch crystallization process. *Chemical Engineering Science*, 63(3):829 – 839, 2008b.
- M. Sheikhzadeh, M. Trifkovic, and S. Rohani. Adaptive MIMO neuro-fuzzy logic control of a seeded and an unseeded anti-solvent semi-batch crystallizer. *Chemical Engineering Science*, 63(5):1261 – 1272, 2008c.
- B. Y. Shekunov and P. York. Crystallization processes in pharmaceutical technology and drug delivery design. *Journal of Crystal Growth*, 211(1-4):122 – 136, 2000.
- B. Y. Shekunov, P. Chattopadhyay, H. H. Y. Tong, and A. H. L. Chow. Particle size analysis in pharmaceuticals: Principles, methods and applications. *Pharmaceutical Research*, 24(2):203 – 227, 2007.

- D. Shi, N. H. El-Farra, M. H. Li, P. Mhaskar, and P. D. Christofides. Predictive control of particle size distribution in particulate processes. *Chemical Engineering Science*, 61(1):268 – 281, 2006.
- L. L. Simon, Z. K. Nagy, and K. Hungerbuhler. Endoscopy-based in situ bulk video imaging of batch crystallization processes. *Organic Process Research & Development*, 13(6):1254 – 1261, 2009a.
- L. L. Simon, Z. K. Nagy, and K. Hungerbuhler. Comparison of external bulk video imaging with focused beam reflectance measurement and ultra-violet visible spectroscopy for metastable zone identification in food and pharmaceutical crystallization processes. *Chemical Engineering Science*, 64(14):3344 – 3351, 2009b.
- L. L. Simon, K. A. Oucherif, Z. K. Nagy, and K. Hungerbuhler. Bulk video imaging based multivariate image analysis, process control chart and acoustic signal assisted nucleation detection. *Chemical Engineering Science*, 65(17):4983 – 4995, 2010.
- B. Srinivasan and D. Bonvin. Real-time optimization of batch processes by tracking the necessary conditions of optimality. *Industrial & Engineering Chemistry Research*, 46(2):492 – 504, 2007.
- B. Srinivasan, D. Bonvin, E. Visser, and S. Palanki. Dynamic optimization of batch processes II. Role of measurements in handling uncertainty. *Computers & Chemical Engineering*, 27(5):761 – 761, 2003a.
- B. Srinivasan, S. Palanki, and D. Bonvin. Dynamic optimization of batch processes I. Characterization of the nominal solution. *Computers & Chemical Engineering*, 27(5):759 – 760, 2003b.
- B. Srinivasan, L. T. Biegler, and D. Bonvin. Tracking the necessary conditions of

- optimality with changing set of active constraints using a barrier-penalty function. *Computers & Chemical Engineering*, 32(3):572 – 579, 2008.
- J. A. K. Suykens and J. Vandewalle. Least squares support vector machine classifiers. *Neural Processing Letters*, 9(3):293 – 300, 1999.
- T. Takagi and M. Sugeno. Fuzzy identification of systems and its applications to modeling and control. *Systems, Man and Cybernetics, IEEE Transactions on*, SMC-15(1):116–132, 1985.
- T. Togkalidou, R. D. Braatz, B. K. Johnson, O. Davidson, and A. Andrews. Experimental design and inferential modeling in pharmaceutical crystallization. *AIChE Journal*, 47(1):160 – 168, 2001a.
- T. Togkalidou, M. Fujiwara, S. Patel, and R. D. Braatz. Solute concentration prediction using chemometrics and ATR-FTIR spectroscopy. *Journal of Crystal Growth*, 231(4):534 – 543, 2001b.
- M. Trifkovic, M. Sheikhzadeh, and S. Rohani. Kinetics estimation and single and multi-objective optimization of a seeded, anti-solvent, isothermal batch crystallizer. *Industrial & Engineering Chemistry Research*, 47(5):1586 – 1595, 2008.
- M. Trifkovic, M. Sheikhzadeh, and S. Rohani. Multivariable real-time optimal control of a cooling and antisolvent semibatch crystallization process. *AIChE Journal*, 55(10):2591 – 2602, 2009.
- H.H. Tung, E. L. Paul, M. Midler, and J. A. McCauley. *Crystallization of organic compounds: An industrial perspective*. John Wiley & Sons, 2009.
- T. van Gestel, J. A. K. Suykens, B. Baesens, S. Viaene, J. Vanthienen, G. Dedene, B. de Moor, and J. Vandewalle. Benchmarking least squares support vector machine classifiers. *Machine Learning*, 54(1):5 – 32, 2004.

- V. N. Vapnik. An overview of statistical learning theory. *IEEE Transactions on Neural Networks*, 10:988 – 999, 1999.
- E. Visser, B. Srinivasan, S. Palanki, and D. Bonvin. A feedback-based implementation scheme for batch process optimization. *Journal of Process Control*, 10:399 – 410, 2000.
- X. Z. Wang, J. C. De Anda, and K. J. Roberts. Real-time measurement of the growth rates of individual crystal facets using imaging and image analysis - a feasibility study on needle-shaped crystals of l-glutamic acid. *Chemical Engineering Research & Design*, 85(A7):921 – 927, 2007.
- C. Welz, B. Srinivasan, and D. Bonvin. Measurement-based optimization of batch processes: Meeting terminal constraints on-line via trajectory following. *Journal of Process Control*, 18(3 - 4):375 – 382, 2008.
- S. Wold, N. Kettanehwoold, and B. Skagerberg. Nonlinear PLS modeling. *Chemometrics and Intelligent Laboratory Systems*, 7(1 - 2):53 – 65, 1989.
- X. Y. Woo, Z. K. Nagy, R. B. H. Tan, and R. D. Braatz. Adaptive concentration control of cooling and antisolvent crystallization with laser backscattering measurement. *Crystal Growth & Design*, 9(1):182 – 191, 2009.
- L. X. Yu, R. A. Lionberger, A. S. Raw, R. D’Costa, H. Wu, and A. S. Hussain. Applications of process analytical technology to crystallization processes. *Advanced Drug Delivery Reviews*, 56:349 – 369, 2004.
- Z. Q. Yu, R. B. H. Tan, and P. S. Chow. Effects of operating conditions on agglomeration and habit of paracetamol crystals in anti-solvent crystallization. *Journal of Crystal Growth*, 279(3 - 4):477 – 488, 2005.
- Z. Q. Yu, P. S. Chow, and R. B. H. Tan. Application of attenuated total reflectance-fourier transform infrared (ATR-FTIR) technique in the monitoring and control

- of anti-solvent crystallization. *Industrial & Engineering Chemistry Research*, 45(1):438 – 444, 2006a.
- Z. Q. Yu, P. S. Chow, and R. B. H. Tan. Seeding and constant-supersaturation control by ATR-FTIR in anti-solvent crystallization. *Organic Process Research & Development*, 10(4):717 – 722, 2006b.
- Z. Q. Yu, J. W. Chew, P. S. Chow, and R. B. H. Tan. Recent advances in crystallization control - An industrial perspective. *Chemical Engineering Research & Design*, 85(A7):893 – 905, 2007.
- G. X. Zhou, M. Fujiwara, X. Y. Woo, E. Rusli, H. H. Tung, C. Starbuck, O. Davidson, Z. H. Ge, and R. D. Braatz. Direct design of pharmaceutical antisolvent crystallization through concentration control. *Crystal Growth & Design*, 6(4):892 – 898, 2006.
- Y. Zhou, R. Srinivasan, and S. Lakshminarayanan. Critical evaluation of image processing approaches for real-time crystal size measurements. *Computers & Chemical Engineering*, 33(5):1022 – 1035, 2009.

Publications and Presentations

KAMARAJU, V. K., CHIU, M. -S., An Integrated Approach for C-control of Antisolvent Crystallization Processes, In *The 8th International Symposium on Advanced Control of Chemical Processes (ADCHEM 2012)*, 762 - 767, Singapore, 10 - 13 July (2012).

KAMARAJU, V. K., SRINIVASAN, B., CHIU, M. -S., NCO-tracking based Control of Semi-batch Antisolvent Crystallization Processes in the Presence of Uncertainties, In *The 12th biannual European Control Conference (ECC 2013)*, 3390 - 3395, Zurich, Switzerland, 17 - 19 July (2013).

KAMARAJU, V. K., CHIU, M. -S., SRINIVASAN, B., Reformulating Real-time Optimal Feedback based on Model Uncertainty, In *10th International Symposium on Dynamics and Control of Process Systems (DYCOPS 2013)*, 756 - 761, Mumbai, India, 18 - 20 December (2013).

KAMARAJU, V. K., CHIU, M. -S., Improved Operation of Concentration Control for Antisolvent Crystallization Processes. *Organic Process Research & Development* (2014), submitted.

KAMARAJU, V. K., SRINIVASAN, B., CHIU, M. -S., Measurement based Optimal Control of Semi-batch Antisolvent Crystallization Processes in the Presence of

Uncertainties, under preparation.

